KERNFORSCHUNGSZENTRUM

KARLSRUHE

Dezember 1976 KFK 2379

Institut für Angewandte Kernphysik

ANNUAL REPORT

Teilinstitut Kernphysik

(July 1, 1975 — June 30, 1976)

Editors:
H. J. Gils and D. Heck

GESELLSCHAFT
FÜR
KERNFORSCHUNG M.B.H.

KARLSRUHE

GESELLSCHAFT FÜR KERNFORSCHUNG M. B. H.

KARLSRUHE

KERNFORSCHUNGSZENTRUM KARLSRUHE

KFK 2379

Institut für Angewandte Kernphysik

A N N U A L R E P O R T

Teilinstitut Kernphysik

(July 1, 1975 - June 30, 1976)

Editors: H.J. Gils and D. Heck

Gesellschaft für Kernforschung mbH, Karlsruhe

Abstract

The activities of the Nuclear Physics Section of the Institute of Applied Nuclear Physics from mid 1975 to mid 1976 are surveyed. The research program comprises the measurement of neutron cross sections, the application of γ ray spectroscopy to problems of the nuclear fuel cycle, the development of a high intensity neutron generator tube, and several investigations in fundamental nuclear physics. In addition, the operation of the two accelerators of the institute, an isochronous cyclotron and a 3 MV Van de Graaff accelerator, are briefly reviewed.

Zusammenfassung

Es wird über die Tätigkeit des Teilinstitutes Kernphysik des Institutes für Angewandte Kernphysik von Mitte 1975 bis Mitte 1976 berichtet. Das Forschungsprogramm umfaßt Messungen von Neutronenwirkungsquerschnitten, Anwendungen der Gammaspektroskopie auf Probleme des Kernbrennstoffzyklus, die Entwicklung einer Neutronengeneratorröhre hoher Intensität und einige Grundlagenuntersuchungen zur Kernphysik. Ferner wird der Betrieb der beiden Beschleuniger des Institutes, eines Isochronzyklotrons und eines 3 MV-Van-de-Graaff-Beschleunigers, kurz geschildert.

The Institute of Applied Nuclear Physics of the Karlsruhe Nuclear Research Centre is engaged in research work on the application of nuclear physics to problems of nuclear energy, solid state physics, medicine, and analysis. These investigations are supported by some fundamental research. This report gives a survey of the work of the Nuclear Physics Section from mid 1975 to mid 1976. Progress of the Nuclear Solid State Physics Section is reported separately.

Measurements of cross sections of neutron induced nuclear reactions are among the main acitivities of the institute. The major part of this work is to provide nuclear data that are required for the design of fast breeder reactors. Here the emphasis is now on cross sections for uranium and transuranium isotopes. Other neutron cross section measurements aim at data relevant to the astrophysical s-process thought to be responsible for heavy element synthesis in stars.

Methods of γ ray spectrometry are applied to problems of the nuclear fuel cycle such as the determination of plutonium in waste and of the isotopic composition of nuclear fuel. A method to measure the enrichment of ^{235}U in light water reactor fuel has been demonstrated in a fuel fabrication plant and will come into routine use in the near future.

The development of the intense neutron generator tube KARIN has also reached the stage of practical application. A neutron cancer therapy unit based on KARIN was installed at the German Cancer Research Centre at Heidelberg, in close operation with an industrial licensee.

In addition to this applied research, a number of experiments in fundamental nuclear physics are carried out, most of them in close cooperation with visiting groups from German universities. A close connection between applied and fundamental work is one of the characteristics of the institute and has led to a stimulating exchange of ideas in either way. Most of the fundamental research makes use of the Karlsruhe Isochronous Cyclotron. One experiment of the last year which deserves special mention is a determination of the neutron distribution in lead nuclei as deduced from the elastic scattering of high energy alpha particles.

The institute operates two accelerators. A 3 MV single stage Van de Graaff accelerator is primarily used for neutron time-of-flight experiments and solid state physics. The Karlsruhe Isochronous Cyclotron, a fixed frequency machine, provides beams of 52 MeV deuterons, 104 MeV alpha particles, 26 MeV protons and low intensities of 156 MeV ^{6}Li ions. The cyclotron is, for the major part of its beam time, used by a large number of groups from other institutes of the research centre, from universities and several other institutes for research in a variety of fields. This report covers only that part of the work at the cyclotron in which staff of the Institute of Applied Nuclear Physics has participated. A separate report on the operation of the cyclotron and on its use outside the field of nuclear physics is available.

G. Schatz

(G. Schatz)

Das Institut für Angewandte Kernphysik des Kernforschungszentrums Karlsruhe beschäftigt sich mit Anwendungen der Kernphysik auf Probleme der Kernenergie, Festkörperphysik, Medizin und Analyse. Diese Untersuchungen werden durch grundlagen-physikalische Arbeiten begleitet. Der vorliegende Bericht gibt einen Überblick über die Arbeiten des Teilinstituts Kernphysik von Mitte 1975 bis Mitte 1976. Über die Tätigkeit des Teilinstituts Nukleare Festkörperphysik wird getrennt berichtet.

Die Messung von Wirkungsquerschnitten neutroneninduzierter Kernreaktionen stellt eines der Hauptarbeitsgebiete des Teilinstituts dar. Der größte Teil dieser Untersuchungen dient der Bereitstellung von Kerndaten,die für den Entwurf schneller Brutreaktoren benötigt werden. Dabei liegt das Schwergewicht z.Z. auf Wirkungsquerschnitten für Uran- und Transuran-Isotope. Andere Messungen von Neutronenwirkungsquerschnitten haben Daten zum Ziel, die für den astrophysikalischen s-Prozess von Bedeutung sind, der für die Erzeugung schwerer Elemente in Sternen verantwortlich gemacht wird.

Methoden der Gammaspektroskopie werden auf Probleme des Kernbrennstoffzyklus angewandt. Beispiele dafür sind die Bestimmung von Plutonium im radioaktiven Abfall und die Messung der Isotopen-Zusammensetzung von Kernbrennstoffen. Eine Methode zur Bestimmung der Anreicherung von ^{235}U im Brennstoff von Leichtwasser-Reaktoren wurde in einer Brennelement-Fabrik demonstriert und wird in der nahen Zukunft routinemäßig eingesetzt werden.

Die Entwicklung des intensiven Neutronengenerators KARIN hat ebenfalls das Stadium der praktischen Anwendung erreicht. Eine darauf basierende Anlage zur Neutronentherapie von Krebs wurde in enger Zusammenarbeit mit einem industriellen Lizenznehmer im Deutschen Krebsforschungszentrum in Heidelberg installiert.

Außer diesen angewandten Forschungsvorhaben wird eine Reihe von Experimenten auf dem Gebiete der Grundlagenkernphysik durchgeführt, die meisten davon in enger Zusammenarbeit mit Gastgruppen deutscher Universitäten. Eine enge Verbindung zwischen angewandter und grundlagenorientierter Forschung ist für das Institut charakteristisch und hat zu einem fruchtbaren Gedankenaustausch zwischen

beiden Gebieten geführt. Die meisten Grundlagenarbeiten nutzen das Isochronzyklotron Karlsruhe. Ein Experiment des letzten Jahres, das besonders erwähnt werden sollte, ist die Bestimmung der Neutronenverteilung in Blei-Kernen aus der elastischen Streuung hochenergetischer Alphateilchen.

Das Institut betreibt zwei Beschleuniger. Ein einstufiger Van-de-Graaff-Beschleuniger von 3 MV wird hauptsächlich für Neutronenflugzeit-Experimente und die Festkörperphysik benutzt. Das Isochronzyklotron Karlsruhe, ein Festfrequenzzyklotron, liefert Strahlen von 52 MeV-Deuteronen, 104 MeV-Alphateilchen, 26 MeV-Protonen und geringe Intensitäten an ^{6}Li-Ionen von 156 MeV. Das Zyklotron wird überwiegend von Gruppen aus anderen Instituten des Kernforschungszentrums und von Universitäten sowie anderen externen Forschungsinstituten für Arbeiten auf den verschiedensten Forschungsgebieten genutzt. In diesem Bericht wurden nur diejenigen der Arbeiten am Zyklotron aufgenommen, an denen Mitarbeiter des Instituts für Angewandte Kernphysik beteiligt waren. Ein getrennter Bericht über den Betrieb des Zyklotrons und seine Nutzung außerhalb der Kernphysik liegt vor und wird auf Anfrage gern zugesandt.

G. Schatz

(G. Schatz)

CONTENTS

		Page
1.	NEUTRON PHYSICS	1
1.1	FUNDAMENTAL RESEARCH	1
1.1.1	Precision Measurements of the Energies of Neutron Resonances in the MeV Range F. Voß, G. Schmalz	1
1.1.2	Elastic Neutron Scattering on ^{16}O and ^{28}Si I. Schouky, S.W. Cierjacks	3
1.1.3	Neutron Installations and Facilities S.W. Cierjacks	5
1.1.4	Study of keV-Resonances in the Total Cross Sections of ^{63}Cu and ^{65}Cu H. Beer, G. Rohr	6
1.1.5	A 4-Parameter Measurement of Kinetic Energies and Velocities of Correlated Fragments from Fission Induced by 550 keV Neutrons R. Müller, F. Käppeler, A. Naqvi, F. Gönnenwein, A. Ernst	6
1.1.6	Investigation of Mass and Energy Distributions and Neutron Yields of Fission Fragments from the ^{233}U (d,pf) Reaction S.W. Cierjacks, Y. Patin, J. Lachkar, J. Sigaud, C. Humeau, Y. Chardine	9
1.1.7	Intermediate Structure in the Capture to Fission Ratio of ^{235}U H. Beer, F. Käppeler	12
1.1.8	Valency Transitions in ^{56}Fe and $^{58,60}Ni$ H. Beer, F. Käppeler	14
1.1.9	The Energy Gap at the Saddle Point Deformation of ^{236}U F. Käppeler, F. Dickmann	15
1.1.10	Neutron Capture Cross Section Measurements of Noble Gas Isotopes Relevant to the Astrophysical S-Process F. Hensley	16

Page

1.2 NUCLEAR DATA 18

1.2.1 Measurements of Neutron Induced Fission Cross Section Ratios at the Karlsruhe Isochronous Cyclotron
S.W.Cierjacks,B. Leugers, K. Kari, P. Brotz, D. Erbe, D. Gröschel, G. Schmalz, F. Voß..... 18

1.2.2 The ^{235}U and ^{238}U Neutron Induced Fission Cross Sections Relative to the H(n,p) Cross Section
B. Leugers,S.W.Cierjacks, P. Brotz, D. Erbe, D. Gröschel, G. Schmalz, F. Voß 18

1.2.3 γ-Ray Production Cross Sections in Inelastic Neutron Scattering on ^{238}U
F. Voß 19

1.2.4 The Total Neutron Cross Section of ^{58}Fe in the Energy Range 7 to 325 keV
H. Beer, Ly Di Hong, F. Käppeler 21

1.2.5 A Method for the Measurement of the Capture Cross Sections of $^{241,243}Am$
F. Käppeler, K. Wisshak 22

1.2.6 A Measurement of the Neutron Capture Cross Section of $^{240,242}Pu$ in the Energy Range 10-100 keV
K. Wisshak, F. Käppeler 24

1.2.7 Measurement of Neutron Radiative Capture in ^{59}Co
R.R. Spencer, H. Beer 26

1.2.8 The Average Number of Prompt Neutron $\bar{\nu}_p$ from Neutron Induced Fission of ^{235}U Between 0.2 and 1.4 MeV
F. Käppeler, R.-E. Bandl..... 27

1.2.9 Measurements of the Neutron Fission Cross Section of ^{241}Am Via Fragment and Neutron Detection
W. Hage, H. Hettinger, S. Kumpf, F. Käppeler, K. Wisshak 27

1.2.10 The Fission Cross Section of ^{239}Pu Around 1 MeV
F. Käppeler 30

Page

2. NUCLEAR REACTIONS AND NUCLEAR SPECTROSCOPY..... 32

2.1 NUCLEAR REACTIONS 32

2.1.1 Measurement of the Vector Analysing Power in Elastic Deuteron-Proton and Deuteron-Deuteron Scattering at 52 MeV
M.S. Abdel-Wahab, V. Bechtold, L. Friedrich, J. Bialy, M. Junge, F.K. Schmidt 32

2.1.2 Investigation of the $\vec{d}+p \rightarrow p+p+n$ Break Up Reaction with Vector Polarized Deuterons of the Karlsruhe Isochronous Cyclotron
M.S. Abdel-Wahab, V. Bechtold, J. Bialy, L. Friedrich, M. Junge, F.K. Schmidt 34

2.1.3 How to Extract Isoscalar Transition Rates from Alpha Particle Scattering Experiments
H. Rebel 36

2.1.4 Differences Between Neutron and Proton Density RMS-Radii of ^{204,206,208}Pb Determined by 104 MeV α-Particle Scattering
H.J. Gils, H. Rebel 37

2.1.5 Experimental Studies of Neutron Collectivities by α-Particle Scattering and Some Implications for Giant Resonance Excitations
H.J. Gils, H. Rebel, W. Knüpfer 38

2.1.6 Nuclear Matter Distribution from Scattering of Strongly Interacting Projectiles
H. Rebel 38

2.1.7 Realistic Coulomb Potentials for Coupled Channel Calculations of α-Particle and ^{16}O Scattering
H. Rebel..... 39

2.1.8 Investigation of the Compound Nuclear Reactions $^{191+193}$Ir, ^{197}Au (^{6}Li,xn+yp) at E_{Li} = 48 - 156 MeV
J. Kropp, H. Klewe-Nebenius, J. Buschmann, H. Rebel, H. Faust, H.J. Gils, J. Rieder, K. Wisshak..... 39

2.1.9 Scattering of ^{6}Li on ^{12}C, ^{90}Zr and ^{208}Pb at E_{Li}=156 MeV
J. Buschmann, H.J. Gils, H. Rebel, H. Klewe-Nebenius, H. Faust, J. Kropp, W. Nowatzke, S. Zagromski..... 43

2.1.10 Study of Prolate-Oblate Effects by Use of Particle-γ Angular Correlations in the Reaction ^{24}Mg $(\alpha,\alpha_1)^{24}$Mg
W. Eyrich, A. Hofmann, U. Scheib, S. Schneider, F. Vogler, H. Rebel..... 47

Page

2.2 NUCLEAR SPECTROSCOPY 49

2.2.1 Experimental Studies of the Level Scheme of ^{143}Eu and a Generalized Decoupling Model Description
K. Wisshak, A. Hanser, H. Klewe-Nebenius, J. Buschmann, H. Rebel, H. Faust, H. Toki, A. Fäßler 49

2.2.2 Experimental Studies of the $4_1^+ \rightarrow 0^+$ Transition in ^{60}Ni by 104 MeV α-Particle Scattering and Conversion Electron Spectroscopy
H. Faust, K. Wisshak, H. Klewe-Nebenius, H. Rebel, H.J. Gils, A. Hanser 49

2.2.3 Level Structure of ^{149}Nd
J.A. Pinston, R. Roussille, H. Börner, H.R. Koch, D. Heck. 52

2.2.4 Rotational States in ^{151}Nd Populated Through Thermal Neutron Capture
J.A. Pinston, R. Roussille, H. Börner, W.F. Davidson, P. Jeuch, H.R. Koch, K. Schreckenbach, D. Heck 52

3. LASER SPECTROSCOPY 54

3.1 A Laser Spectrometer for Measurements of Nuclear Moments of Instable Isotopes
G. Nowicki, S. Göring, H. Rebel, G. Schatz 54

3.2 Method and Apparatus for Producing Atomic Beams of Neutron Deficient Radioactive Barium Isotopes for Laser Experiments
B. Feurer, A. Hanser 56

4. THEORY 58

4.1 Finite Velocities in the Dynamics of Nuclear Fission
E.F. Chaffin, F. Dickmann 58

4.2 Dependence of the Fission Mass Parameter on Pairing Strength, Shell Structure and Mass Asymmetry
E.F. Chaffin, F. Dickmann 60

4.3 Division of Energy Between Nuclear Collective and Internal Degrees of Freedom
E.F. Chaffin, F. Dickmann 64

Page

5. APPLIED NUCLEAR PHYSICS 68

5.1 NUCLEAR FUEL ANALYSIS 68

5.1.1 Gamma-Ray Spectrometry for In-Line Measurements of ^{235}U Enrichment in a Nuclear Fuel Fabricating Plant
P. Matussek, H. Ottmar 68

5.1.2 In-Process Control of ^{235}U Enrichment in a LWR Fuel Fabricating Plant
H. Ottmar, P. Matussek 68

5.1.3 Assay of Plutonium in Process Wastes from Fuel Fabrication Plants
M.R. Iyer, H. Ottmar 69

5.1.4 Plutonium Isotopic Analysis by High Resolution Gamma-Ray Spectrometry
H. Ottmar, M.R. Iyer 72

5.1.5 Gadolinium Concentration Measurements in Poisoned BWR Fuel Pellets by X-ray Fluorescence Analysis
P. Matussek, I. Michel-Piper, H. Ottmar, S. Heger 74

5.1.6 A Portal Monitor for the Detection of Fissile Materials
P. Matussek, I. Michel-Piper 77

5.2 ELEMENTAL ANALYSIS 80

5.2.1 Activation-Analysis of Manganese Nodules with 14 MeV Neutrons
H. Eberle 80

5.2.2 Investigation of Bulk Density Determination and Filling Level Indication in the MANKA Manganese Nodule Analysis System
H. Eberle 80

5.2.3 Trace Element Analysis by Proton Induced X-Ray Fluorescence
H. Sobiesiak, F. Käppeler 82

5.2.4 Suppression of Radioactive Background in Ion Induced X-Ray Analysis
H. Sobiesiak, D. Heck, F. Käppeler 84

Page

5.3 MEDICAL APPLICATIONS..... 85

5.3.1 Radioactive Purity of ^{125}Xe Samples for Medical Applications
W. Comper, S. Göring, A. Hanser..... 85

5.3.2 Recent Developments in the Production of ^{123}I at the Karlsruhe Isochronous Cyclotron
K.H. Assmus, F. Michel, H. Münzel, F. Schulz, R. Schütz, H. Schweickert..... 86

5.3.3 The High Power 14 MeV Neutron Generator Tube KARIN
K.A. Schmidt, H. Dohrmann..... 89

5.3.4 Installation of a Neutron Generator Tube for Cancer Therapy
K.A. Schmidt, H. Dohrmann..... 89

6. TECHNICAL DEVELOPMENTS..... 93

6.1 CYCLOTRON..... 93

6.1.1 Operation Summary of the Karlsruhe Isochronous Cyclotron
F. Schulz, H. Schweickert..... 93

6.1.2 Computer Controlled Beam Diagnostic at the Karlsruhe Isochronous Cyclotron
W. Kappel, W. Karbstein, W. Kneis, J. Möllenbeck, D. Hartwig, G. Schatz, H. Schweickert..... 96

6.1.3 Further Developments on the Computer Controlled Cyclotron Operation
W. Kappel, W. Karbstein, W. Kneis, J. Möllenbeck, H. Schweickert..... 97

6.1.4 New Computer Controlled Power Supplies for the Correction Coils of the Cyclotron
W. Kappel, G. Klinger, E. Schönstein.....100

6.1.5 Design of the New Correction Coils for the Cyclotron
V. Bechtold, L. Friedrich, Ch. Rämer, F. Schulz, L. Wiss.....101

6.1.6 Capacitive Current Measurement at the Internal Beam of the Cyclotron
G. Haushahn, K. Heidenreich, W. Maier, E. Röhrl.....103

Page

6.1.7 Status Report of the Axial Injection System at the Karlsruhe Isochronous Cyclotron
G. Haushahn, J. Möllenbeck, G. Schatz, F. Schulz, H. Schweickert.....104

6.1.8 Polarized Deuterons of a Lambshift Ion Source Accelerated by the Karlsruhe Isochronous Cyclotron
V. Bechtold, L. Friedrich, D. Finken, G. Strassner, P.Ziegler..105

6.2 VAN DE GRAAFF ACCELERATOR.....106

6.2.1 Operation of the Van de Graaff Accelerator
A. Ernst, D. Roller, H. Schreiber, J. Nadasdy.....106

6.2.2 Present Status of the Computer Based Van de Graaff Control and Supervisory System
A. Ernst.....107

6.2.3 Ion Optical Calculations of Focusing a 3 MeV Ion Beam to Micron Diameters
D. Heck.....108

6.2.4 Third Order Transfer Matrix Elementsof Octopoles
D. Heck.....110

6.3 ION SOURCES.....111

6.3.1 Penning Ion Source Improvements
J. Biber, H. Kuhn, F. Schulz.....111

6.3.2 Experimental Investigations of Charge Exchange Processes in Lambshift Sources with Argon and Krypton for Production of D^--Ions
V. Bechtold, L. Friedrich, G. Strassner.....112

6.3.3 LASCO, the Polarized Ion Source at the Cologne HV-FN7 Tandem Accelerator
V. Bechtold, L. Friedrich, P. Ziegler.....113

6.4 DETECTORS.....115

6.4.1 A Gas Scintillator Arrangement for Measurements of Fission Fragments at High α-Background
B. Leugers, K. Kari.....115

Page

6.4.2 A Spherical Avalanche Detector with Good α-Discrimination
M.A. Kazerouni, F. Käppeler.....116

6.4.3 Accurate Calibration of a 50 cm^3 Ge(Li) Detector in the Energy Range from 0.9 to 11 MeV
H. Beer.....118

6.5 COMPUTER DEVELOPMENT.....120

6.5.1 Configuration of the New Cyclotron Experimental Computer
G. Ehret, H. Hanak, W. Karbstein, B. Kögel.....120

6.5.2 An ADC Multiparametric System for Nova Computers
W. Karbstein.....122

6.5.3 A BASIC Data Acquisition and Analysis Program for the Experiment Computer NOVA 2 at the Van de Graaff Accelerator
K. Wisshak, H. Sobiesiak.....124

6.5.4 An Interactive Beam Transport Optimization Program with Graphic Facilities in BASIC
W. Kneis.....125

6.5.5 A Keyboard Input Handler for DGC FORTRAN IV on NOVA 2 Computers
H. Sobiesiak.....128

6.5.6 Supplementary Subroutines for the Coupled Channels Code ECIS-Karlsruhe
H.J. Gils.....129

6.5.7 Program IONBEAM
D. Heck, E. Kasseckert.....130

7. PUBLICATIONS AND CONFERENCE CONTRIBUTIONS.....133

8. PERSONNEL.....138

1. NEUTRON PHYSICS

1.1. FUNDAMENTAL RESEARCH

1.1.1 Precision Measurements of the Energies of Neutron Resonances in the MeV Range

F. Voß and G. Schmalz

With the aim of removing existing discrepancies in the neutron energy determination in different laboratories, the INDC has initiated activities to remeasure the energies of neutron resonances which can be recommended as calibration standards. To contribute to these efforts we have examined highly resolved total cross sections of some light nuclei for suitable resonances. The criteria were the following: (i) the resonances should be narrow, (ii) they should be isolated, (iii) they should be symmetrical, (iv) the cross section should be high, (v) the material should be easily available. Although not all conditions could be fulfilled, oxygen and magnesium proved to be suitable elements.

The total cross sections were measured at the 187 m flight path of the Karlsruhe fast neutron time-of-flight spectrometer with a channel width of 1 ns. The neutron energies were calculated from the flight path length L and the neutron time-of-flight t_n taking into account relativistic corrections. The relative error is given as in the nonrelativistic case by

$$\left(\frac{\Delta E_n}{E_n}\right)^2 = 4 \left[\left(\frac{\Delta L}{L}\right)^2 + \left(\frac{\Delta t_n}{t_n}\right)^2 \right]$$

The flight path length has recently been measured with an overall uncertainty of 1.5 mm. The accuracy of t_n is given by the precision with which the position of the prompt γ-peak (defining the zero of the time scale) and the position of the resonance maxima and minima can be determined. The position of the γ-peak is monitored during the measurement and is known to better than 0.5 channels. The precision determining the resonance peak (dip) position is limited by the width of the resonance and by the statistical uncertainty. In most cases an accuracy of less than one channel could be obtained without any fitting procedure.

The resonance energies are summarized in table 1 for oxygen and in table 2 for magnesium.

Table 1

Position of resonance maxima in the total cross section of oxygen (E_n in keV)

Present experiment	Cierjacks /1/	Johnson et al. /2/	Davis et al. /3/
1652.5 ± 0.35	1651 ± 1	1651 ± 2	
1835.4 ± 0.4	1833 ± 1	1833 ± 2	
3212.4 ± 0.6			
3441.3 ± 0.7			
3768.1 ± 1.2	3765 ± 4		3765 ± 3
5125.0 ± 1.9	5122 ± 4		5122 ± 4
5918.9 ± 2.4	5906 ± 7		5914 ± 5
6402.7 ± 3.6	6386 ± 8		6395 ± 7
7201.3 ± 3.2	7193 ± 9		7200 ± 8

Table 2

Position of resonance maxima (minima) in the total cross section of magnesium

E_n (keV)	ΔE_n (keV)	E_n (keV)	ΔE_n (keV)
1022.7	0.2	2262.6	1.5
1280.9	0.25	2821.9	1.5
1567.4 (min)	0.3	3044.7	0.9
1710.2	0.7	3870.9	1.8
1814.2	0.7	4228.9	1.4
2078.9	0.9	4864.3	1.8

The errors given in the tables can further be reduced to a few tenths of a channel by fitting the cross section curves around the resonance energies. If desired by the users an additional improvement could be achieved by measurements with the smallest channel width of our time analyser (0.25 ns). In this case an accuracy of 10^{-2} keV at 1 MeV, i.e. $\Delta E_n/E_n = 10^{-5}$ seems to be obtainable.

References

/1/ S. Cierjacks; Proc. of the 2nd Intern. Conf. on Nuclear Data for Reactors, Helsinki, June 15-19, 1970, Vol. II (IAEA, Vienna, 1970) 219

/2/ J.C. Davis, F.T. Noda; Nucl. Phys. A134 (1969) 361

/3/ C.H. Johnson et al.; Proc. Conf. on Neutron Cross Sections and Technology, Washington, D.C., March 1968 (NBS Spec. Publ. 299, 1968) 851

1.1.2 Elastic Neutron Scattering on ^{16}O and ^{28}Si

I. Schouky and S.W. Cierjacks

Experimental determination of the neutron resonance structure of light nuclei near doubly closed shells or subshells provide a good means to test the validity of the modern microscopic theories of nuclear reactions. For these nuclei a rather simple nuclear configuration is expected for nuclear excitations in the few MeV range, representing only a few quasiparticle states. In the range below A = 40 the nuclei ^{16}O and ^{28}Si are favourable candidates for neutron structure studies. Although investigated by various groups, the level structure of these nuclei was not yet well known (Si) or still uncompletely known (O). We, therefore, have performed new high resolution measurements of the differential elastic scattering cross sections in the range from 0.5 - 6 MeV and analyzed these data in connection with our previous results on high resolution total neutron cross sections. Such high resolution data provide a good opportunity for an unambiguous assignment of spins and parities. This possibility is based on the fact that the resonance shapes are very sensitive to spin and parity as a function of the scattering angle. The differences are most apparent at the angles where the Legendre polynomials of the corresponding partial waves cross the zero axis, i.e. the interference terms in the cross sections change sign.

In the energy range between 0.5 and 6 MeV where only a few partial waves contribute to neutron resonance scattering we have applied the a-few-angle method described elsewhere /1/ for spin and parity assignments. The combined analysis of high resolution total cross sections and a-few-angle differential elastic scattering cross sections provided accurate spin and parity assignments for 34 resonances in ^{17}O between 0.5 and 6 MeV and for 21 of the 35 ^{29}Si-resonances observed in the energy region from 0.5 - 2 MeV. In the latter case of silicon it is expected that the inclusion of all measured scattering angles, an analysis of which is underway, will provide further spin and parity assignments of not yet identified neutron resonances.

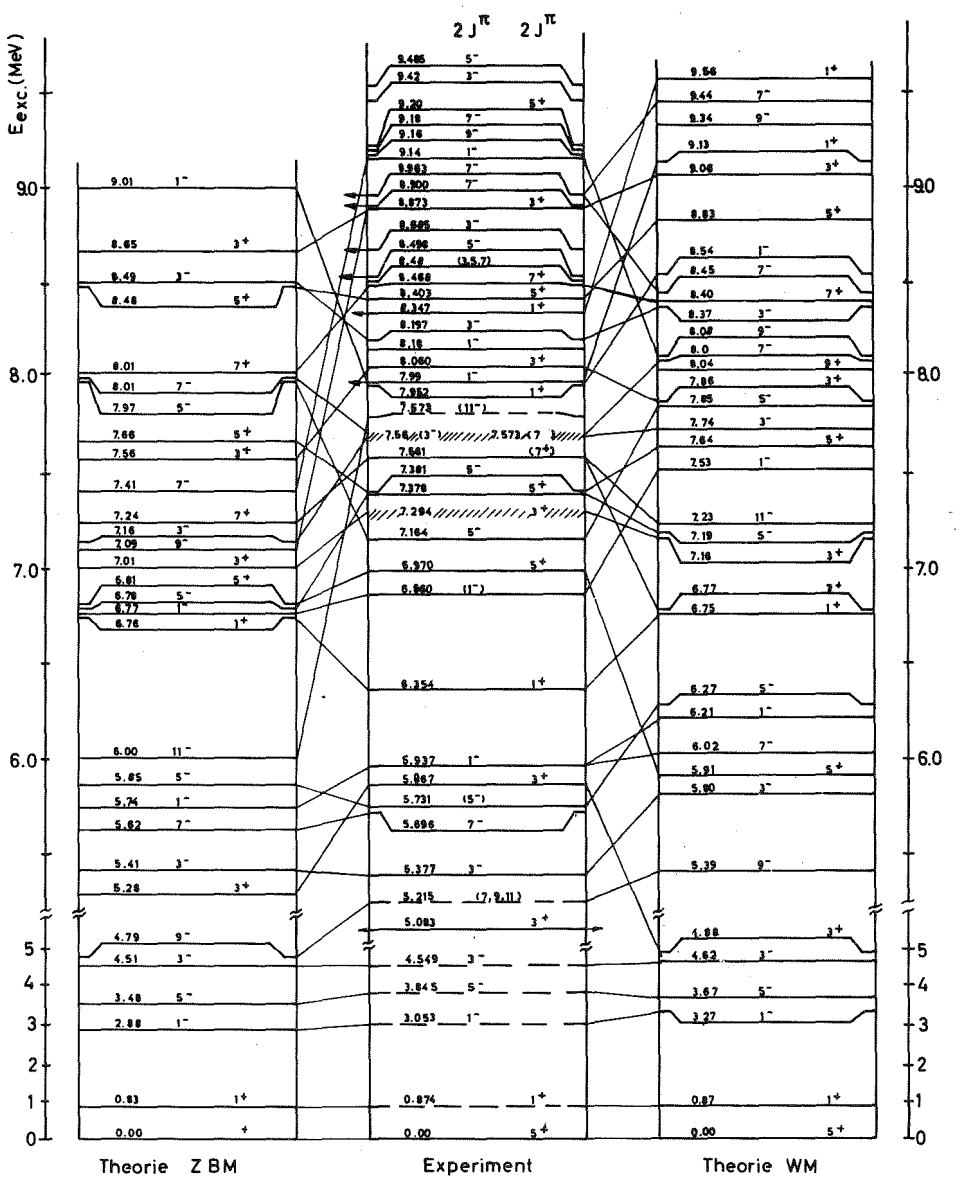

Fig. 1 Level scheme of ^{17}O. Comparison of the present experimental results with model calculations of Wildenthal and McGrory /2/ and Zucker et al . /3/. The data of the present analysis in the middle (solid line) are supplemented by the five known levels below neutron binding energy and two high spin levels not yet observed in neutron experiments (dotted lines). Equivalent levels in the measured and the calculated schemes are connected by solid lines.

The identification of the spin structure of ^{17}O for all measured neutron resonances has encouraged a comparison with recent theoretical predictions /2,3/ obtained from calculations in the generalized shell model. A comparison of present results with theory is shown in fig. 1. The experimental results are summarized in the central level scheme. In addition to levels assigned in our work (indicated by solid lines) this scheme contains the five known levels below the neutron binding energy and two high spin levels at 5.215 and 7.575 MeV observed in charged particle reactions only (indicated by the dotted lines). Corresponding levels in the measured and the predicted schemes are connected by solid lines.

Comparisons with calculations of Wildenthal and McGrory (WM) show an almost one-to-one correspondence indicating that the adopted multiparticle-multihole basis was realistic. If this is adopted the calculations show that most of the levels of this nucleus have a rather complicated multiparticle-multihole character except the ground and first excited states and the broad $d_{5/2}$ state at 5.083 MeV.

The model calculations of Zucker et al. (ZBM) are restricted to particle-hole excitations in the $1p_{1/2}$, $2s_{1/2}$ and the $1d_{5/2}$ orbits only and thus to excitations less complex than 5 p - 4 h states. This theory therefore provides less levels than those of Wildenthal and McGrory and cannot account likewise for all observed resonances.

References

/1/ G.J. Kirouac, J. Nebe; Nucl. Phys. A154 (1970) 36

/2/ B.H. Wildenthal, J.B. McGrory; Phys. Rev. C7 (1973) 714

/3/ A.P. Zucker, B. Buick, J.B. McGrory; Contr. Int. Conf. on Properties of Nuclear States, Montreal, 1969, p. 193

1.1.3 Neutron Installations and Facilities*

S.W. Cierjacks

A survey of the major accomplishments in the field of neutron facilities and installations during the past decade is presented. In particular the progress in developing accelerator-based pulsed neutron devices with a conti-

nuous energy spectrum are considered. The availability of these neutron facilities for all types of total and partial neutron interaction studies is demonstrated. Future implications for neutron research facilities are briefly summarized .

* Proceedings of the Int. Conf. on the Interactions of Neutrons with Nuclei, Lowell (Mass.), July 1976, to be published

1.1.4 Study of keV-Resonances in the Total Cross Sections of ^{63}Cu and ^{65}Cu*

H. Beer and G. Rohr+

Neutron total cross sections of ^{63}Cu and ^{65}Cu have been determined in the energy range 34 - 150 keV by means of transmission measurements. With an R-matrix shape fit analysis of the transmission data, s-wave and $\ell > 0$ wave resonance parameters were derived. The s-wave resonance parameters were used to calculate strength functions and to establish width and spacing distributions. A previously reported spin dependence of the strength function could not be confirmed. In the case of ^{63}Cu indications for intermediate structure were found.

* Z. Physik A277 (1976) 181; Int. Conf. on the Interactions of Neutrons with Nuclei, Lowell (Mass.) July 1976

+ Present address: CBNM-Euratom Geel (Belgium)

1.1.5 A 4-Parameter Measurement of Kinetic Energies and Velocities of Correlated Fragments from Fission Induced by 550 keV Neutrons

R. Müller+, F. Käppeler, A. Naqvi, F. Gönnenwein+, and A. Ernst++

The progress in the description of the fission process during the past years was mainly concentrated on the deformation of the nucleus from its ground state to the saddle point. This phase of fission proceeds rather slowly but from thereon the deformation changes so rapidly that the dynamical aspects play an important role. For an improvement of the theoretical description more experimental information on this phase of fission is necessary.

The scission point can be characterized by the properties of the fission fragments, like their mass distribution, as well as the distribution of kinetic energy and the number of fission neutrons, both as a function of fragment mass.

Up to now these quantities have been measured mainly for fission induced by thermal neutrons and for spontaneously fissioning isotopes. At higher excitation energies such experiments suffer from the available intensities. To improve this situation we have designed a double time-of-fligth experiment which allows the determination of energy and velocity of correlated fragments from neutron induced fission in the MeV range. The measurement was performed at the Karlsruhe 3 MV pulsed Van de Graaff accelerator which was operated with a repetition rate of 5 MHz, a pulse width of 500 psec, and an average proton current of 20 μA. The pulse pick-up signals were fed into an ultrafast sampling oscilloscope and the pulse shape was continuously analyzed by a computer. The computer was able to re-adjust the machine parameters so that the short pulse width could be maintained over long periods.

As a first isotope we investigated ^{235}U because for this isotope there exists already information at thermal energies. In addition the average number of fission neutrons shows distinct structure in the higher keV range, which indicates some influence of the saddle point on the scission configuration. Neutrons were produced via the ^{7}Li (p,n) reaction on a water cooled target very close to the fissile sample. The neutron spectrum was measured during the experiment by time-of-flight techniques; it was determined to lie within 550 $\pm$ 50 keV FWHM. The fission sample was an evaporated layer of 150 $\mu g/cm^2$ U_3O_8 on a 30 $\mu g/cm^2$ carbon foil. After a flight path of 860 mm the fission fragments were detected by 3 solid state detectors on each side of the sample. The fragment energy determination was achieved by calibrating the solid state detectors with Cf-sources. The fragment velocity was measured by the time of their arrival at the detector versus the pulse pick-up signal. Thus no time-zero detector was required. The zero point of the time scale was determined by a measurement with a short flight path of 90 mm.

In a first run about 20 000 events were collected, 4000 of which are analyzed up to now. These preliminary results are shown in fig. 1 as black points in comparison with results from Schmitt et al. /1/ which were measured

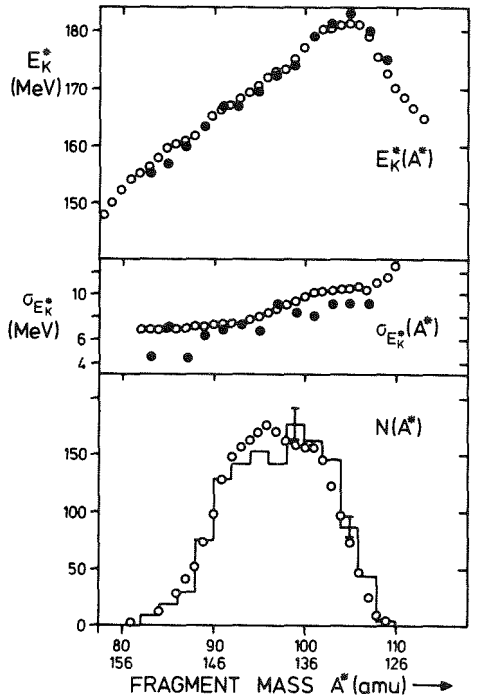

Fig. 1 Preliminary results in comparison to the data at thermal energies of Ref. /1/ (open points)

top: Total kinetic energy E_K^* before neutron evaporation

middle: Variance of the kinetic energy

bottom: Mass distribution before neutron evaporation

at thermal energies. The upper part shows the total kinetic energy E_K^* before neutron evaporation as a function of fragment mass. Both data sets agree within the uncertainties. The variance of the kinetic energy which is shown in the middle of fig. 1 seems to be systematically lower than the thermal values. At the bottom the fragment mass distribution before neutron evaporation is given. The histogram represents our results which agree well with the distribution of Schmitt except for the region at the top. There, our values seem to peak at higher fragment masses, but as the error bars indicate, these deviations are not very significant. The comparison might be more conclusive after all events are analyzed.

For the future work, this experiment has shown that a thinner ^{235}U layer is desirable because small angle scattering in the sample significantly disturbed the collinearity of the fragments.

+ Physikalisches Institut der Universität Tübingen
++ Van.de Graaff operating group

References

/1/ H.W. Schmitt, J.H. Neiler and F.J. Walter; Phys. Rev. 141 (1966) 1146

1.1.6 Investigation of Mass and Energy Distributions and Neutron Yields of Fission Fragments from the ^{233}U (d,pf) Reaction

S.W. Cierjacks, Y. Patin[+], J. Lachkar[+], J. Sigaud[+], C. Humeau[+], and Y. Chardine[+]

The study of dynamical aspects of the fission process, which include inertial and damping (or viscosity) effects, has received increasing attention in fission physics. Effects of this kind are of importance for a proper description of the fissioning system during the crossing of the fission barrier and in the descent from the saddle point to scission. Information about the nature and the influence of dynamical effects on the fission process can in principle be obtained from experimental studies of the variation of fragment masses, energies and neutron yields with excitation energy of the fissioning system. Experimental informations of this type are, however, rather scarce, due to intensity problems arising in the respective measurements.

In the described work a kinematically complete experiment was carried out at the Tandem accelerator of the Service de Physique Nucléaire of the Centre d'Etudes de Bruyères-le-Châtel employing the ^{233}U(d,pf)-reaction. In order to determine both pre- and post-neutron emission masses and energies a simultaneous measurement of the energies and the velocities of both fission fragments was performed. The excitation energy of the fissioning system was provided from an additional observation of the energies of protons emitted in the (d,pf)-reaction.

The experiment carried out in early 1975 and described elsewhere /1/ has partially been analyzed in the period covered by this report. In the analysis pre-neutron fragment masses and energies were calculated from the fragment velocities employing the non relativistic energy-velocity relation and the equation for momentum conservation. For an independent derivation of pre-neutron emission masses and energies it was necessary to replace the initial pre-neutron emission velocities of the fragments by the measured average final velocities. Such a treatment is reasonable, since neutron emission was shown to be in general symmetric about 90^{o} in the center of mass system of the fragments. The calculation of post-neutron emission quantities involved a modified version of the Schmitt-method /2/.

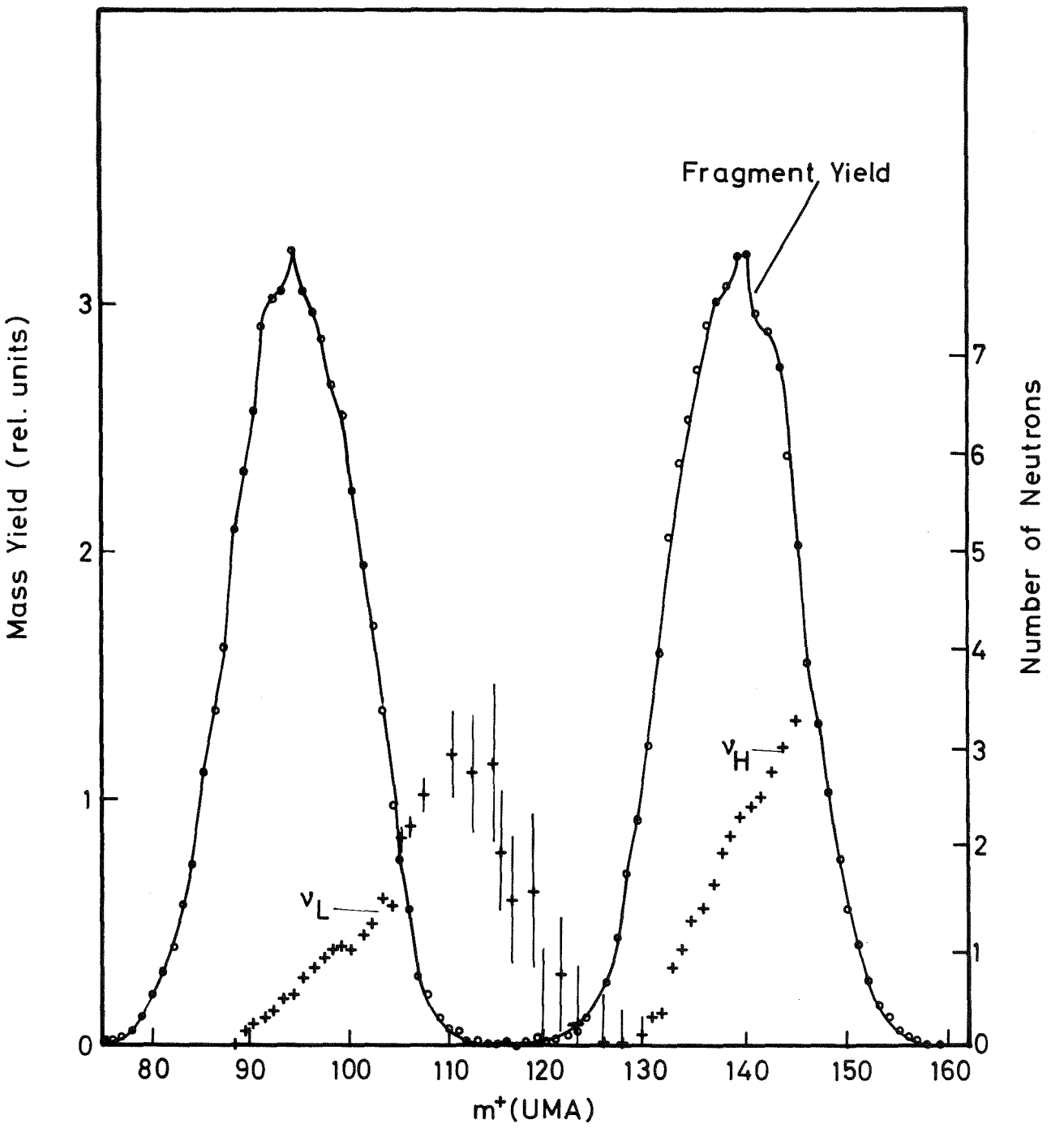

Fig. 1 Pre-neutron emission mass distribution of fission fragments and number of neutrons as a function of fragment mass obtained in ^{233}U (d,pf)-fission. The preliminary results are obtained from a small fraction of the totally accumulated 10^6 fission events and are consistent with average fragment masses of 95.0 and 139.2 for the light and the heavy fragment, respectively.

Together with the pre-neutron emission quantities, the post-neutron emission masses were used to derive the number of neutrons emitted as a function of fragment mass. In addition the variation of the total kinetic energy of both fission fragments with ^{234}U-excitation was determined by inclusion of the (d,p)-proton spectra. A first, preliminary result of the analysis is shown in fig. 1. In this diagram the pre-neutron emission mass yield for a small fraction of the totally accumulated 10^6 fission events is plotted on an arbitrary scale. The derived distribution is consistent with an average mass of 95.0 amu for the light fragment and of 139.2 amu for the heavy fragment in agreement with a result obtained by Unik /3/ from neutron induced fission. The second curve in the diagram represents the corresponding mass dependent neutron yield obtained from the same sample of analyzed events. The total number of neutrons emitted from both fragments is consistent with the average number of neutrons derived from (n,f)-measurements /3/.

+ Service de Physique Nucléaire, Centre d'Etudes de Bruyères-le-Châtel (France)

References

/1/ Y. Patin, S. Cierjacks, J. Lachkar, J. Sigaud, C. Humeau, J. Chardine; Centre d'Etudes de Bruyères-le-Châtel Report, CEAN-N 1875 (1976) Contributions B-III-4, B-III-5

/2/ J. Lachkar, J. Sigaud, Y. Patin, J. Chardine, C. Humeau ; Centre d'Etudes de Bruyères-le-Châtel Report, CEA-R 4715 (1975)

/3/ J.P. Unik, J.E. Gindler, L.E. Glendenin, K.F. Flynn, A. Gorski, R.K. Sjoblom ; Proc. of the Symp. on the Phys. and Chem. of Fission, Rochester 1973, Vol. II (IAEA, Vienna, 1973) p. 19

1.1.7 Intermediate Structure in the Capture to Fission Ratio of ^{235}U

H. Beer and F. Käppeler

The capture to fission ratio, α, of ^{235}U in the energy range 10 to 500 keV was measured at the Karlsruhe 3 MV pulsed Van de Graaff accelerator with a large liquid scintillator tank /1/. A time-of-flight experiment was designed to determine simultaneously absolute values of α with minor and relative values with high energy resolution (2 ns/m). The high resolution data allowed to search for intermediate structure in the capture to fission ratio caused by the fission cross section /2/. Intermediate structure should show up in the capture to fission ratio more pronounced than in the fission cross section itself as fluctuations from the entrance channel, i.e. from the neutron widths are eliminated and the capture widths are known to be independent of neutron energy. So far in reactor calculations the capture to fission ratio was assumed to be a smooth function of energy. Structure in α might therefore lead to substantial corrections of previous results.

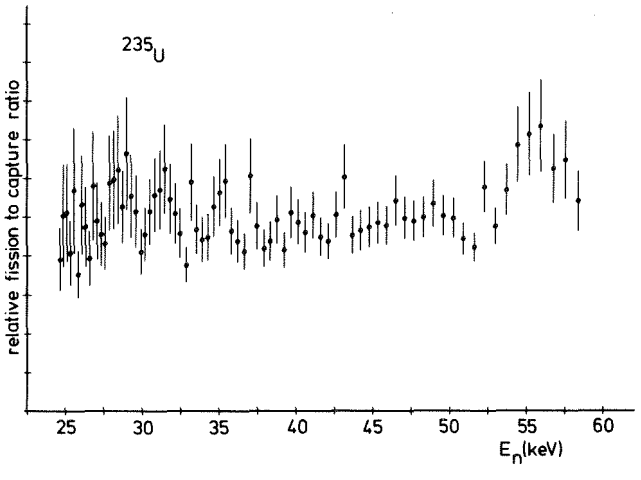

Fig. 1 Shape of the fission to capture ratio.

Fig. 1 shows the high resolution data in the energy range 25 to 60 keV. As the fission cross section is supposed to cause the fluctuations, the fission to capture ratio has been plotted. The structure is much larger - about a factor of 2 - than in the fission cross section itself. Several statistical tests applied to the data showed that the probability for a random origin of the fluctuations is less than 10^{-3}.

A mechanism known to lead to intermediate structure in fission is the enhancement of fission widths by states in the second well of a double-humped barrier. This model has successfully explained intermediate structure in subthreshold fission (see for instance ref. /3/). For intermediate structure originating from fission above the barrier as in our case no definite interpretation has been developed. The fission channel scheme for s-wave resonances of ^{235}U+n established by Lynn /4/ for the liquid drop model suggests partially open channels for some of the available transition states at the saddle point. Recently, a measurement of Keyworth et al. /5/ using a polarized ^{235}U target and a polarized neutron beam to separate the spin 3^- and 4^- contributions of the s-wave interaction showed that intermediate structure of ^{235}U fission is associated with a partially open spin 4^- channel. The important consequence of this result was the prediction of pronounced structure in the capture to fission ratio, just as it has been observed in the present measurement.

References

/1/ H. Beer, F. Käppeler; Report KFK 2223 (1975) p. 22

/2/ E. Migneco, P. Bosignore, G. Lazano, J.A. Wartena, H. Weigmann; Proc. Conf. on Nucl. Cross Sect. and Technology, Washington, D.C., March 1975 , ed. R.A. Schrack, C.A. Bowman, Vol. II (NBS Spec. Publ. 425, 1975)p. 607

/3/ H. Weigmann; Z. Physik 214 (1968) 7

/4/ J.E. Lynn; Proc. Conf. Nucl. Data for Reactors, Paris, Oct. 1966 Vol. II (IAEA, Vienna 1967) p. 89

/5/ G.A. Keyworth, M.S. Moore, J.D. Moses; Proc. of a NEANDC/NEACRP Specialists Meeting on Fast Neutron Fission Cross Sections of U-233, U-235, U-238 and Pu-239, Argonne, June 1976, to be published

1.1.8 Valency Transitions in ^{56}Fe and $^{58,60}Ni$

H. Beer and F. Käppeler

High energy transitions from neutron capture resonances in ^{56}Fe and in $^{58,60}Ni$ have been investigated by a time-of-flight experiment in the energy range 7-70 keV with a 50 cm^3 Ge(Li) detector using the Karlsruhe pulsed 3 MV Van de Graaff accelerator /1,2/. The Ge(Li) efficiency was measured in a separate experiment with calibrated sources and thermal capture γ-ray lines of known intensites /3/. The neutron flux was determined with a ^{235}U gas scintillation chamber /4/. The high energy transitions of s-wave resonances and their partial radiation widths $\Gamma_{\gamma p}$ are summarized in table 1.

Table 1. Partial radiation widths of s-wave resonances

	Resonance energy E_o (keV)	Energy of final state E_f (MeV)	Final state spin J_f^π	Tot. rad. width Γ_γ (eV)	$\Gamma_{\gamma p}$ (eV)		
					Experimental	Theoretical	
						Valency model /5/	Shell model approach /6/
^{56}Fe	27.7	0 0.014	$1/2^-$ $3/2^-$	1.4	0.145±0.023 0.035±0.013	0.20 0.17	0.49 0.42
^{58}Ni	15.4	0 0.471	$3/2^-$ $1/2^-$	2.1	0.124±0.017 0.110±0.019	0.47 0.21	0.90 0.40
^{60}Ni	12.5	0 0.283	$3/2^-$ $1/2^-$	3.4	0.514+0.072 0.289∓0.046	0.36 0.29	0.76 0.58

The experimental results have been compared with theoretical calculations assuming single particle capture which is expected to play a dominant role in the 3 s giant resonance mass region of the investigated nuclei. Table 1 gives theoretical estimates calculated with the valency capture model of Lynn /5/ and the shell model approach of Cugnon /6/. In spite of the simplicity of these models the an-order-of-magnitude agreement between theoretical and experimental values is remarkably good.

The determined partial radiation widths, associated with a single particle capture mechanism, contribute about 10-20 % to the total widths. One can assume that capture via compound nucleus formation amounts to about 0.55 eV in the mass region of the studied nuclei /7/. It is, therefore, apparent that compound nucleus formation and single particle capture are too small to account

for the entire total radiation widths. The residual sizeable contribution may be ascribed to another simple excitation mode like doorway state formation.

References

/1/ H. Beer, R.R. Spencer, F. Käppeler ; Proc. 2nd Int. Symp. on Neutron Capture γ-Ray Spectr. and Related Topics, Petten, Sept. 1974, (RCN Petten, the Netherlands 1975) p. 285

/2/ H. Beer, R.R. Spencer, F. Käppeler ; Proc. Conf. of Nucl. Cross Sections and Technology, Washington, March 1975, ed. R.A. Schrack, C.A. Bowman Vol. II (NBS Spec. Publ. 425, 1975) p. 816

/3/ Contribution 6.4.3

/4/ F. Käppeler; Neutr. Standard Ref. Data, Vienna, Nov. 1972, (IAEA, Vienna, 1974) p. 213

/5/ J.E. Lynn ; The Theory of Neutron Resonance Reactions (Clarendon Press, Oxford, 1968)

/6/ J. Cugnon; Nucl. Phys. A263 (1976) 61

/7/ S.F. Mughabghab; Phys. Lett. 35B (1971) 469

1.1.9 The Energy Gap at the Saddle Point Deformation of ^{236}U*

F. Käppeler and F. Dickmann

A steep increase in the fission cross section of ^{235}U at 0.95 MeV neutron energy was interpreted as due to the onset of quasi particle excitations in ^{236}U. Together with the result of a recent evaluation of the ^{236}U fission barrier an improved value of the energy gap at the saddle point deformation $2\Delta_s = 1.79 \pm 0.2$ MeV was determined. This value is discussed with respect to current assumptions on the deformation dependence of the pairing force parameter G.

* Proceedings of a NEANDC/NEACRP Specialists Meeting on Fast Neutron Fission Cross Sections of U-233, U-235, U-238 and Pu-239, Argonne, June 28-30, 1976, to be published.

1.1.10 Neutron Capture Cross Section Measurements of Noble Gas Isotopes Relevant to the Astrophysical S-Process

F. Hensley

The majority of the chemical elements with $A \gtrsim 56$ found in the universe are formed by nuclear reactions taking place in stars /1/. The most important mechanisms are the neutron capture in the r- and s-process. In the s-process, beginning from the nucleus ^{56}Fe, successive captures occur at a rate that is slow compared to the beta decay half-lives of the synthesized nuclei, so that the process follows the valley of stability. Low neutron fluxes that lead to capture rates of 10^{-5} - 10^{-3} per year and Maxwellian distributed energies ($\langle E_n \rangle \sim 30$ keV) satisfying this description are found in red giant stars, which are thought to be the site of the s-process.

In this model, the product $N_A \langle \sigma_A \rangle$ of the natural abundance of the isotope with mass A with its Maxwellian averaged neutron capture cross section provides a tool to deduce the chronology of the s-process material synthesis. The abundances entering this quantity are usually determined by measurements on certain types of meteorites which are assumed to represent the original isotopical composition formed in the star. Because of the volatility of the noble gases, their measured abundances bear great uncertainties so that for accurate values of $N_A \langle \sigma_A \rangle$ precise determinations of $\langle \sigma_A \rangle$ are necessary.

The Karlsruhe pulsed Van de Graaff accelerator will be used as a neutron source for the investigation of the capture cross section of the stable Krypton isotopes in the energy region 3 keV $\leq E_n \leq$ 100 keV. Krypton is of special interest as there exist two isotopes (^{80}Kr, ^{82}Kr) which are built up by the s-process only and thus allow a test of the validity of the $N_A \langle \sigma_A \rangle$ correlations. The branching of the s-process path at ^{79}Se due to the beta decay of this isotope with a half-life of 7×10^4 y together with $N_A \langle \sigma_A \rangle$ of the two pure s-process isotopes is generally used to determine the time between two neutron captures during nucleosynthesis. With the values of $\langle \sigma_A \rangle$ this time can be determined. Finally in the neutron capture cross section of ^{86}Kr one may expect effects such as intermediate structure due to neutron shell closure at N = 50.

For these measurements an apparatus was designed to produce liquid samples of inert gas allowing the investigation of one liter gas of separated isotopes at standard conditions. The gas is condensed into a sample chamber of

1.91 cm^3 volume. By continuously reducing the volume containing the isotope, the gas pressure can be kept above the vapour pressure of the liquid and so $\sim$90 % of the material can be liquified. The temperature in the cryostat is kept constant by a regulation circuit and determined independently by measuring the vapour pressure of the sample. With the knowledge of the density and the geometric size of the sample, one can determine the irradiated amount of material.

For the neutron capture measurements with the neutron time-of-flight method the prompt γ-rays will be detected with a C_6D_6 liquid scintillator using the Maier-Leibnitz pulse height weighting technique. The expected precision of $\sim$10 % is more than sufficient for astrophysical considerations.

References

/1/ E.M. Burbridge, G.R. Burbridge, W.A. Fowler and F. Hoyle; Rev. Mod. Phys. 29 (1957) 547

1.2 NUCLEAR DATA

1.2.1 Measurements of Neutron Induced Fission Cross Section Ratios at the Karlsruhe Isochronous Cyclotron*

S.W.Cierjacks, B. Leugers, K. Kari, P. Brotz, D. Erbe, D. Gröschel, G. Schmalz, and F. Voß

Ratios of the fission cross sections of ^{238}U and ^{239}Pu relative to ^{235}U were measured with the fast neutron time-of-flight facility at the Karlsruhe Isochronous Cyclotron. With the continuous energy neutron source the entire range from 0.5 - 30 MeV was covered in one experiment. In the experiments gas scintillation counting of the fission fragments and coincidence techniques were employed. Typical energy resolutions range between 0.7 % at 0.5 MeV and 3 % at 30 MeV. For the $^{238}U/^{235}U$ ratio most of the data have counting statistics smaller than 3 %, for the $^{239}Pu/^{235}U$ counting statistics does not exceed 1.5 %.

* Proc. of a NEANDC/NEACRP Specialists Meeting on Fast Neutron Fission Cross Sections of U-233, U-235, U-238 and Pu-239, Argonne, June 28-30, 1976, to be published

1.2.2 The ^{235}U and ^{238}U Neutron Induced Fission Cross Sections Relative to the H(n,p) Cross Section*

B. Leugers, S.W.Cierjacks, P. Brotz, D. Erbe, D. Gröschel, G. Schmalz, and F. Voß

The fission cross sections of ^{235}U and ^{238}U have been measured with the fast neutron time-of-flight facility at the Karlsruhe Isochronous Cyclotron in the range from 1-20 MeV. Fission events were detected with gas scintillation counters requiring coincidences from both fission fragments. The fast neutron flux was measured with a telescope like proton recoil detector. The transmission flux detector allowed a simultaneous measurement of the neutrons at the fission foil position. The fission cross sections have counting uncertainties of less than $\sim$3 % for most of the ^{235}U data points and of less than

$\sim$ 4 % for most of the ^{238}U data points.

*Proc. of a NEANDC/NEACRP Specialists Meeting on Fast Neutron Fission Cross-Sections of U-233, U-235, U-238 and Pu-239, Argonne, June 28-30, 1976, to be published

1.2.3 γ-Ray Production Cross Sections in Inelastic Neutron Scattering on ^{238}U

F. Voß

The inelastic scattering cross section of ^{238}U is one of the important quantities in calculating reactors, but it is still insufficiently known. Large discrepancies exist between measured microscopic data and the result of integral experiments. A quantitative description of spectrum measurements /1,2/ requires significantly smaller inelastic scattering cross sections than those recommended in the evaluated data files KEDAK 3 and ENDF/B-IV. In order to contribute to the solution of this problem we investigated the deexcitation γ-rays of ^{238}U following inelastic neutron scattering.

The principle of the experimental set-up at the Karlsruhe fast neutron time-of-flight spectrometer has been described elsewhere /3/. A ring shaped scattering sample of natural uranium having an inner diameter of 12 cm, an outer diameter of 24 cm,and a thickness of 0.97 mm was placed at a flight path of 57.894 m. The γ-rays were detected in a 42 cm^3 Ge(Li) detector at an average angle of 125°. The neutron flux was measured with NE 102 plastic scintillation counter.

The two associated signals (time-of-flight, pulse height) of the Ge(Li)-detector were digitized in a LABEN TIME-SORTER UC/KB and a fast ADC, respectively, and processed in a CDC 3100 on-line computer. Time-of-flight spectra were accumulated for the photopeaks of interest and for suitably chosen regions in the Compton background.

The counting rates were corrected off-line for Compton background and for time dependent and time independent background peaks. From the corrected photopeak areas and the neutron flux the γ-ray production cross sections were calculated. These were corrected for γ-ray self absorption in the sample (12 - 22 %), flux attenuation (1.5 %),and multiple scattering (3 - 20 %). The

last correction was determined with a Monte-Carlo program /3/ which had been modified to include fission neutrons.

Because of the high background from the radioactive decay of uranium and its daughters the time-of-flight spectra had to be averaged over 100 channels to get a reasonable statistical accuracy. Excitation functions for the following levels and γ-ray energies have been obtained:

E_x	E_γ
680 keV	635 keV
731 keV	584 keV
927+931 keV	882+886 keV
997 keV	952 keV
1060 keV	1015 keV
1061 keV	1061 keV

As an example the cross section for E_γ = 635 keV is given in fig. 1. The error bars include statistical accuracy and uncertainties in multiple scattering corrections and in background subtraction. The systematic errors

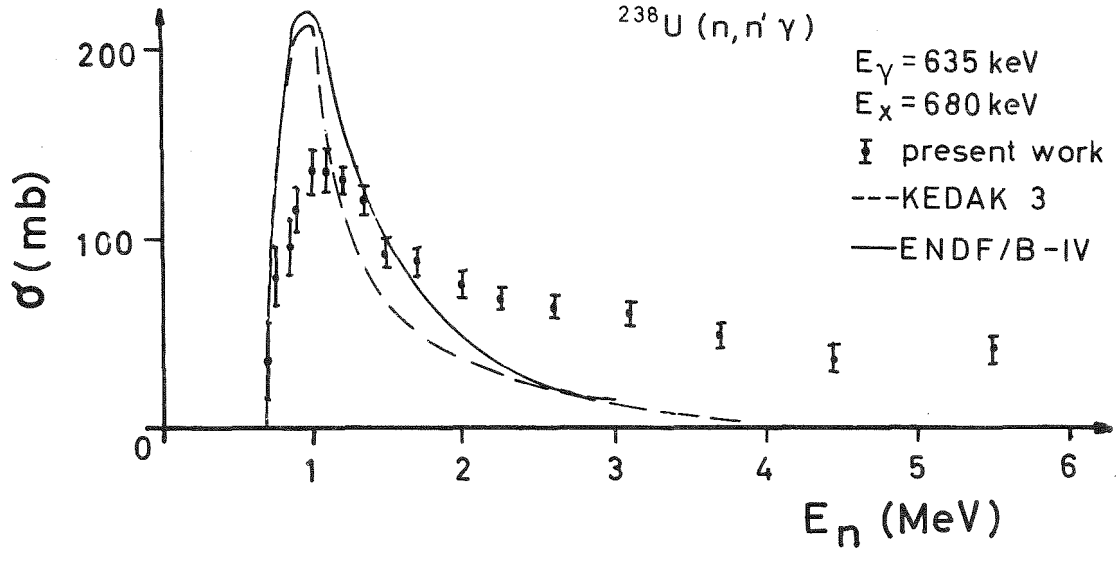

Fig. 1 $\sigma_{n,n'\gamma}$ of ^{238}U for E_γ = 635 keV. Comparison of measured cross sections with values from the evaluated data files KEDAK 3 and ENDF/B-IV.

from the flux measurement and the Ge(Li) detector efficiency are estimated to be less than 11 %. For comparison the γ-ray production cross sections calculated from the KEDAK 3 and ENDF/B-IV inelastic scattering cross sections and the known branching ratios /4/ are also shown in fig. 1. The discrepancies above approximately 1.5 MeV could qualitatively be accounted for by the feeding from higher levels. However, at low energies the measured cross sections are up to 30 % lower than the evaluated data. This discrepancy is greater than the experimental errors even when allowing 10 % error in the branching ratio. A similar situation is found for the other five excitation functions. These results would confirm the conclusions from spectrum measurements that in the energy range from 1 to 3 MeV the inelastic scattering cross sections should be reduced by 20-30 %.

References

/1/ H. Bluhm; Report KFK 1798 (1973)
/2/ R.P. Corcuera; Nucl. Sci. Eng. 58 (1975) 278
/3/ F. Voß; Report KFK 1611 (1972); Thesis Universität Karlsruhe (1972)
/4/ W.R. McMurray, I.J. van Heerden; Z. Physik 253 (1972) 289

1.2.4 The Total Neutron Cross Section of ^{58}Fe in the Energy Range 7 to 325 keV*

H. Beer, Ly Di Hong+, and F. Käppeler

The total neutron cross section of ^{58}Fe has been determined in the energy range 7-325 keV by a transmission measurement using enriched ^{58}Fe samples. The data have been shape fitted by means of an R-matrix multi-level formalism to extract resonance parameters for s- and $\ell > 0$ wave resonances. The s-wave strength function was determined to $S_o = (4.3 \pm 1.9) \times 10^{-4}$.

*Report KFK 2337 (1976)

+Universität Heidelberg

1.2.5 A Method for the Measurement of the Capture Cross Sections of ^{241,243}Am

F. Käppeler and K. Wisshak

During the high burn-up in advanced reactors and by successive recycling of the fuel elements the amount of higher Pu- and transplutonium-isotopes grows to a considerable fraction of the fuel investment. Their high neutron emission rate due to spontaneous fission and (α,n) reactions makes the handling of these isotopes difficult and their inconvenient half-lives of about 10^3 y cause problems with respect to nuclear waste management. For a more quantitative understanding of the build-up of these isotopes an improvement of the basic neutron cross sections is necessary. Up to now, very few experimental information about the respective capture cross sections is available above 10 keV neutron energy.

Capture cross section measurements of transuranium isotopes are difficult because of the high γ-background from natural decay. Although most of the associated γ-radiation has low energies below 100 keV a 3 g sample of ^{241}Am, for example, shows also high energy γ-rays around 650, 350 and 200 keV with intensities of 3 to 6 x 10^6 sec^{-1}. In the case of ^{243}Am the situation is even worse because the decay of the short lived daughter ^{239}Np feeds to more than 80 % levels between 220 and 400 keV in ^{238}Pu. This means that a 3 g sample of ^{243}Am emits about 10^{10} γ-rays/sec with energies between 200 and 350 keV.

As a consequence of this high γ-ray background a high neutron flux must be available at the position of the capture sample, in order to optimize the signal-to-background ratio. Such high neutron fluxes can be obtained for example at10 to 15 cm distance from the target of a Van de Graaff accelerator. With the fast pulsing systems and fast γ-detectors a sufficient neutron energy resolution can be achieved in this geometry below 100 keV.
The following contribution /1/ gives details of such an experiment.
Because of the short neutron flight path only relatively small γ-detectors can be used. We preferred a conventional Moxon-Rae detector rather than a total energy detector because of its low efficiency for the soft γ-component of the radioactive decay. Under the experimental conditions given below it should be possible to measure the capture cross section of ^{241}Am even with an oxide sample. In this case it is assumed that the backgrounds from (α,n) re-

actions in the ^{241}Am sample and from spontaneous fission of ^{240}Pu are of comparable influence.

The extremely high background from the decay of ^{243}Am and its daughter, however, requires an additional shielding of the γ-ray detector. In fig. 1 the most intense γ-rays from a 3 g ^{243}Am sample above 220 keV are shown as dotted lines. After shielding the sample by 2 cm lead, the intensity is reduced (the factor is given by the solid curve) to values indicated with bars.

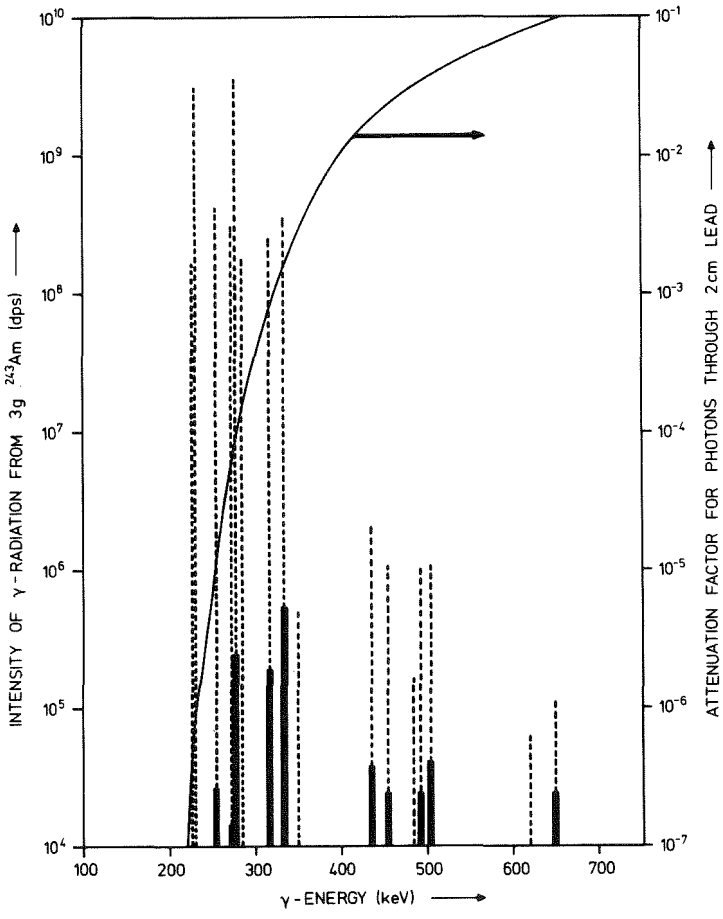

Fig. 1 The dotted lines represent the intensities of γ-ray transitions from the decay of 3 g ^{243}Am. The solid curve gives the attenuation factor of 2 cm lead (right scale). The black bars indicate the respective γ-ray intensities shielded by 2 cm lead.

This residual background can be discriminated by the experiment. Of course, the lead thickness of 2 cm is an extreme value, which can be reduced as long as the background can be handled. One could expect that such a heavy shielding affects the properties of the Moxon-Rae detector. Therefore it has to be shown, that the efficiency per MeV of incident γ-rays remains more or less independent of γ-ray energy. Fortunately the transmission coefficient of lead has the proper energy dependence to keep the detector working. Fig. 2 gives the efficiency per MeV of a common, unshielded Moxon-Rae detector

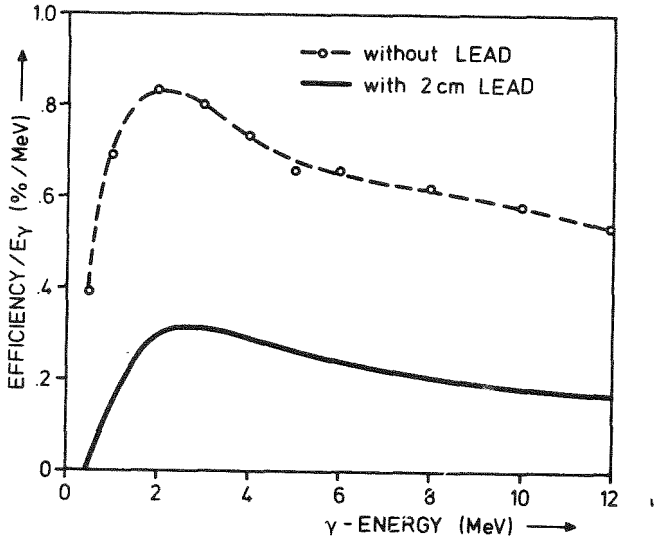

Fig. 2 The upper curve gives the efficiency per MeV of incident γ-ray of a common Moxon-Rae detector (ref./2/). The curve below demonstrates the efficiency per MeV with a shielding of 2 cm lead. The shape is even smoother with γ-energy while the efficiencyis reduced by a factor of 2.5.

with a 2.58 cm thick graphite converter as it was calculated by Iyengar et al. /2/. It can be seen that the additional shielding by 2 cm lead makes the detector response even more independent from γ-energy without a too large reduction of the efficiency.
From the above considerations the direct measurement of the capture cross sections of both important Am isotopes can be performed with our existing technique.

References

/1/ Contribution 1.2.6

/2/ K.V.K. Iyengar, B. Lal, M.L. Jhingan; Nucl. Instr. Meth. 121 (1974)33

1.2.6 A Measurement of the Neutron Capture Cross Section of ^{240,242}Pu in the Energy Range 10 - 100 keV

K. Wisshak and F. Käppeler

Measurements of the neutron capture cross sections of Plutonium isotopes are recommended with high priority in the World Request List of Nuclear Data (WRENDA). These cross sections are necessary to calculate neutron flux and criticality in fast reactors and to estimate the build-up of actinides with higher Z-values during the burn-up cycle.

The essential part of the experimental setup is shown in the schematic drawing of fig. 1. Neutrons were produced via the $^{7}Li(p,n)^{7}Be$ reaction with the pulsed proton beam (2.5 MHz frequency, 600 psec pulse width and 10-15 μA intensity) of the Karlsruhe Van de Graaff accelerator.

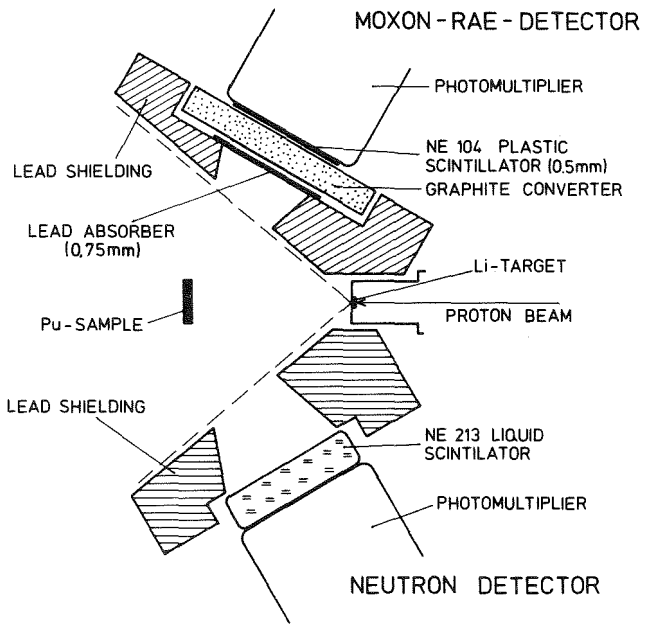

Fig. 1 The experimental arrangement of the capture cross section measurement of ^{240}Pu.

The proton energy has been adjusted 10 and 20 keV above the reaction threshold. Using a thick lithium target a kinematically collimated neutron flux was produced with an opening angle of 30^{o} and 45^{o} and an energy spectrum of E_n = 10-70 keV and E_n = 5-90 keV, respectively. The neutron energies were determined by time-of-flight. The flight paths used were 13 and 6.5 cm giving an energy resolution of ± 10 %.

The plutonium samples (3 g $^{240}PuO_2$ enriched to 98.3 % and 8 g $^{242}PuO_2$ enriched to 77 %) were canned in 0.1 mm thick stainless steel and in 0.3 mm thick PVC foils. The capture γ-rays were detected in a Moxon-Rae detector shielded by 0.75 mm of lead against the low energy γ-rays of the Pu-samples. To reduce systematic errors, the capture cross sections of the Pu-isotopes were measured relative to the well known cross sections of ^{197}Au and ^{238}U. To take into account that the Moxon-Rae detector is sensitive to fission γ-rays, too, we used a neutron detector (NE 213 with pulse shape discrimination) to measure fission events simultaneously. The correlation between fission γ-ray and fission neutron spectra was determined with a ^{235}U sample. To correct for capture events from scattered neutrons a graphite sample was used.

The four samples (Pu, reference, ^{235}U, graphite) were mounted on a sample changer, which was controlled by a beam current integrator. For each sample individual time-of-flight and analog spectra of the two detectors were recorded. A time-of-flight spectrum of the ^{240}Pu sample measured with the Moxon-Rae detector is shown in fig. 2. In this spectrum, the time independent background due to the γ-radiation of the sample etc. and the time

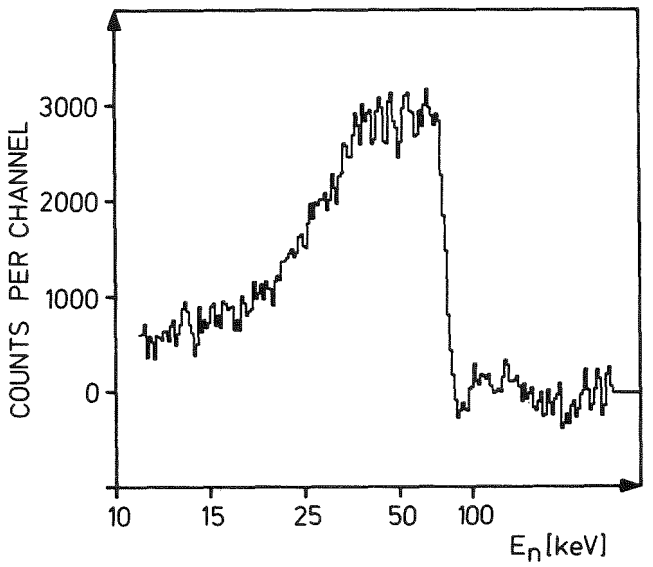

Fig. 2 Time-of-flight spectrum of capture events from the ^{240}Pu sample after background correction .

dependent background caused by the stainless steel canning, sample holder, etc. have been subtracted. From the shape of the γ-peak an overall time resolution of 1.5 nsec FWHM was found. The data analysis is still in progress; we hope to determine the capture cross section of the Pu-isotopes with an uncertainty of about 10 %.

1.2.7 Measurement of Neutron Radiative Capture in ^{59}Co*

R.R. Spencer[+] and H. Beer

The neutron capture cross section of ^{59}Co has been measured in the energy range from 6 to 200 keV using an 800 ℓ liquid scintillator detector in conjunction with a pulsed 3 MV Van de Graaff accelerator as a neutron source. The excellent time resolution of the system (2.8 nsec FWHM) permitted derivation of radiation widths for single s-wave resonances to 50 keV neutron energy. Average radiation widths of 0.564 ± 0.024 eV and 0.486 ± 0.016 eV were found for seven J = 3 resonances and ten J = 4 resonances, respectively. No significant correlation between Γ_n^o and Γ_γ was

found for either spin state. The Maxwellian-averaged cross section for kT = 30 keV was found to be 38 mb over the region from 0.0253 eV to 200 keV neutron energy.

* Nuclear Science and Engineering 60 (1976) 390

+ Present address: Oak Ridge National Laboratory, Oak Ridge, Tennessee 37830 (USA)

1.2.8 The Average Number of Prompt Neutrons $\bar{\nu}_p$ from Neutron Induced Fission of ^{235}U Between 0.2 and 1.4 MeV*

F. Käppeler and R.-E. Bandl+

For the clarification of existing discrepancies in the energy dependence of $\bar{\nu}_p$ for ^{235}U an experiment was performed which was based on a method independent of current techniques. A considerable reduction of background and correction problems was achieved by renouncing on an absolute measurement. Thus the resulting systematic uncertainty was 0.6 %. In the energy range between 0.2 and 1.4 MeV the shape of $\bar{\nu}_p$ was measured at 22 points in steps of 50 keV with an average energy resolution of 3.3 %. Repetition of several runs with modified experimental conditions ensured the consistent reproduction of the results. It was found that $\bar{\nu}_p$ of ^{235}U shows distinct deviations of up to 2 % from a linear energy dependence.

* Annals of Nuclear Energy 3 (1976) 31

+ Present address: BBC, Postfach 351, 68 Mannheim

1.2.9 Measurements of the Neutron Fission Cross Section of ^{241}Am Via Fragment and Neutron Detection

W. Hage+, H. Hettinger+, S. Kumpf+, F. Käppeler, and K. Wisshak

The build-up of the hazardous transplutonium isotopes in power reactors is determined by the respective neutron capture and fission cross sections. In many cases the accuracy of the available experimental data is not sufficient for a detailed description of the build-up process. The measurement of relevant capture cross sections has already been discussed in this report/1/.

Fission cross section measurements of these isotopes are also difficult because of the high α-background from natural decay. Especially ^{241}Am shows a very high α-rate of more than 10^{8} mg^{-1} sec^{-1}. Below the threshold at about 800 keV, the fission cross section of ^{241}Am shows a small sub-threshold component of less than about 50 mb below 200 keV. Above threshold values of 1 to 2 b are reported. As we intended to cover the neutron energy range from 10 to 1200 keV it seemed reasonable to use different techniques because the cross sections are too different at the lower and upper end of the energy range.

a: Neutron detection

At present we are running the cross section measurement in the low energy region via the detection of fission neutrons. As it is difficult to use absolutely calibrated liquid scintillation detectors we are determining σ_f of ^{241}Am relative to the fission cross section of ^{235}U. In this case one can get the cross section ratio by correcting for the different fission neutron energy spectra; if this procedure implies too large uncertainties, this method allows at least a measurement of the energy dependence of the cross section ratio.

The measurement is performed at the pulsed 3 MV Van de Graaff accelerator with a short flight path of a few cm between neutron target and fissile samples. The distance between the samples and the neutron detector is about 20 cm. The samples are mounted on a 4 position sample changer. We are using a pellet of 3 g ^{241}Am oxide with some aluminium as a binder and canned into 0.2mm stainless steel, a dummy sample with depleted uranium instead of Am, an empty position for background determination and a 7 g sample of ^{235}U. Fig. 1 shows the measured time-of-flight spectra of the ^{241}Am and the ^{235}U samplesat a neutron energy of 220 ± 20 keV. While the ^{235}U spectrum is almost free of background, the ^{241}Am spectrum contains a considerable amount of time independent background which is caused by neutrons from (α,n) reactions with ^{18}O and Al. The time resolution is sufficient for a clear separation of time correlated γ-radiation so that the fission neutron distributions are well isolated and the background subtraction can be performed without problems. The cross section measurement via neutron detection can be extended up to about 1 MeV. The fission neutron distribution in the TOF-spectra is too broad for a separation of the 2^{nd} neutron group of the $^{7}Li(p,n)$ reaction, so that this contribution has to be corrected for above 650 keV.

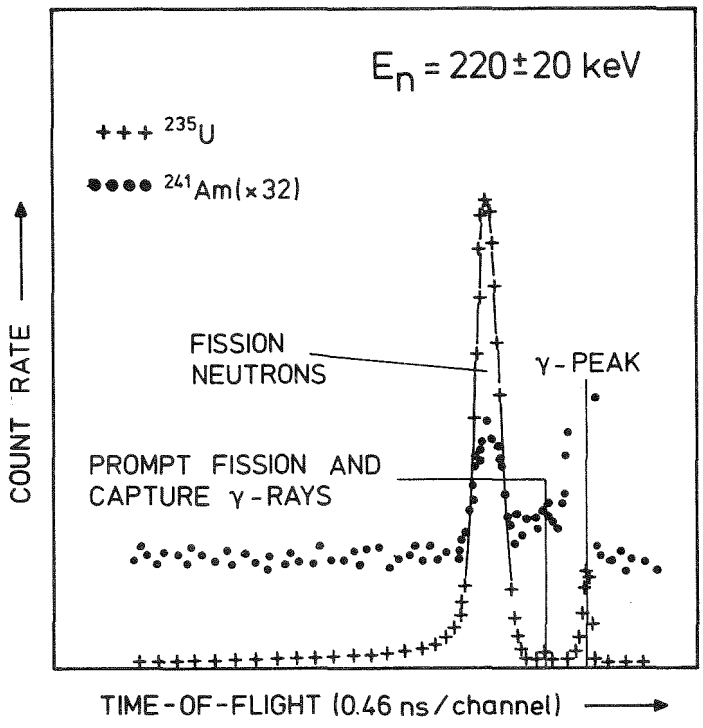

Fig. 1 Time-of-flight spectra from the fission cross section measurement of ^{241}Am relative to ^{235}U via the fission neutrons. The time independent background in the ^{241}Am spectrum stems from (α,n) reactions.

b: Fragment detection

The more common technique for fission cross section measurements is based on the detection of fission fragments. This technique requires less corrections and allows a better accuracy. We are preparing an experiment with a gas scintillation counter which yields a good time resolution and thus a good signal to background ratio in time-of-flight measurements with monoenergetic neutrons. Again the ^{241}Am fission cross section will be measured relative to the fission cross section of ^{235}U. Up to now there are still problems with the high α-background of the Am sample. In order to discriminate it, a He-N-mixture is used as a counter gas in which the ranges of α-particles are considerably larger than the counter dimensions cutting off that part of their range where the specific ionization is high. This improves the α-discrimination by pulse height by a factor of about 2-3. Further α-suppression is achieved by a coincidence between both fragments of a fission event. Aluminium was found to be a suitable backing foil which can withstand the high α-dose sufficiently long /2/. As the fragment absorption losses in the backing foil (about 20 % in 4 π measurements) make an accurate determination of the detector efficiency difficult, we are intending to use the "threshold cross section method" suggested by Behrens and Carlson/3/ for the determination of the cross section ratio. The measurements with this technique will start late in 1976 and will cover the neutron energy range from about 500 to 1200 keV.

+ Euratom, Ispra (Italy)

References

/1/ Contributions 1.2.5 and 1.2.6

/2/ J.v. Audenhove and J. Pauwels; Euratom Geel (Belgium), private communication (1976)

/3/ J.W. Behrens, G.W. Carlson; Proc. of a NEANDC/NEACRP Specialists Meeting on Fast Neutron Fission Cross-Sections of U-233, U-235, U-238 and Pu-239, Argonne, June 28-30, 1976, to be published

1.2.10 The Fission Cross Section of ^{239}Pu Around 1 MeV

F. Käppeler

Contrary to ^{235}U only a few absolute measurements of the ^{239}Pu fission cross section exist in the fast neutron energy range. The importance of this cross section for fast breeder reactors was the reason for this new measurement. It was felt that additional information might be useful as cross check to those fission cross section values of ^{239}Pu which are calculated from the cross section ratios and the fission cross section of ^{235}U.

The experimental arrangement is given in fig. 1. Neutrons are produced by the pulsed 3 MV Van de Graff accelerator (pulse width 1 nsec, repetition rate 5 MHz, average current 20 μA) via the ^{7}Li(p,n) reaction. A collimator shields all heavier parts of the detectors against the neutron flux in order to avoid corrections due to scattered neutrons. The neutron energy spectrum (determined by the ^{7}Li-target thickness) is measured by a ^{6}Li-glass detector at a flight path of 134.5 cm. The second neutron group of the ^{7}Li(p,n) reaction is discriminated by time-of-flight in the fission detector and by pulse height in the proton-recoil telescope detector for flux determination. This neutron flux detector is the same as described earlier /1/. The fission detector is a gas scintillation chamber operated with a mixture of 85 % Argon and 15 % Nitrogen. As is indicated in fig. 1 a thin sample backing allows the detection of both fission fragments. This is necessary to suppress the α-background from the ^{239}Pu decay. However, as one fragment always has to penetrate the backing foil, the respective energy loss - especially at large angles with respect to the neutron direction - might cause the scintillation

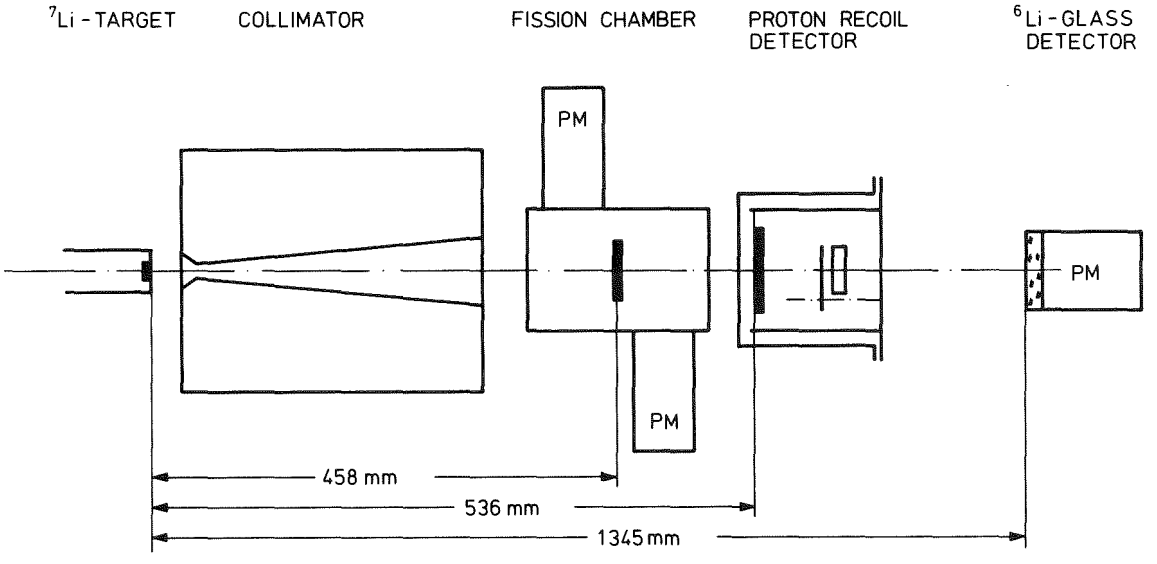

Fig. 1 Experimental set-up for the fission cross section measurement of ^{238}Pu around 1 MeV neutron energy.

pulses to fall below the electronic threshold. This fraction of lost fission events is difficult to determine. To avoid too large uncertainties a method for the direct measurement of the detector efficiency was applied: Trace amounts of ^{252}Cf were added to the solution from which the sample was electrosprayed. This spontaneously fissioning component was determined by low geometry counting which can be done without background problems. Then the count rate measured under the experimental conditions immediately allows to calculate the detector efficiency. For a sample of 70 µg/cm^2 Pu on a VYNS-backing of about 80 µg/cm^2 the efficiency was found to be 90 $\pm$ 2.5 %. An overall uncertainty of about 4 % is estimated for the final results.

References

/1/ F. Käppeler; 2nd IAEA Panel on Neutron Standards Reference Data, Vienna, Nov. 1972 (IAEA, Vienna, 1974) p. 75

2. NUCLEAR REACTIONS AND NUCLEAR SPECTROSCOPY

2.1 NUCLEAR REACTIONS

2.1.1 Measurement of the Vector Analysing Power in Elastic Deuteron-Proton and Deuteron-Deuteron Scattering at 52 MeV

M.S. Abdel-Wahab[+], V. Bechtold, L. Friedrich, J. Biały[+], M. Junge[+], and F.K. Schmidt[+]

In the frame of experimental investigations of few nucleon reactions and for preparation of break-up experiments the vector analysing power in elastic d-p- and d-d-scattering has been measured. These measurements were carried out at the Karlsruhe isochronous cyclotron with the vector polarized deuteron beam of 52 MeV.

In fig. 1 the measured vector analysing power of the elastic d-d-scattering at 52 MeV is given as a function of the center of mass angle. In consequence of identity of projectile and target particle the curve has to be antisymmetric around $\theta_{cm} = 90^{o}$. A significant maximum of $i\,T_{11} = 0.32$ at an angle of $\theta_{cm}=65^{o}$ has been found. Comparing this results with earlier measurements from Berkeley at 40 MeV there is nearly the same shape and maximum in the analysing power. Hence the reported increase of the maximum analysing power with increasing energy discontinues above this energy region.

The measured vector analysing power of the elastic d-p-scattering at 52 MeV is shown in fig. 2. There is a maximum of the analysing power $i\,T_{11} = 0.25$ at $\theta_{cm} = 135^{o}$ and a minimum of $i\,T_{11} = 0.11$ at $\theta_{cm} = 114^{o}$. The curve is very similar compared with the Berkeley data, except of the minimum, which is deeper in the data of this work. In fig. 3 this energy dependence of the vector analysing power is demonstrated in a contour plot using data of this work and data of several other experiments. Fig. 3 shows the well known fact that substantial values of the vector analysing power are observed only above energies higher than 20 MeV. A maximum of the analysing power of $i\,T_{11} = 0.25$ may be expected in the region of 50 MeV from the shape of lines with equal analysing power. From theoretical point of view the low angle region is of most interest. As shown by Doleschall /2/ the calculated vector analysing power in this region is most sensitive on the nuclear potentials involved. The contour plot shows that useful experimental data

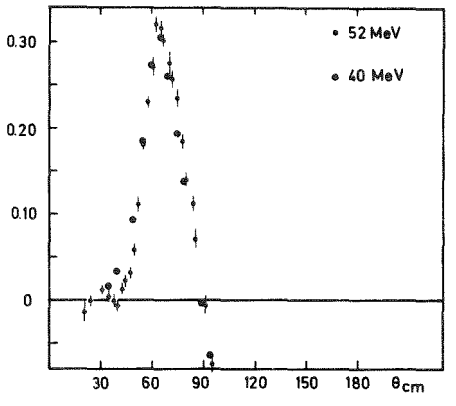

Fig. 1 The vector analysing power i T_{11} of the elastic scattering of polarized deuterons by deuterons at 52 MeV. For comparison measurements of Berkeley /1/ are shown in addition.

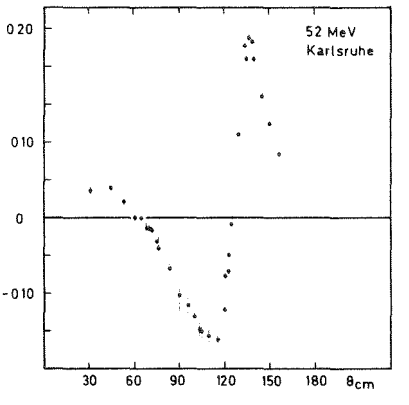

Fig. 2 The vector analysing power i T_{11} of the elastic scattering of polarized deuterons by protons at 52 MeV.

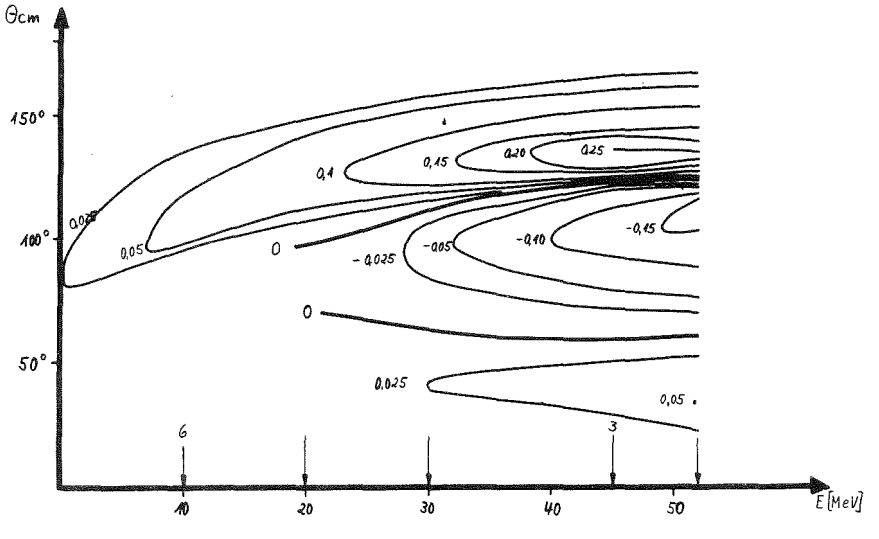

Fig. 3 Contour plot of the analysing power i T_{11} of elastic scattering of deuterons by protons in the energy range from 1 to 52 MeV.

needed for this discussion can be achieved only in an energy region higher than 45 MeV.

+ Institut für Experimentelle Kernphysik der Universität Karlsruhe

References

/1/ H.E. Conzett, W. Dahme, R.M. Larimer, Ch. Leemann, J.S.C. Mc Kee; Fourth International Symposium on Polarization Phenomena in Nuclear Reactions, Zürich (Switzerland) August 1975

/2/ P. Doleschall; Nucl. Phys. A220 (1974) 491

2.1.2 Investigation of the $\vec{d}+p \rightarrow p+p+n$ Break-up Reaction with Vector Polarized Deuterons of the Karlsruhe Isochronous Cyclotron

M.S. Abdel-Wahab+, V. Bechtold, J. Bialy+, L. Friedrich, M. Junge+, and F.K. Schmidt+

Few nucleon experiments are of fundamental interest in providing information on nuclear forces which cannot be extracted from nucleon-nucleon experiments. Especially the three body problem is solvable and therefore probably helpful in reducing ambiguities of the nuclear potentials /1/.

Special reaction mechanism of the d+p → p+p+n are studied defining complete kinematic conditions by measuring coincident proton pairs at two definite angles /2/. The "quasi two particle" inelastic scattering process

$$d + p \rightarrow p + d^{*} + 2.2 \text{ MeV}$$

produces a so-called "Final State Interaction" d^{*} = (n,p) pair with relative energy zero. In this case the three particle reaction matrix element $|T_{fi}|^2$ can be written in the following form

$$|T_{fi}|^2 = F_{np} |\ T_{fi}{}^{o}|^2 .$$

The enhancement factor F_{np} can be calculated from low energy n-p s-wave scattering. The n-p pair will be produced in the singlet or in the triplet state, therefore two different enhancement factors and two different matrix elements $|T_{fi}^{OS}|^2$ and $|T_{fi}^{OT}|^2$ have to be considered, which give the production rates of the FSI n-p pair. This "Watson Model" was used to determine the cross sections for production of the FSI singlet and triplet pair /2/ (see fig. 1).

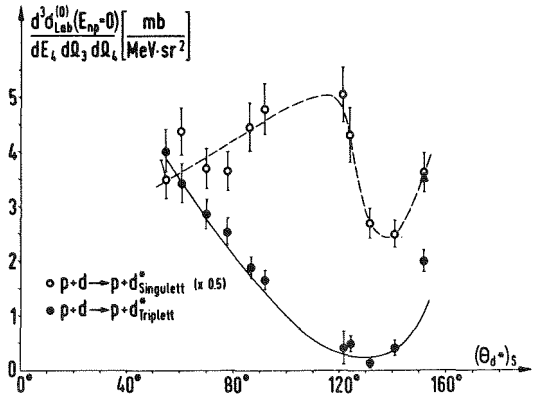

Fig. 1 The angular distribution of the three-particle cross section for the production of final state interacting singlet and triplet n-p pairs at relative energy $E_{np} = 0$. The solid curve is the result of a calculation which connects the three particle cross section quantitatively with the cross section of elastic p-d scattering (taken from ref. /2/).

Exact three body calculations with separable potentials describe these three particle cross sections with equal success /3/. Since the agreement with the cross section measurement is achieved using only N-N s-wave scattering no analysing power is predicted. But experiments at Berkeley /4/ with polarized protons and first results of Karlsruhe (fig. 2) with vector polarized deuterons show analysing powers of nearly the same shape as in the corresponding elastic scattering process. From the present state of the theoretical treatment this result is difficult to understand, particularly for the following reason. The measured analysing power can be evaluated from the analysing power of the singlet and triplet FSI as follows:

$$iT_{11} = \frac{iT_{11}^S \cdot \sigma^S + iT_{11}^T \sigma^T}{\sigma^S + \sigma^T}$$

Because of the much higher singlet cross section the iT_{11} is dominated by the singlet analysing power. Therefore the shape of the singlet analysing power seems to be fairly similar to the elastic $\vec{d}$-p scattering, in which the deuteron is in the triplet state. On the contrary only the triplet FSI cross section could be shown to be similar in shape to the elastic scattering cross section /2/.

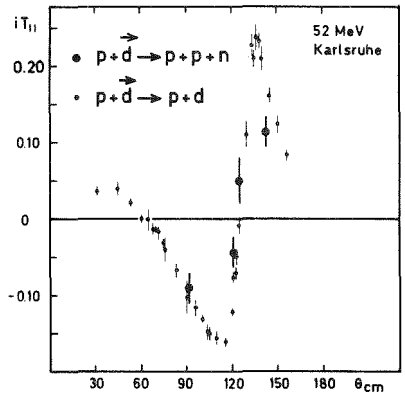

Fig. 2 The analysing power i T_{11} of the n-p FSI pair in comparison with the analysing power of the elastic $\vec{d}$-p scattering process.

+ Institut für Experimentelle Kernphysik der Universität Karlsruhe

References

/1/ W. Kluge; Fortschritt der Physik 22 (1974) 691

/2/ H. Brückmann, W. Kluge, M.Matthäy, L. Schänzler, K. Wick, Nucl. Phys. A157 (1970) 209

/3/ W. Kluge, R. Schlüfter, W. Ebenhöh; Nucl. Phys. A228 (1974) 29

/4/ F.N. Rad, H.E. Conzett, R. Roy, F. Seiler; Fourth Int. Symp. on Polarization Phenomena in Nuclear Reactions, Zürich (Switzerland) August 1975

2.1.3 How to Extract Isoscalar Transition Rates from Alpha Particle Scattering Experiments*

H. Rebel

Various methods proposed for determining isoscalar transition rates are briefly discussed and demonstrated by an application to 146 MeV α-particle scattering from ^{16}O for excitation energies up to the E2 giant resonance region (table). Satchler's theorem relating the moments of a folded potential to moments of the nucleon distributions has been empirically studied for various cases of 104 MeV α-particle scattering.

Table Isoscalar transition rates from $^{16}O(\alpha, \alpha')^{16}O$ compared to electromagnetic results

E_x MeV	I^π	G_L [s.p.u.]				S(IS) [%]	S(EL) [%]
		RC-BP	CC-BP	Folding	Electromagn.		
6.13	3^-	13.6 11.0 ± 1.7[a]	4.9 ± 0.7	13.9 ± 1.2	14.1 ± 1.5[b]	13 ± 1	13 ± 1
6.92	2^+	3.6		2.4 ± 0.3	3.0[c]	9 ± 1	11
11.52	2^+	2.2		1.5 ± 0.1	2.1[c]	9 ± 0.5	13
18.4	2^+	1.1		0.7 ± 0.05	0.43[c]	7 ± 0.5	4
15.9–27.3	2^+	5.9	2.4 ± 0.3	4.3 ± 0.2	1.7[c,d]	47 ± 2	21 ± 9[d]

RC-BP: Real coupling results – Bernstein procedure
CC-BP: Complex coupling results – Bernstein procedure
S: Fraction of the energy-weighted sum rule
[a] A. M. Bernstein
[b] S. J. Skorka et al.
[c] A. Hotta et al.
[d] $E2$ strength for the excitation region of 20–30 MeV

* Z. Physik A277 (1976) 35

2.1.4 Differences Between Neutron and Proton Density RMS-Radii of $^{204,206,208}Pb$ Determined by 104 MeV α-Particle Scattering*

H.J. Gils and H. Rebel

Differential cross sections of elastic scattering of 104 MeV α-particles from $^{204,206,208}Pb$ have been measured with high angular accuracy. The analyses are based on a folding model treating the proton and neutron distributions independently. The proton distributions were taken from precise electron scattering results. The neutron distributions were parametrized by a modified Gaussian the parameters of which were varied in order to fit the experimental cross sections. The resulting rms-radii of the neutron distributions exceed the rms-radii of the proton distributions by $\Delta r = 0.22 \pm 0.09$ fm for ^{204}Pb, $\Delta r = 0.19 \pm 0.09$ fm for ^{206}Pb and $\Delta r = 0.30 \pm 0.07$ fm for ^{208}Pb.

* Phys. Rev. C13 (1976) 2159; KFK-Nachrichten 8/1 (1976) 29

2.1.5 Experimental Studies of Neutron Collectivities by α-Particle Scattering and Some Implications for Giant Resonance Excitations*

H.J. Gils, H. Rebel, and W. Knüpfer+

Using recently measured differential cross sections for elastic and inelastic α-particle scattering from ^{208}Pb at E_α = 104 MeV we studied the question whether the collectivities of protons and neutrons in the strong collective 3^-_1-state (2.615 MeV) are different or not. Adopting the experimental B(E3) value and the proton transition densities from electron scattering experiments we extract the corresponding quantities of the neutron part from an analysis of the α-particle scattering data. Significant differences revealing a different neutron collectivity are found. Furthermore we test results of recent RPA-calculations, which very well reproduce the proton density found in "model independent" analyses of (e,e') measurements. A satisfactory description of α-particle scattering by the microscopically predicted transition densities is obtained if the neutron part is assumed to be different from the proton part whereby a larger transition radius for the neutrons is required. On the basis of these results and of further theoretical studies the (α,α') cross sections for the E2 giant resonance excitation in ^{208}Pb are calculated.

* Proc. of the XIV Intern. Winter Meeting on Nuclear Physics, Bormio (Italy) January 19-24, 1976; Nuov. Cim. (in press)

+ Institut für Theoretische Physik der Universität Erlangen-Nürnberg

2.1.6 Nuclear Matter Distribution from Scattering of Strongly Interacting Projectiles*

H. Rebel

Nucleon and α-particle scattering has been reviewed with the aspect of the information on the nuclear matter distribution, in particular at the surface, and on size and shape of nuclei. Considering various experimental situations some problems of interpretation and procedures of the analysis are discussed. The limits and the particular type of nuclear information are illustrated by various recent examples of low and medium energy proton and

α-particle scattering.

*Proc. of the EPS Conference on "Radial Shape of Nuclei", Cracow (Poland) June 22-25, 1976, ed. by A. Budzanowski, A. Kapuścik and A. Bobrouska, to be published; Report KFK 2330 (1976)

2.1.7 Realistic Coulomb Potentials for Coupled Channel Calculations of α-Particle and ^{16}O Scattering*

H. Rebel

The customary approximations in treating the Coulomb potentials in DWBA- and Coupled Channel calculations of nuclear scattering from deformed nuclei are studied. The formalism and numerical procedures for computing the potentials and Coulomb excitation form factors from realistic charge distributions of projectile and target nucleus are described. The calculated differential cross sections for the cases ^{238}U $(\alpha,\alpha')^{238}U$ and ^{28}Si $(^{16}O,^{16}O')$ ^{28}Si demonstrate the distinct influence of the shape of the Coulomb potential for bombarding energies not far away from the Coulomb barrier.

*Report KFK 2247 (1976)

2.1.8 Investigation of the Compound Nuclear Reactions $^{191+193}Ir$, ^{197}Au $(^{6}Li,xn+yp)$ at E_{Li} = 48 - 156 MeV

J. Kropp+, H. Klewe-Nebenius+, J. Buschmann, H. Rebel, H. Faust+, H.J. Gils, J. Rieder+, and K. Wisshak

Studies of the compound nuclear reactions $^{191+193}Ir$, ^{197}Au $(^{6}Li,xn+yp)$ at the 156 MeV ^{6}Li-beam by means of in-beam γ-ray spectroscopy /1/ have been continued and the analyses of the data have been extended especially to reactions with charged particles in the exit channel. Experimental excitation functions for a variety of compound nuclear reactions have been compared to predictions of a more refined preequilibrium model (hybrid model /2/), which - in contrast to models used previously-is able to calculate absolute cross sections, too. In fig. 1 experimental excitation functions (drawn as smooth curves through the experimental points) are compared to theoretical predictions. The calculated excitation functions well reproduce shapes and thresholds of the experimental curves in most cases, but show strong discrepancies

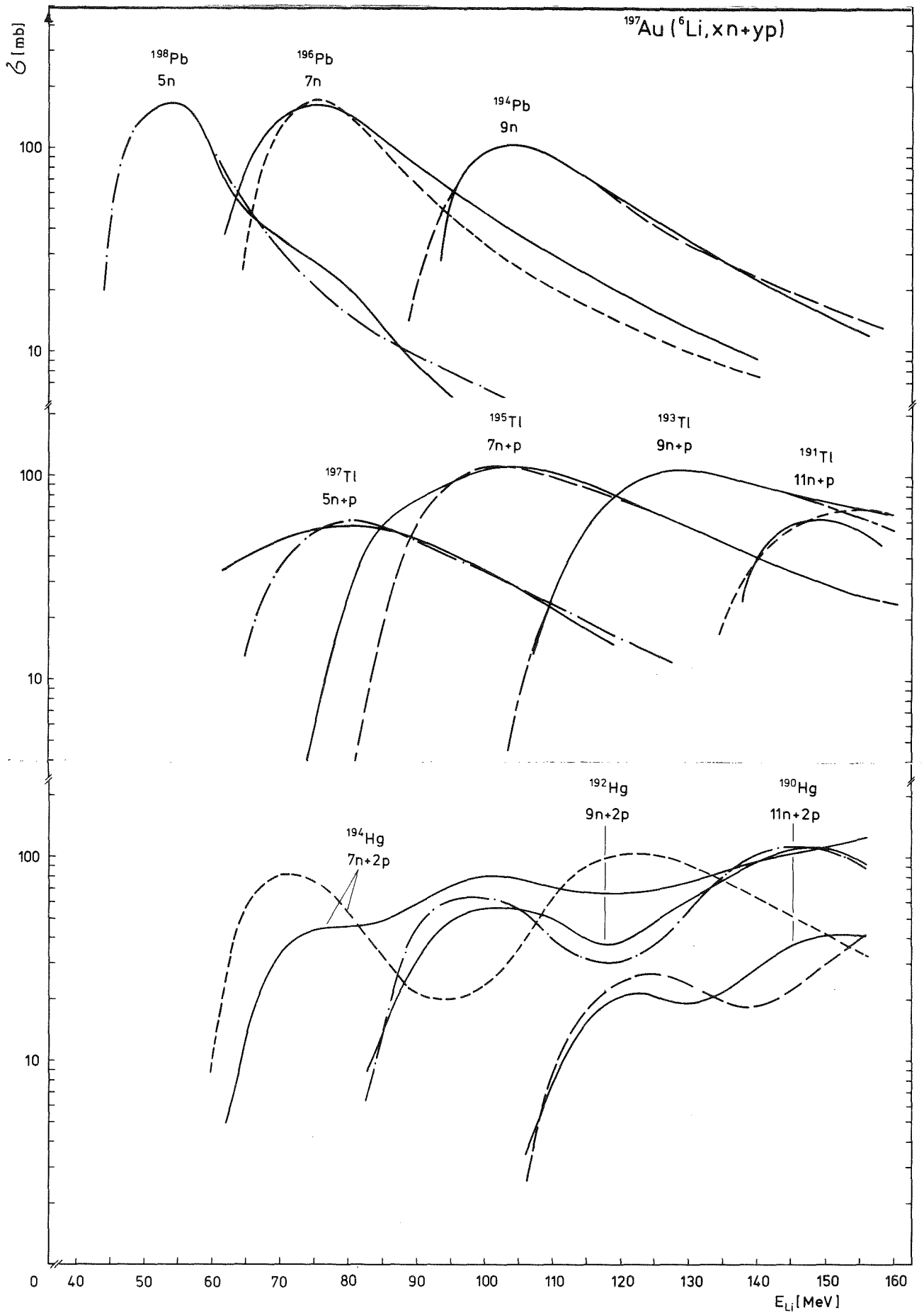

Fig. 1 Examples of the measured (——) excitation functions compared to the theoretical predictions. The theoretical cross sections have been reduced by the factors given in table 1.

in absolute cross sections. The reduction factors by which the theoretical curves have to be devided, have values up to 7 for (^{6}Li,xn)-reactions, but they are considerably smaller for the reactions with outgoing protons (^{6}Li, xn+1(2)p).

Table 1 Reduction factors F for adjusting the calculated cross sections to the experimental excitation functions for all reactions R studied.

Target										
^{197}Au	R	5n		7n		9n				
	F	6.5		6.5		6.5				
	R	5n+p		7n+p		9n+p		11n+p		
	F	2.2		2		2.8		3.5		
	R	6n+2p		7n+2p		8n+2p	9n+2p	10n+2p	11n+2p	
	F	0.15		0.3		0.4	0.9	1.8	3.7	
$^{191+193}$Ir	R	(3+5)n	(4+6)n	(5+7)n		(6+8)n	(7+9)n	(9+11)n	(10+12)n	(11+13)n
	F	6.5	7	6.9		6.8	5.1	6.9	6.8	7.7
	R	(3+5)n+p		(5+7)n+p						
	F	2		2.2						

Since for (α,xn) reactions /3/ no such discrepancies were observed, the strong deviations for the (^{6}Li,xn) reactions are probably due to a strong reaction channel correlated with the ^{6}Li projectile which is not taken into account when calculating the total compound nucleus formation cross sections in theory.

We started, therefore, an investigation of ^{6}Li break-up which is expected to have a large cross section. Particle specific spectra obtained from the analysis of data measured with an E-ΔE telescope are shown in fig. 2. Broad α-particle and deuteron bumps are observed, with maxima at energies corresponding to the velocity of the primary projectiles. From a comparison with the elastically scattered ^{6}Li-particles a rough estimate for the differential break-up cross section of 1.5 b/sr at $\theta_{Lab} = 15^{o}$ is obtained.

The increase of (^{6}Li,xn+yp) cross sections compared to the (^{6}Li,xn) cross sections, which is in contrast to theoretical predictions (c.f. the reduction factors in table 1) may be explained by a kind of "internal break-up" where a capture of α-particle or deuteron clusters into highly lying

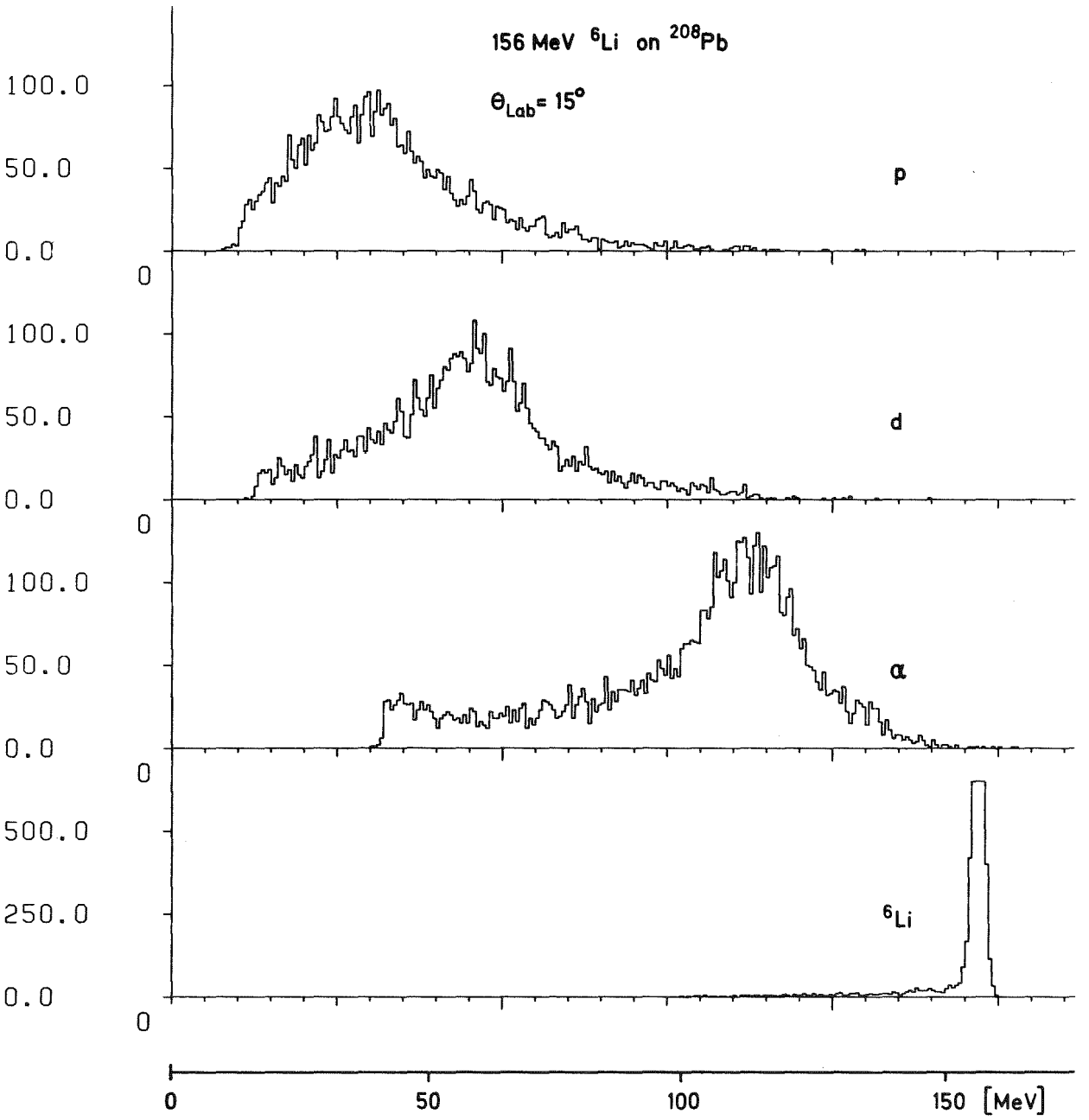

Fig. 2 Particle specific spectra from the reaction ^{208}Pb (^{6}Li; p,d,α,^{6}Li) measured at E_{Li} = 156 MeV and θ_{Lab} = 15°.

states of the target nucleus induces (α,xn) or (d,xn) compound nuclear reactions interfering with the (^{6}Li,xn+p) and (^{6}Li,xn+2p) reactions, respectively. The second break-up particle would then be reemitted via a direct reaction process.

A further investigation of these processes which is necessary to clarify these hypotheses, is planned for the near future by measuring e.g. the angular distribution of break-up particles, α-d coincidences, coincidences

between break-up particles and γ-rays of the final nuclei of compound nuclear reactions, and excitation functions of the break-up process.

+ Physikalisches Institut der Universität Heidelberg

References

/1/ J. Kropp, J. Buschmann, H. Klewe-Nebenius, H. Rebel, H. Faust, K. Wisshak; Report KFK 2223 (1975) 42

/2/ M. Blann; Phys. Rev. Lett. 28 (1972) 757

/3/ P. Jahn, H.J. Probst, A. Djaloeis, W.F. Davidson, C. Mayer-Böricke; Nucl. Phys. A209 (1973) 333

2.1.9 Scattering of ^{6}Li on ^{12}C, ^{90}Zr and ^{208}Pb at E_{Li} = 156 MeV

J. Buschmann, H.J. Gils, H. Rebel, H. Klewe-Nebenius+, H. Faust+, J. Kropp+, W. Nowatzke, and S. Zagromski

Scattering experiments with the 156 MeV ^{6}Li beam have been started at the Karlsruhe Isochronous Cyclotron. The experiments used the big scattering chamber (130 cm ∅) installed at beam line 5 which includes the monochromator magnet. In order not to loose intensity in the external beam transport system the monochromator magnet was used in the dispersionless mode. Thus the energy spread of the primary beam amounted to about 600 keV FWHM. The beam spot on the target had a diameter of about 2 mm and the beam divergence was estimated to be less than 0.2^{o} FWHM. The maximum beam current on the target was 7 nA.

Scattered particles with masses between 6 and 9 amu were detected by four ΔE-E telescopes of Si surface barrier detectors mounted on the same movable arm in the scattering chamber with angular distances of 1.5^{o} between each other. Each telescope consisted of one ΔE detector of 300 μm thickness and one E detector of 4 mm thickness being sufficient to stop ^{6}Li ions up to their maximum energy. The electronic set-up consisted of standard NIM-modules. In the ΔE branches biased amplifiers were used in order to select and stretch the pulse height window, which referres to the energy loss of ^{6}Li, ^{7}Li, and ^{9}Be ions, and to suppress smaller pulses caused by particles lighter than A=6. The data were accumulated and stored on magnetic tape event by event

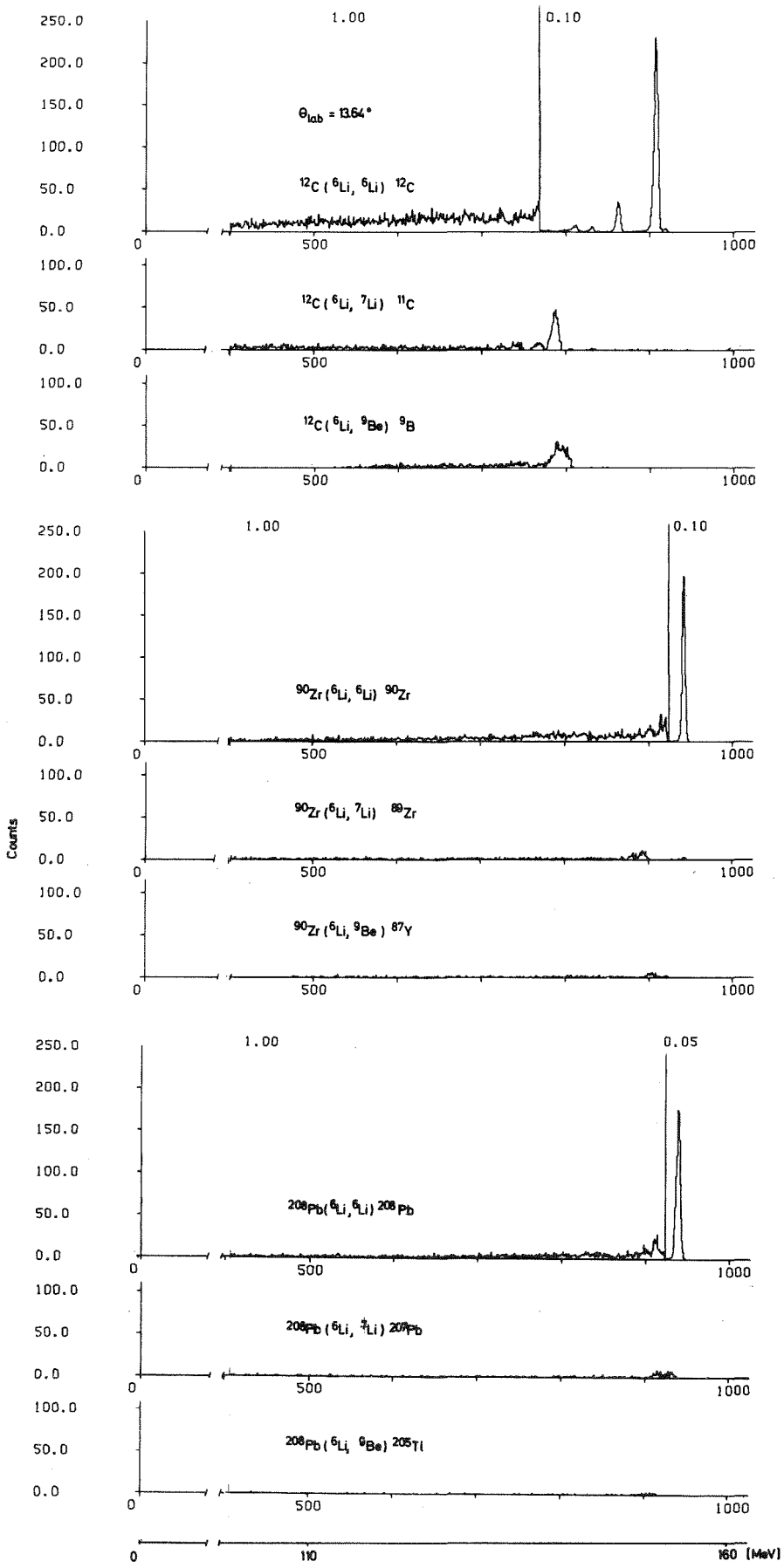

Fig. 1

Particle specific spectra of ^{6}Li induced nuclear reactions on ^{12}C, ^{90}Zr, and ^{208}Pb targets, respectively.

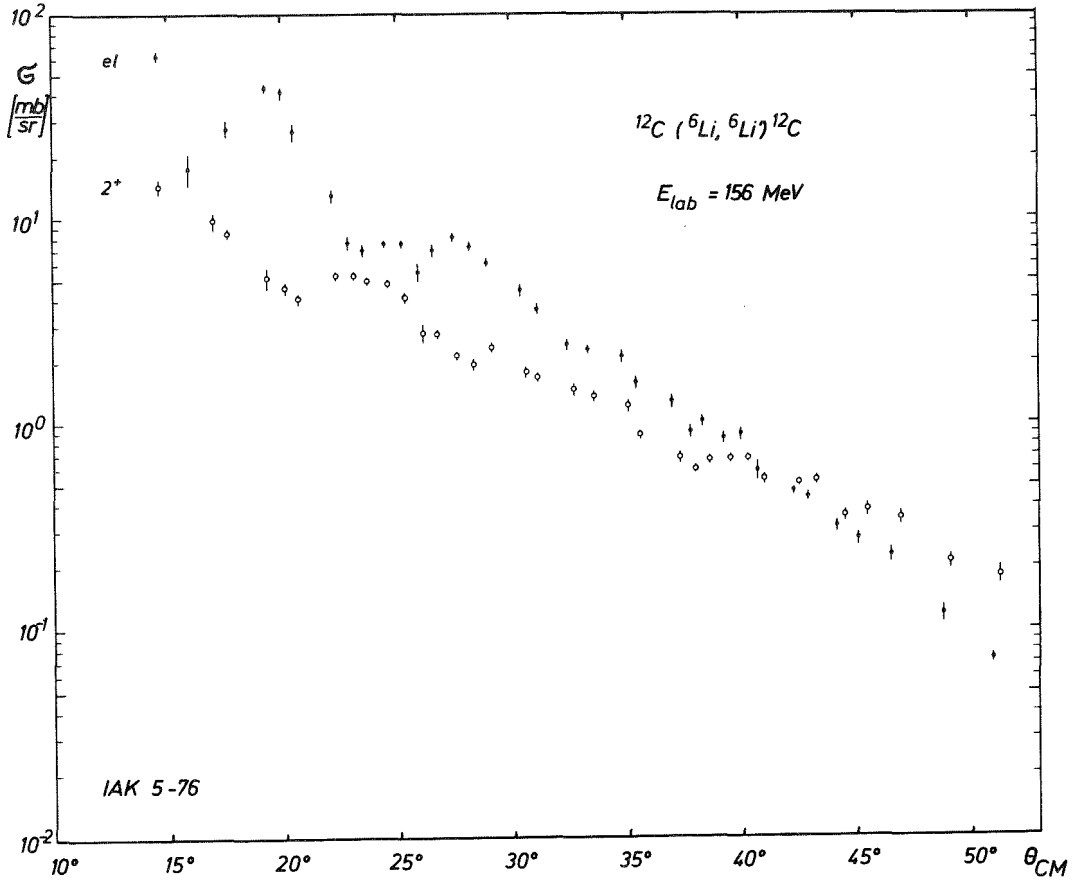

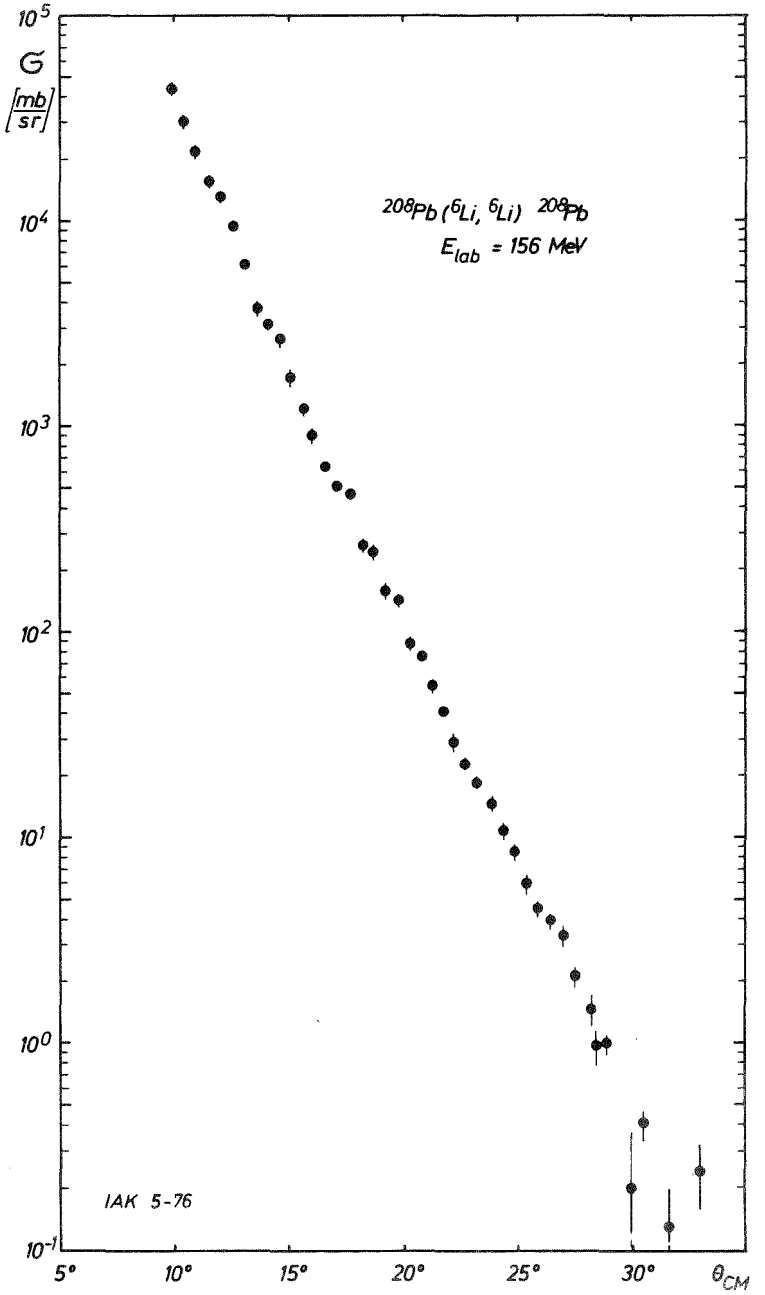

Fig. 2 Preliminary results of elastic and inelastic scattering cross sections $^{12}C(^{6}Li, ^{6}Li)^{12}C$ and $^{208}Pb(^{6}Li, ^{6}Li)^{208}Pb$.

in the list mode by a ND 4400 multiparameter analyzer /1/ and a Geoscience multichannel analyzer. Particle identification was performed by an off-line method /2,3/ after the measurements.

The targets used were a natural C target of 8.3 mg thickness and isotopically enriched (∿99 %) targets of ^{90}Zr and ^{208}Pb of 4.8 mg and 8 mg thickness, respectively. Angular distributions of ejected ^{6}Li, ^{7}Li and ^{9}Be particles have been measured between $\theta_{Lab} = 10^{o}$ and $\theta_{Lab} = 32^{o}$ in steps of 0.5^{o} for ^{12}C and ^{208}Pb. For ^{90}Zr only a few spectra at forward angles have been measured. In fig. 1 the particle specific spectra are shown for the three target nuclei. Preliminary results of elastic and inelastic scattering cross sections of ^{12}C and ^{208}Pb are shown in fig. 2.

+Physikalisches Institut der Universität Heidelberg

References

/1/ The analyzer was kindly placed at our disposal by the Max-Planck-Institut für Kernphysik, Heidelberg

/2/ F.S. Goulding, D.A. Landis, J. Cerny and R.H. Pehl; Nucl. Instr. Meth. 31 (1964) 1

/3/ W. Nowatzke; Report (unpublished) ; J. Buschmann, H.J. Gils and W. Nowatzke; to be published

2.1.10 Study of Prolate-Oblate Effects by Use of Particle - γ Angular Correlations in the Reaction $^{24}Mg(\alpha,\alpha_1)^{24}Mg$

W. Eyrich+, A. Hofmann+, U. Scheib+, S. Schneider+, F. Vogler+, and H. Rebel

Particle-γ angular correlations in the reaction $^{24}Mg\ (\alpha,\alpha_1)^{24}Mg$ for E_α = 104 MeV have been studied at the Karlsruhe Isochronous Cyclotron. The double differential cross section $\frac{d^2\sigma}{d\Omega_\alpha\, d\Omega_\gamma}$ has been measured for 126 combinations of angles (ϕ_α, ϕ_γ) in the reaction plane. From the experimental angular correlation function $W(\phi_\gamma) = A + C \sin^2 2(\phi_\gamma - \phi_2)$ the absolute squares of reaction amplitudes from the ground state to the magnetic substates of the first excited state have been determined (cf. ref. /1/). The differential cross sections, the correlation parameters A, C, ϕ_2, and the reaction amplitudes have been analyzed by a coupled channels procedure with a $0^+-2_1^+-4^+$ coupling on the basis of a rotational model description of ^{24}Mg. In these analyses both the extended optical model and a semimicroscopic folding model have been applied.

Previous analyses of cross sections have shown that it is possible to determine deformation parameters from α-scattering experiments /2/. The present study shows that α-γ-angular correlation data are considerably more sensitive to the sign of the quadrupole deformation parameter β_2 than the differential cross section. In fig. 1 the best fits of the folding model analyses for $\beta_2<0$ and $\beta_2>0$ are compared with the experimental cross sections. Both fits can reproduce the experimental data favouring the positive sign of β_2. Fig. 2 shows the experimental correlation parameter C along with coupled channels calculations using the same parameters as obtained from the cross section fits in fig. 1. One can see that C is strongly affected by the sign of the deformation and gives clear evidence for a prolate shape of ^{24}Mg. (The same result has been obtained also from the extended optical potential analyses). The characteristic differences in C between calculations for $\beta_2 > 0$ and $\beta_2 < 0$ were found to be independent of the potential parameters used. Therefore α-γ correlation studies provide an interesting source of detailed information on nuclear deformation with sensitive discrimination of prolate and oblate shapes.

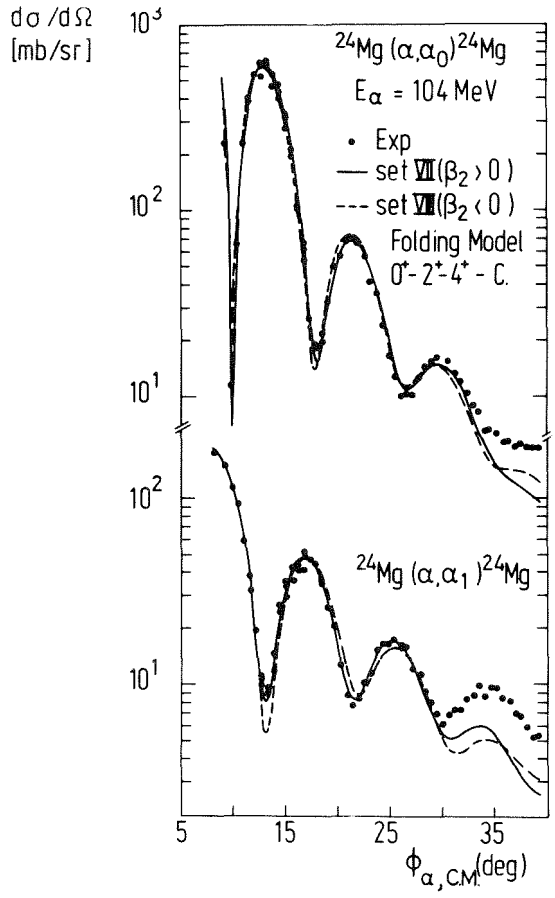

Fig. 1: Experimental differential cross sections for ^{24}Mg (α,α_0) and ^{24}Mg (α,α_1) along with folding model calculations for prolate and oblate deformation.

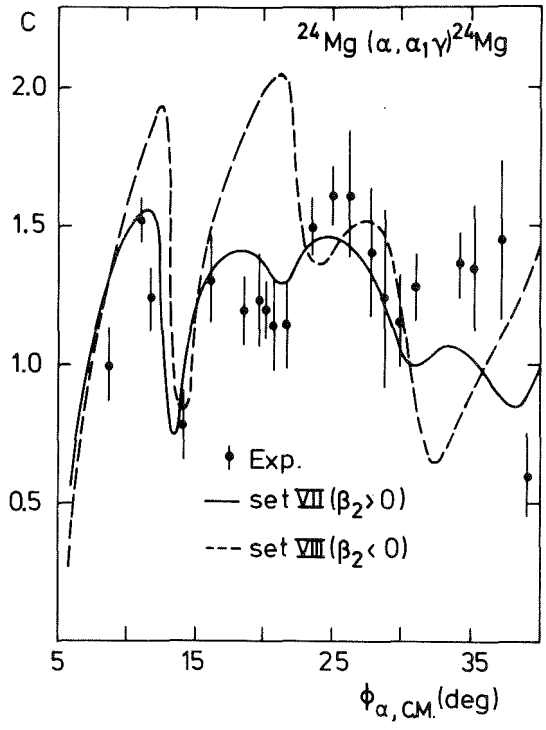

Fig. 2: The angular correlation parameter C of the reaction ^{24}Mg ($\alpha,\alpha_1\gamma$) in comparison with folding model calculations for prolate and oblate deformation.

+Physikalisches Institut der Universität Erlangen-Nürnberg

References

/1/ H. Wagner et al.; Phys. Lett. 47B (1973) 497

/2/ H. Rebel et al., Nucl. Phys. A182 (1972) 145

2.2 NUCLEAR SPECTROSCOPY

2.2.1 Experimental Studies of the Level Scheme of ^{143}Eu and a Generalized Decoupling Model Description*

K. Wisshak, A. Hanser, H. Klewe-Nebenius+, J. Buschmann, H. Rebel, H. Faust+, H. Toki++, and A. Fäßler++

Excited levels of ^{143}Eu have been investigated by nuclear spectroscopy methods. We measured γ-rays and conversion electron singles spectra as well as $\gamma\gamma$-coincidences from mass separated ^{143m}Gd sources (108 s) prepared after the irradiation of ^{144}Sm with 78 MeV α-particles. In addition in-beam data were obtained by measuring γ-ray singles spectra, angular distributions and $\gamma\gamma$-coincidences, following the ^{144}Sm (α, 4n+p,γ) reaction. A level scheme for ^{143}Eu comprising 19 levels is proposed, spin assignments or at least restrictions are given. The deduced experimental level scheme can be reproduced semiquantitatively by a generalized decoupling model which takes into account an asymmetric deformation of the core and a variable moment of inertia. Additionally, the results are discussed in the limit of the weak coupling model.

* Z. Physik A277 (1976) 129

+ Physikalisches Institut der Universität Heidelberg

++ Kernforschungsanlage Jülich, IKP and Universität Bonn

2.2.2 Experimental Studies of the $4_1^+ \rightarrow 0^+$ Transition in ^{60}Ni by 104 MeV α-Particle Scattering and Conversion Electron Spectroscopy

H. Faust+, K. Wisshak, H. Klewe-Nebenius+, H. Rebel, H.J. Gils, and A. Hanser

In addition to the well established permanent hexadecapole deformation of deformed nuclei there is considerable experimental evidence for a collective hexadecapole motion in spherical nuclei from inelastic scattering of electrons, protons and α-particles. Tab. 1 compiles some results for closed shell nuclei. The conspicuous feature indicated in the table is the correla-

Table 1 Measured L=4 transition rates from various experiments

	N = 28	Z = 28		N=82	Z=82	
	^{50}Ti	^{58}Ni	^{60}Ni	^{140}Ce	^{202}Pb	^{204}Pb
(α,α')	5.4 ± 0.8	3.8 ±0.7		(6.0)*		
(e,e')	4.7 ± 0.15	2.2 ±0.7	4.1 ± 0.8	20. ± 4.		
$4_1^+ \rightarrow 0^+$ decay					4.6 ± 0.8	2.3 ±0.5
$E_{4_1^+}/E_{2_1^+}$	1.72	1.70	1.88	1.305	1.40	1.42

B(L4; $4_1^+ \rightarrow 0^+$) - Results [W.u.]

* Standard - DWBA Result

tion between the relative lowering of the energetic positions of the 4_1^+ states and the enhanced E4 transition probabilities. Good agreement is found in cases where the α-particle cross sections are analyzed on the basis of a folding procedure/1/. In some favourable cases the direct cross-over $4_1^+ \rightarrow 0^+$ decay could be observed despite of the extreme E4/E2 branching ratios of about 10^{-4} - 10^{-8}. We have started a detailed experimental study of the case of ^{60}Ni. The result of inelastic 104 MeV α-particle scattering is displayed in fig. 1. The found hexadecapole transition rate of $G_4 = 5.5 \pm 0.8$ s.p.u. corresponds to an E4/E2 branching ratio of 10^{-8} - 5 x 10^{-8} with an uncertainty due to the ill-known lifetime of the 4_1^+ state of ^{60}Ni. It is interesting to look to what extent this result is consistent with a direct observation of the $4_1^+ \rightarrow 0^+$ decay. By use of an improved version of the mini orange conversion electron spectrometer /2/ we searched for the conversion electrons of this decay. The present results and the experimental set-up is shown in fig. 2. From the measurements we deduce an upper limit for the branching ratio of 1 x 10^{-7}.

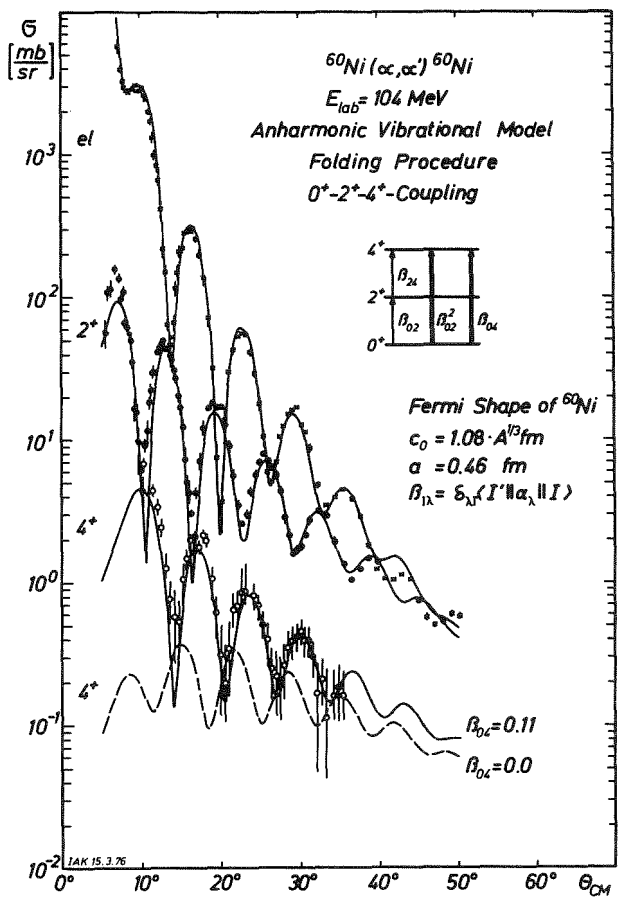

Fig. 1 ^{60}Ni (α,α') cross sections and results of the analysis.

+Physikalisches Institut der Universität Heidelberg

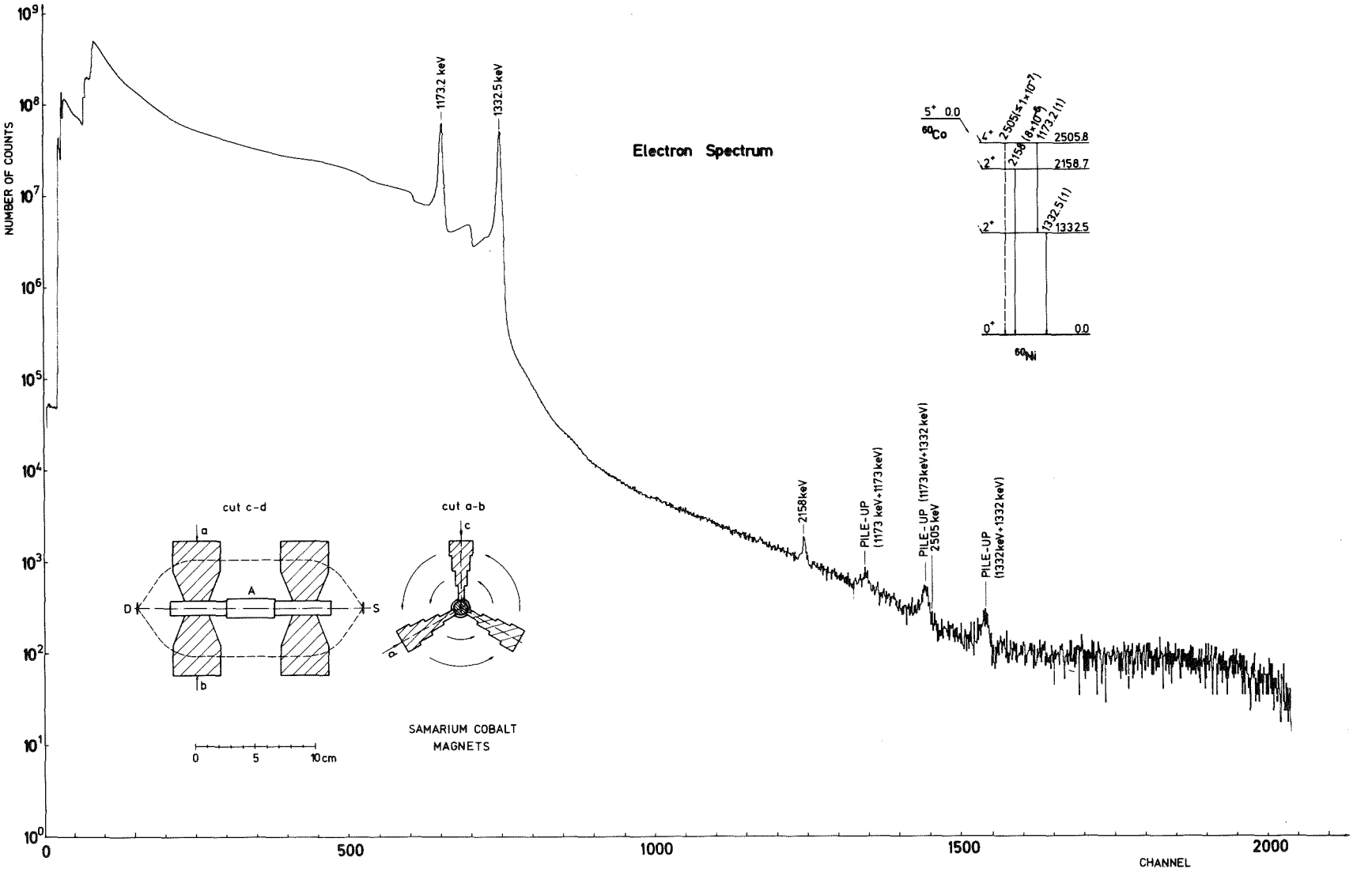

Fig. 2 Conversion electron spectrum of a ^{60}Co-source. The special arrangement of the spectrometer reduces the background of low energy electrons from ß-decay as well as from Compton scattering. The peaks are denoted with the γ-ray transition energy. The electron-electron-pile-up-lines are shifted to low energies by the K-electron binding energy of ^{60}Ni; they are also broadened to the low energy tail by the double absorption effect in the target (2 mg/cm^2).

References

/1/ H.J. Gils and H. Rebel; Z. Physik A274 (1975) 259;
H. Rebel; Z. Physik A277 (1976) 35

/2/ J. van Klinken, F. Feenstra, K. Wisshak, H. Faust;
Nucl. Instr. Meth. 130 (1975) 427

2.2.3 Level Structure of ^{149}Nd*

J.A. Pinston[+], R.Roussille[+], H. Börner[++], H.R. Koch[++], and D. Heck

The level structure of ^{149}Nd has been established from the study of the prompt γ-rays following thermal neutron capture in ^{148}Nd. Within the energy range $26 < E_\gamma < 520$ keV the γ-radiation has been analysed with one of the three bent crystal spectrometers installed at the Grenoble high-flux reactor. Measurements with Ge(Li) detectors operated in Compton suppression and pair mode covered the energy range $0.1 < E_\gamma < 4.9$ MeV. Gamma-gamma coincidences have been taken with two Ge(Li) detectors at the Karlsruhe research reactor FR2. Using all these data a level scheme is proposed for ^{149}Nd comprising 23 excited states up to 920 keV. For most levels spin and parity values are proposed. The present level energies, spins and parities are in excellent agreement with the results found in (^{3}He,α) and (d,t) reactions.

* Nucl. Phys. A264 (1976) 1

+ Institut Laue-Langevin, Grenoble (France)
++ Kernforschungsanlage Jülich, IKP

2.2.4 Rotational States in ^{151}Nd Populated Through Thermal Neutron Capture*

J.A. Pinston[+], R. Roussille[+], H. Börner[++], W.F. Davidson[+], P. Jeuch[+], H.R. Koch[++], K. Schreckenbach[+], and D. Heck

The level scheme in the nucleus ^{151}Nd has been studied following neutron capture by observing the γ-rays and conversion-electrons with curved-crystal

spectrometers, a Ge(Li) detector and a ß-spectrometer. A comprehensive level scheme up to ≃1 MeV was established. It is shown that the present level scheme energies differ from those previously found in a ^{150}Nd (d,p) reaction study by a systematic shift of 27 keV. The binding energy of the last neutron in ^{151}Nd was deduced. For most levels spin and parity values are proposed and an identification of bands with Nilsson-model configurations is given.

* Nucl. Phys. A 270 (1976) 61

+ Institut Laue-Langevin, Grenoble (France)

++ Kernforschungsanlage Jülich, IKP

3. LASER SPECTROSCOPY

3.1 A Laser Spectrometer for Measurements of Nuclear Moments of Instable Nuclides

G. Nowicki, S. Göring, H. Rebel, G. Schatz

Measurements of isotope shifts and hyperfine splittings in atomic spectra give information about rms radii and nuclear moments of atomic nuclei. With tunable narrow band dye lasers excellent light sources are available for a selective excitation of hyperfine levels. Their intensity is sufficiently high to allow measurements on samples containing only very few atoms. We are building up a laser spectrometer for high resolution atomic spectroscopy of shortlived nuclides produced with the cyclotron beam. The principle of the experiment - atomic beam fluorescence spectroscopy with optical heterodyning using two cw dye lasers - is described in ref. /1/. The present status of the experimental set-up the main functions of which have been tested in the last year with regard to the spectroscopy of light Barium isotopes, is briefly characterized by the following features:

a: Spectral properties of the dye lasers:

The dye laser is pumped by the 514.5 nm radiation of a commercial cw Argon ion laser. We use a dye solution of 30 mg/ℓ Rhodamin 504 in 75 % H_2O + 25 % CH_3OH with some drops of cyclooctotetraen. With a pumping power of 1.2 W the dye laser emits 10 mW in a single mode at 553.5 nm (the $^1S_o - {}^1P_1$ resonance line of Ba atoms) when used with two fixed intracavity glass etalons. Intensity stability is within 10 % and the frequency jitter of the free running laser is about 26 MHz. To reduce both, intensity and frequency fluctuations, we have designed a new dye-cell. Because of the fixed etalons the single mode tuning range without mode hopping is only about 160 MHz. This will be extended to some GHz by using tunable air spaced etalons.

b: Frequency locking:

A precise reference frequency for optical heterodyning is provided by one laser locked to a known atomic transition, e.g. $^1S_o - {}^1P_1$ of ^{138}Ba. The control signal is deduced from the resonance fluorescence of a well collimated atomic beam, thus preventing Doppler broadening of the reference frequency. By taking the difference between the fluorescence signal and a signal proportional to the laser intensity as the error signal the laser is locked to one side of the resonance line. The resulting line shape is shown in fig. 1 (left signal). The residual line width of approximately 10 MHz is

partly due to the natural line width of the reference line (19 MHz). This is demonstrated by locking the laser in a similar way to one side of the transmission fringe of a confocal Fabry-Pêrot with a resolution of 10 MHz FWHM. This reduces the line width to 6.5 MHz (central signal of fig. 1).

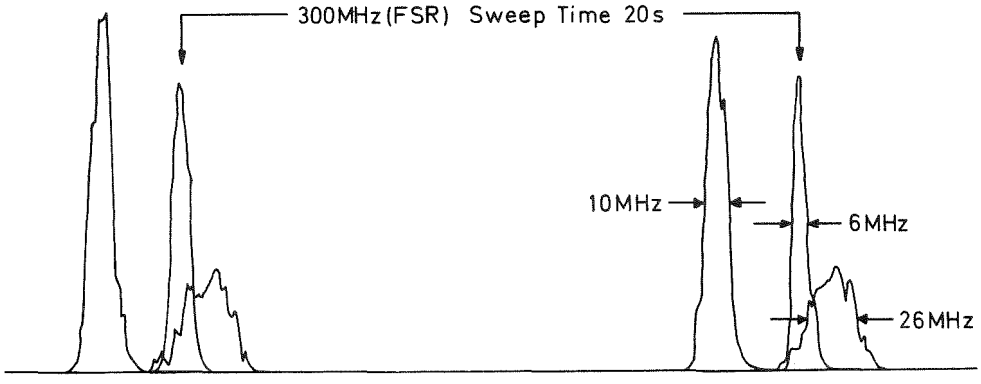

Fig. 1 Transmission fringes from a confocal Fabry-Pêrot with free spectral range of 300 MHz and a finesse of ∿20. The fringe patterns result from free running laser, laser locked to a confocal Fabry-Pêrot and locked to resonance fluorescence of Barium (from right to left).

So, when locking the reference laser to the transition of a stable isotope we expect a laser band width smaller than the respective natural line width, which should be sufficient for our measurements.

c: Optical heterodyning:

The exact resonance frequency of the isotope under investigation is to be measured by mixing parts of the two laser signals (reference laser and exciting laser) on a fast diode and analyzing the difference frequency with a microwave spectrum analyzer. We tested this apparatus by mixing two modes of one dye laser. Thus we got a measure for the coherence of the dye laser light, as the frequency jitter is nearly the same for both resonator modes. The result with the two modes $TEM_{n,o,o}$ and $TEM_{n+5,o,o}$ differing by 1286 MHz was a mode width of 20 kHz corresponding to a coherence length of 15 km.

d: Fluorescence from a small number of atoms:

We checked the efficiency of our fluorescence light detecting system by counting the fluorescence photons from Ba and Na atomic beams at different oven temperatures. Without lock-in technique it was possible to detect fluorescence from 5×10^3 atoms/s in the presence of a background counting rate of 5 kHz (scattered light of the laser beam) at 5 mW laser power. With the drastically reduced background of the new atomic beam apparatus /2/ it should be possible to detect the fluorescence of about 100 atoms/s.

References

/1/ S. Göring et al., Report KFK 2223 (1975) p. 56; p. 59

/2/ Contribution 3.2

3.2 Method and Apparatus for Producing Atomic Beams of Neutron Deficient Radioactive Barium Isotopes for Laser Experiments

B. Feurer, A. Hanser

In the planned measurements of isotope shifts and hyperfine structures of instable barium isotopes atomic beam resonance fluorescence spectroscopy will be employed /1/. As first examples we intend to investigate the isotopes ^{131}Ba and ^{129}Ba. Preliminary studies show that atomic beams of ^{131}Ba and of ^{129}Ba can be produced with sufficient intensity in the following way: Highly enriched ^{134}Ba and ^{130}Ba are irradiated with deuterons of 50 MeV and 30 MeV, respectively. The barium isotope of interest which is produced via a short-lived lanthanum isotope is separated electromagnetically. By the mass separation process, it is implanted into a collector material. We implant into silicon because barium can be heated off from silicon almost quantitatively at a temperature of about 1300°C. The heating off is performed in the atomic beam oven which has a "long exit channel" for a crude focusing of the atomic beam. From the results of preliminary studies we expect atomic beam intensities of 10^5 atoms/sec (^{131}Ba) and of 4×10^3 atoms/s (^{129}Ba), respectively, if we limit the beam divergence to $\pm$ 0.4° in the direction of the laser beam (resulting in negligible Doppler broadening) and to $\pm$ 0.6° perpendicular to the laser beam determined by the laser beam cross section). This beam intensity will be available for about 1.5 hours per experimental run. Especially in the case of ^{129}Ba, however, we have to cope with a substantial contamination by stable barium isotopes.

For the planned experiment a new atomic beam apparatus has been constructed. In the design care was taken that measurements are not disturbed by a high background caused by laser light scattered in the experimental set-up. If a laser beam of 1 mW power passes through the new apparatus the background count rate is only increased by 20 counts/s, measured with a multiplier of 14 % quantum efficiency for Ba light. This has been achieved by long, wide entrance

and exit tubes for the laser beam, sharply edged diaphragms within the tubes and thoroughly blackening the inner surfaces of the apparatus. On the other hand the solid angle for collecting the resonance light on a photomultiplier is about 22 % of 4 π. The oven of this apparatus can be heated up to 1300°C. At present the oven gives rise to a yet too high count rate of scattered photons coming from the brightly glowing oven at high temperature. This is to be removed by some modifications of the apparatus or by a suitable interference filter. The atomic beam oven has three exit channels lying in the plane perpendicular to the laser beam. So the atomic beam intensity will be increased and the duration of measuring decreased by the same factor with respect to the values given above. This means that the signal to noise ratio will be improved. Moreover, the apparatus has a device for detecting a beam of radioactive atoms. The atoms leaving the atomic beam oven at an angle of more than one degree with respect to the beam axis are collected on a small aluminium sheet (with a hole of 3 mm diameter for the central part of the beam which is used for the experiment). After s short collection time the sheet can be brought to a γ-detector. A magazine with 30 sheets allows a frequent repetition of this operation.

It is estimated that one can record 10^8 counts and 5×10^6 counts per run in the cases of ^{131}Ba and ^{129}Ba, respectively, using the described apparatus and assuming the beam intensities given above, provided the laser stays on resonance for the whole duration of the experiment.

References

/1/ Contribution 3.1

4. THEORY

4.1 Finite Velocities in the Dynamics of Nuclear Fission

E.F. Chaffin and F. Dickmann

The cranking model which has been used to obtain effective mass parameters for studies of fission dynamics is extended to higher order in the collective velocities. Thus we investigate the question whether and up to which collective energy the cranking model is applicable in fission theory. Our starting point is a model Hamiltonian H which depends on particle coordinates $\underline{r}$, momenta $\underline{p}$ and on a set of real coordinates α characterizing the shape of the nucleus. The eigenvectors $|j(\alpha)\rangle$ and eigenvalues of the Schrödinger equation

$$(H(\underline{r},\underline{p},\alpha) - \varepsilon_j(\alpha))\ |j(\alpha)\rangle = 0 \tag{1}$$

are functions of the collective variables. The operator

$$P_n = \frac{\hbar}{i}\frac{\partial}{\partial\alpha_n} \tag{2}$$

which generates a change of the variable α_n, is non-hermitian, because the right hand side of the equation

$$P_n \langle a(\alpha)|b(\alpha)\rangle = -\langle P_n\, a|b\rangle + \langle a|P_n b\rangle \tag{3}$$

is non zero in general for two arbitrary states a and b. For two orthonormalized eigenstates j and ℓ of the Hamiltonian, however, the left hand side of eq. (3) is zero and we define

$$\langle j|P_n|\ell\rangle = \langle P_n j(\alpha)|\ \ell(\alpha)\rangle = \langle j(\alpha)|\ P_n\ \ell(\alpha)\rangle\ . \tag{4}$$

The phases of the eigenstates j can be chosen so that the matrix elements of P_n are pure imaginary quantities. Consequently the diagonal elements are zero

$$\langle j|P_n|j\rangle = \langle j|P_n|j\rangle^* = 0\ . \tag{4}$$

We now use the operators P_n as Lagrange constraints to generate a collective motion. In particular we determine the ground state vector $|\psi\rangle$ of the modified Hamiltonian

$$H' = H - V$$

where

$$V = \sum_n \dot{\alpha}_n \frac{h}{i} \frac{\partial}{\partial \alpha_n} \quad . \tag{5}$$

The real collective velocities $\dot{\alpha}_n$ play the role of Lagrange constraints. With the ansatz

$$|\psi\rangle = |0(\alpha)\rangle + |\psi^{(1)}\rangle + |\psi^{(2)}\rangle + |\psi^{(3)}\rangle + \ldots \tag{6}$$

where the vector $\psi^{(i)}$ is of i'th order in the velocities and

$$\langle 0(\alpha)| \psi^{(i)}\rangle = 0 \tag{7}$$

one obtains in standard Rayleigh Schrödinger perturbation theory taking advantage of eq. (4)

$$\begin{aligned} |\psi^{(1)}\rangle &= |R\ V_0\rangle, \\ |\psi^{(2)}\rangle &= |R\ V\ \psi^{(1)}\rangle, \\ |\psi^{(3)}\rangle &= |R\ V\ \psi^{(2)}\rangle - |R\ \psi^{(1)}\rangle\langle 0|\psi^{(1)}\rangle. \end{aligned} \tag{8}$$

The operator R is defined by

$$R = \sum_{j\neq 0} |j\rangle \frac{1}{\varepsilon_j - \varepsilon_o} \langle j| \quad . \tag{9}$$

The energy increase above the groundstate energy ε_o is given by the expression

$$T = \frac{\langle\Psi|H-\varepsilon_o|\Psi\rangle}{\langle\Psi|\Psi\rangle} = \langle\psi^{(1)}|H-\varepsilon_o|\psi^{(1)}\rangle(1-\langle\psi^{(1)}|\psi^{(1)}\rangle)$$

$$+ \langle\psi^{(1)}|H-\varepsilon_o|\psi^{(3)}\rangle + \langle\psi^{(2)}|H-\varepsilon_o|\psi^{(2)}\rangle + \langle\psi^{(3)}|H-\varepsilon_o|\psi^{(1)}\rangle \tag{10}$$

up to fourth order in the collective velocities.

Using relation (3) this expression can be rewritten in a form where the velocity potential V (eq. (5)) operates only on eigenstates of the Hamiltonian and on matrix elements:

$$T = \langle V\,0|R|\,V\,0\rangle$$

$$+\ 3 \sum_{j\neq 0} \frac{1}{\varepsilon_j - \varepsilon_o} \left(\langle V\,j|R|V\,0\rangle + V\ \langle j|R|V\,0\rangle\right)^2 \qquad (11)$$

$$-\ 3\ \langle V\,0|R|V\,0\rangle\langle V\,0|R^2|V\,0\rangle$$

$$+\ 2\ V\left[\sum_{j\neq 0} \langle V\,0\ |R^2|j\rangle\ (\langle V\,j|R|V\,0\rangle + V\langle j|R|V\,0\rangle)\right].$$

The first term on the right hand side of eq. (11) is the familiar cranking model expression. It is of second order in the collective velocities. The remaining fourth order terms represent the first nonvanishing correction. The cranking model can be valid only up to velocities where the correction is small compared to the first term.

We have evaluated expression (11) numerically for a two-center oscillator Hamiltonian, i.e. a generalized Nilsson model which allows the nucleus to fission. A pairing force is used as residual interaction. The variables α characterize the shape of the potential. The velocity potential V (eq. (5)) is thus a one body operator. When applied to an eigenstate of the Hamiltonian it changes the quasiparticle (Q.P.) number of the state by zero plus or minus two. Thus the excited states occuring in eq. (11) are two Q.P.-states except for the first term in the second line where j may also be a four Q.P.-state. The calculations have been done for protons of ^{236}U and one collective degree of freedom. This degree was chosen to describe the motion across the second saddle point, it consists essentially of a separation of the centers of the oscillators. The results are presented in ref. /1/.

References

/1/ Contribution 4.2

4.2 Dependence of the Fission Mass Parameter on Pairing Strength, Shell Structure and Mass Asymmetry

E.F. Chaffin and F. Dickmann

The nuclear energy for the fission degrees of freedom is dependent on the pairing strength, shell structure, and mass asymmetry. We present here results

showing that higher order correction terms, depending on higher order powers of the collective velocities, are especially strongly varying with these variables.

When a tractable form for the energy increase T of the nucleus above the ground state potential energy ε_o has been found (see the previous article), one gets

$$T = \frac{1}{2}\{B_{AD} + (B_1^{2QP} + B_1^{4QP} + B_2 + B_3 + B_4 + B_5 + B_6)\,\dot{\alpha}^2\}\,\dot{\alpha}^2$$

where

$$B_{AD} = 2\,\hbar^2 \sum_{\substack{k \\ k=0}} \frac{\left|\langle 0|\frac{\partial}{\partial\alpha}|k\rangle\right|^2}{\varepsilon_k - \varepsilon_o}$$

$$B_1^{2QP} + B_1^{4QP} = 6\,\hbar^4 \sum_{\substack{k \\ k\neq 0}} \frac{1}{\varepsilon_k - \varepsilon_o} \left[\sum_{\substack{j \\ j\neq 0}} \frac{\langle 0|\frac{\partial}{\partial\alpha}|j\rangle\langle j|\frac{\partial}{\partial\alpha}|k\rangle}{\varepsilon_j - \varepsilon_o}\right]^2$$

$$B_2 = -6\,\hbar^4 \left(\sum_{\substack{k \\ k\neq 0}} \frac{\left|\langle k|\frac{\partial}{\partial\alpha}|0\rangle\right|^2}{\varepsilon_K - \varepsilon_o}\right)\left(\sum_{\substack{j \\ j\neq 0}} \frac{\left|\langle j|\frac{\partial}{\partial\alpha}|0\rangle\right|^2}{(\varepsilon_j - \varepsilon_o)^2}\right)$$

$$B_3 = 2\,h^4 \sum_{\substack{k \\ k\neq 0}} \frac{1}{\varepsilon_k - \varepsilon_o} \left|\frac{\partial}{\partial\alpha} \frac{\langle k|\frac{\partial}{\partial\alpha}|0\rangle}{\varepsilon_k - \varepsilon_o}\right|^2$$

$$B_4 = 4\,\hbar^4 \sum_{\substack{k \\ k\neq 0}} \frac{\langle 0|\frac{\partial}{\partial\alpha}|k\rangle}{\varepsilon_k - \varepsilon_o} \frac{\partial}{\partial\alpha}\left(\frac{1}{\varepsilon_k - \varepsilon_o} \frac{\partial}{\partial\alpha} \frac{\langle k|\frac{\partial}{\partial\alpha}|0\rangle}{\varepsilon_k - \varepsilon_o}\right)$$

$$B_5 = 8\,\hbar^4 \sum_{\substack{k \\ k\neq 0}} \sum_{\substack{j \\ j\neq 0}} \frac{\langle 0|\frac{\partial}{\partial\alpha}|k\rangle\langle k|\frac{\partial}{\partial\alpha}|j\rangle}{(\varepsilon_k - \varepsilon_o)(\varepsilon_j - \varepsilon_o)} \left[\frac{\partial}{\partial\alpha} \frac{\langle j|\frac{\partial}{\partial\alpha}|0\rangle}{\varepsilon_j - \varepsilon_o}\right]$$

$$+ 4\,\hbar^4 \sum_{\substack{k \\ k\neq 0}} \sum_{\substack{j \\ j\neq 0}} \frac{\langle 0|\frac{\partial}{\partial\alpha}|k\rangle\langle k|\frac{\partial}{\partial\alpha}|j\rangle}{(\varepsilon_k - \varepsilon_o)^2} \left[\frac{\partial}{\partial\alpha} \frac{\langle j|\frac{\partial}{\partial\alpha}|0\rangle}{\varepsilon_j - \varepsilon_o}\right]$$

$$B_6 = 4\,\hbar^4 \sum_{\substack{k \\ k\neq 0}} \sum_{\substack{j \\ j\neq 0}} \frac{\langle 0|\frac{\partial}{\partial\alpha}|k\rangle}{\varepsilon_k - \varepsilon_o} \left[\frac{\partial}{\partial\alpha} \frac{\langle k|\frac{\partial}{\partial\alpha}|j\rangle}{\varepsilon_j - \varepsilon_o}\right] \frac{\langle j|\frac{\partial}{\partial\alpha}|0\rangle}{\varepsilon_j - \varepsilon_o} \quad .$$

Here B_1^{2QP} and B_1^{4QP} are separated according to whether the intermediate states $|k\rangle$ are two quasi-particle (2QP) or four quasiparticle (4QP) states.

Table 1 Dependence of mass parameter on pairing strength. Δ is in MeV, B_{AD} in $\hbar^2$/MeV, and all other quantities in $\hbar^4$/MeV^2 units.

Δ	B_1^{2QP}	B_1^{4QP}	B_2	B_3	B_4	B_5	B_6	B_{Corr}	B_{AD}
1.07	792.3	560.6	-866.7	438.8	405.2	1481.1	7.5	2701.9	39.9
1.18	707.0	458.0	-698.6	352.6	256.0	1296.6	4.4	2376.1	37.2
1.35	585.6	331.2	-497.7	255.7	218.0	1071.3	1.6	1964.9	32.2
2.47	199.3	58.7	-82.5	65.6	75.0	373.9	-0.2	687.0	17.3

If we make some simple approximations, such as replacing summations by integrals, it can be shown that the adiabatic mass is given approximately by

$$B_{AD} \cong \frac{1}{16} \left| < \frac{\partial h}{\partial \alpha} >_{AV} \right|^2 \frac{\rho}{\Delta^2}$$

(See for example ref. /1/). Here $<\frac{\partial h}{\partial \alpha}>_{AV}$ is some average value of the matrix elements, expected to vary slowly with deformation. In practice it is found that the quantity ρ should not be put equal to the single particle level density ρ_{SP}, but needs to be modified to take into account the large contributions of levels close to but not exactly at the fermi level:

$$\rho \rightarrow \rho_{SP} \ (1 + \omega \ \Delta^2).$$

It then emerges that for the region of physical interest, log-log plots show that B_{AD} varies approximately as the inverse first power of Δ.

Similar approximations may be used to estimate the dependence of the higher order terms. For example, the terms involving four quasiparticle intermediate states are given by:

$$B_1^{4QP} = 6 \sum_{\xi\eta\chi\zeta} \frac{1}{E_\xi + E_\eta + E_\chi + E_\zeta} \left[\frac{<0|\frac{\partial}{\partial\alpha}|\xi\ \bar{\eta}><\xi\ \bar{\eta}|\frac{\partial}{\partial\alpha}|\xi\bar{\eta}\chi\bar{\zeta}>}{E_\xi + E_\eta} + \frac{<0|\frac{\partial}{\partial\alpha}|\chi\bar{\zeta}><\chi\ \bar{\zeta}|\frac{\partial}{\partial\alpha}|\xi\ \bar{\eta}\chi\bar{\zeta}>}{E_\chi + E_\zeta} \right]^2$$

$$\cong \frac{3}{2\Delta} \left| \frac{1}{16} \left(<\frac{\partial h}{\partial \alpha}>_{AV}\right)^2 \frac{\rho}{\Delta^2} \right|^2.$$

The same arguments as before show that this agrees with the Δ^{-3} dependence which we actually find in practice.

In summary, the terms B_1^{4QP} and B_2 are found to vary as the inverse third power of Δ, while B_1^{2QP}, B_4, B_5 and B_6 vary as the inverse 1.7 power of Δ and B_3 as the inverse 2nd power. Thus the relative importance of the various terms seems to be strongly Δ dependent, and it is important to know the actual value of Δ in regions of deformations important to the fission process, i.e. at the saddle point.

Table 2 Dependence of mass parameter on shell structure

κ	Δ	B_1^{2QP}	B_1^{4QP}	B_2	B_3	B_4	B_5	B_6	B_{Corr}	B_{AD}
0.0577	1.07	792.3	560.6	-866.7	438.8	405.2	1481.1	7.5	2701.9	39.9
0.0400	1.07	615.7	358.8	-556.9	315.2	202.9	1080.0	1.2	2038.3	33.6

By changing the values of the $\vec{\ell}\cdot\vec{s}$ and $\vec{\ell}^2$ coupling constant κ, we can study the dependence of the mass parameter on the shell structure. When the pairing strength is readjusted so that the Δ is the same as before, there still remain peculiarities of the individual levels close to the fermi energy, as we can see in table 2. Thus the shell structure can have an appreciable effect.

The results for the asymmetric saddle point are of special physical interest, and are shown in the second row of table 3. In principle, the above discussion of pairing and shell structure dependent effects applies here as well.

Table 3 Dependence of mass parameter on mass asymmetry

	Δ	B_1^{2QP}	B_1^{4QP}	B_2	B_3	B_4	B_5	B_6	B_{Corr}	B_{AD}
Symm.	1.07	792.3	560.6	-866.7	438.8	405.2	1481.1	7.5	2701.9	39.9
Asymm.	1.08	597.8	531.7	-875.7	416.8	155.4	1119.5	10.0	1955.5	38.0

Our results show that even though there is a partial cancellation of corrections, the resultant term B_{Corr} is appreciable. In order to obtain

an estimate for the applicability of the cranking model we rewrite our initial equation

$$T = \frac{1}{2} (B_{AD} + B_{Corr} \dot{\alpha}^2) \dot{\alpha}^2$$

in the form

$$T = T_o (1 + \frac{2 B_{Corr}}{B_{AD}} T_o)$$

where

$$T_o = \frac{1}{2} B_{AD} \dot{\alpha}^2$$

may be approximately estimated by setting it equal to the pre-scission kinetic energy. From the first row of table 1 one obtains

$$\frac{2 B_{Corr}}{B_{AD}^2} = 3.39 \text{ MeV}^{-1}$$

Thus the corrections to the adiabatic model become large if T_o is only a fraction of an MeV. This casts severe doubt upon the usefulness of the adiabatic model as a starting point for a dynamic theory of fission.

References

/1/ V.M. Strutinsky, et al.; Rev. Mod. Phys. 44 (1972) 320

4.3 Division of Energy Between Nuclear Collective and Internal Degrees of Freedom

E.F. Chaffin and F. Dickmann

The energy increase induced by introducing finite collective velocities as in the previous articles /1,2/ can be of two types. The first is a kinetic energy associated with a collective or coherent motion of the nucleons, and the second is a heating of the internal particle motion in a non-coherent or random manner. In order to establish equations of motion for the collective variables α , one would like to be able to separate out the collective inertia and the viscous heating. Boneh, Blocki and Myers /3/, following a suggestion of S.E. Koonin, calculated the collective kinetic energy

obtained from a single particle shell model without residual interaction, by assuming that the collective velocity distribution $\vec{v}(\vec{r},t)$ can be deduced from the probability current density

$$\vec{j}_{a_n}(\vec{r},t) = \frac{h}{2mi}\left(\Psi^*_{a_n}(\vec{r},t)\vec{\nabla}\Psi_{a_n}(\vec{r},t) - \Psi_{a_n}(\vec{r},t)\vec{\nabla}\Psi^*_{a_n}(\vec{r},t)\right) \tag{1}$$

Thus

$$\vec{v}(\vec{r},t) = \frac{h}{\rho(\vec{r},t)}\ \mathrm{Im}\left(\sum_{n=1}^{N}\Psi^*_{a_n}(\vec{r},t)\vec{\nabla}\Psi_{a_n}(\vec{r},t)\right) \tag{2}$$

where Im denotes taking the imaginary part, and $\rho(\vec{r},t)$ is given by

$$\rho(\vec{r},t) = m\sum_{n=1}^{N}\Psi^*_{a_n}(\vec{r},t)\Psi_{a_n}(\vec{r},t) \tag{3}$$

where the a_n label the filled single particle orbitals. We present here an extension of this formula to the case of a many-body wavefunction including correlations, and discuss its consequences for the nature of the contributions to the collective kinetic energy.

In the case where $\Psi = \Psi(\vec{r}_1, \vec{r}_2, \ldots, \vec{r}_N)$ is a single Slater determinant, the expression for the density distribution

$$\rho(\vec{r},t) = m\sum_{i=1}^{N}\langle\Psi|\ (\vec{r}-\vec{r}_i)\ |\Psi\rangle \tag{4}$$

reduces to the single form of eq. (3). Similarly, the expression

$$\vec{v}(\vec{r},t) = \frac{h}{\rho(\vec{r})}\ \mathrm{Im}\ \langle\Psi|\ \sum_{i=1}^{N}\delta(\vec{r}-\vec{r}_i)\nabla_i\ |\Psi\rangle \tag{5}$$

is an appropriate generalization of eq. (2) for the collective velocity.

If we assume a single quasi-particle Hamiltonian one may expand the wavefunction $|\Psi\rangle$ in terms of the BCS ground state plus quasiparticle excitations:

$$|\Psi\rangle = c_o|0_{BCS}\rangle + \sum_{\nu\bar{\omega}} C_{\nu\bar{\omega}}|\ \nu\bar{\omega}\rangle + \sum_{\xi\bar{\eta}\chi\bar{\zeta}} C_{\xi\bar{\eta}\chi\bar{\zeta}}|\ \xi\bar{\eta}\chi\bar{\zeta}\rangle \tag{6}$$

where, in first non-trivial order one obtains

$$C_o = 1$$

$$C_{\nu\bar{\omega}} = i\alpha \frac{|\langle \nu\bar{\omega}|\frac{\partial}{\partial\alpha}|0_{BCS}\rangle|^2}{E_\nu + E_\omega} \qquad (7)$$

$$C_{\xi\eta\chi\zeta} = 0$$

using the fact that $C_{\nu\bar{\omega}}$ is pure imaginary, we find

$$\langle\Psi|\sum_{i=1}^{N}\delta(\vec{r}-\vec{r}_i)\nabla_i|\Psi\rangle \tilde{=} \sum_{\nu\bar{\omega}} U_\nu V_\omega C_{\nu\bar{\omega}} \{\langle\Psi_\omega|\vec{r}\rangle\nabla_{\vec{r}}\langle\vec{r}|\Psi_\nu\rangle - \langle\Psi_\nu|\vec{r}\rangle\nabla_r\langle\vec{r}|\Psi_\omega\rangle\}$$

$$+ \sum_{\nu\bar{\omega}} U_\nu V_\omega C_{\nu\bar{\omega}} \{\langle\Psi_{\bar{\nu}}|\vec{r}\rangle\nabla_{\vec{r}}\langle\vec{r}|\Psi_{\bar{\omega}}\rangle - \langle\Psi_{\bar{\omega}}|\vec{r}\rangle\nabla_r\langle\vec{r}|\Psi_{\vec{r}}\rangle\} \qquad (8)$$

From this expression one may conclude that, in lowest order, the contributions to the collective velocity from $\nu = \omega$ type eigenstates $|\nu\bar{\nu}\rangle$ are zero. In higher order one finds that they contribute through wavefunction renormalization and through the four quasiparticle terms. We thus find the change of the occupation amplitudes for having a pair of particles in an orbital and its time reversed counterpart can have no contribution to the collective kinetic energy, in lowest order in the coordinate velocities α.

In the context of the cranking model and its extension to higher order, one sees that in lowest order, the collective part of the energy increase should not include contributions from $|\nu\bar{\nu}\rangle$ excitations. For the asymmetric saddle mass parameter discussed in the previous article /2/, this exclusion reduces the adiabatic mass from 38 $\hbar^2$/MeV to 28 $\hbar^2$/MeV. In higher order, such a separation is not definable in an unambiguous manner. One expects that the use of a proper Lagrange constraint operator for the cranking would induce only collective motion, and knows that, for example, in the case of rotations no $|\nu\bar{\nu}\rangle$ excitations are induced by the Lagrange operator J_x (see ref. /4/). In the case under consideration here, however, one sees that both collective motion and internal motions are induced by finite velocities for the collective variables.

References

/1/ Contribution 4.1

/2/ Contribution 4.2

/3/ Y. Boneh, J. Blocki, W.D. Myers, Proc. of the 4th International Workshop

on Gross Properties of Nuclei and Nuclear Excitations, Hirschegg, (Austria) 1976, ed. F. Beck, E.R. Hilf, W.D. Myers, Technische Hochschule Darmstadt, Report No. AED-Conf.-76-015-000 (1976) p. 77

/4/ S.T. Belyaev; Mat. Fys. Medd. Dan. Vid. Selsk. 31, no. 11 (1959)

5. APPLIED NUCLEAR PHYSICS

5.1 NUCLEAR FUEL ANALYSIS

5.1.1 Gamma Ray Spectrometry for In-Line Measurements of ^{235}U Enrichment in a Nuclear Fuel Fabricating Plant*

P. Matussek and H. Ottmar

The nondestructive enrichment assay technique using gamma ray spectrometry has been applied for in-line monitoring the ^{235}U enrichment in a LWR fuel fabricating plant. The in-line system measures continuously the enrichment of low-enriched UO_2 powder prior to pelletizing with relative precisions and accuracies of $\simeq$ 0.5 % at two sigma. The precisions obtained during a continuous four-week run are consistent with counting statistics proving the insensibility of the system to environmental influences. The effect of variable sample age upon the assay accuracy has been studied more in detail both in the laboratory and at field sites. If present, it can be eliminated through proper calibration procedures. A new calibration technique based upon reference samples having the same enrichment but different ages has been successfully used to calibrate the in-line system.

* Proceedings of the Symposium on the Safeguarding of Nuclear Materials, Vienna, 20-24 October 1975, Vol. II (IAEA, Vienna, 1976) p. 223

5.1.2 In-Process Control of ^{235}U Enrichment in a LWR Fuel Fabrication Plant*

H. Ottmar and P. Matussek

This paper describes experiences on the use of the nondestructive ^{235}U enrichment assay technique using gamma ray spectrometry. Main emphasis is given to in-process enrichment measurements on low-enriched uranium oxide powder in a LWR fuel fabrication plant. The results from in-line measurements performed under real in-plant conditions demonstrate that the gamma technique provides an efficient tool for reliable enrichment control on a real-time basis. Details of a computerized system which is intended for extensive enrichment and process control in a fuel fabrication plant are given. In addition, laboratory enrichment analyses on powder and pellet

samples have been performed using NaI and Ge(Li) spectrometers. It can be concluded from these measurements that the accuracies now attained in gamma-spectrometric enrichment analyses compare favourably with those available from routine mass spectrometry.

*International Seminar on Nuclear Fuel Quality Assurance, Oslo (Norway), 24-28 May, 1976, Paper IAEA-SR-7/29, to be published

5.1.3 Assay of Plutonium in Process Wastes from Fuel Fabrication Plants

M.R. Iyer+ and H. Ottmar

Since the wastes from fuel fabrication plants and chemical laboratories to a large extent consist of low density material (paper, rags, gloves etc.) and usually are not mixed with fission products, the high sensitivity gamma technique for plutonium assay can be preferably applied to this category of wastes. The present work was aimed at standardizing the measurement of fissile plutonium in wastes using gamma spectrometry with a NaI detector. The method is a multi-group one which can give the total fissile plutonium content (^{239}Pu and ^{241}Pu) after correcting for matrix attenuation by using an external plutonium source. It can also check for the possibility of the presence of plutonium bearing materials with significant self-absorption, which usually cannot be corrected for by making a transmission measurement.

Fig. 1 gives the typical gamma spectrum of a plutonium sample as obtained with a NaI detector. To assay the fissile plutonium content (^{239}Pu and ^{241}Pu) in the waste samples, the energy groups as indicated in fig. 1 have been selected. *Group 1 (180 to 240 keV)* can be taken as a quantitative measure of the ^{241}Pu content for samples having a wide range of isotopic compositions. Counts to *Group 2 (290 to 470 keV)* arise mainly from ^{239}Pu and ^{241}Pu and to a lesser extent from ^{241}Am. Since ^{241}Am goes on slowly building up in plutonium samples its contribution is dependent on the age of the sample. For samples having less than 5 % ^{241}Pu and ages less than 2 years, the contribution from ^{241}Am to *Group 2* can be neglected and the counts may be regarded as due to ^{239}Pu and ^{241}Pu only. The energy *Group 3 (375 to 470 keV)* has been optimized to include counts due to ^{239}Pu preferentially. Computer simulated gamma spectra from plutonium of various

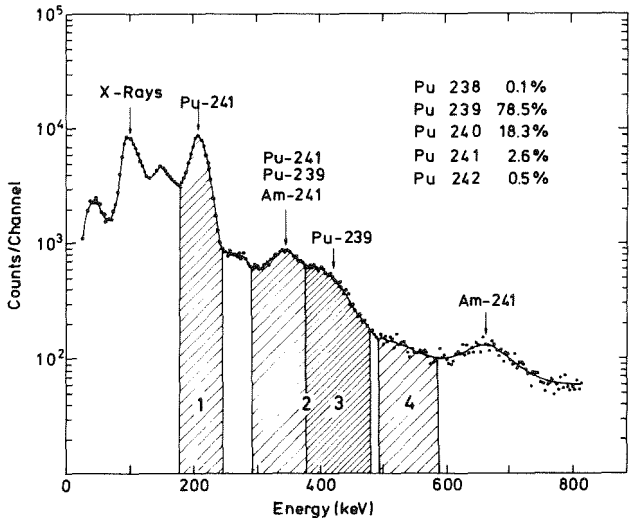

Fig. 1 Typical gamma spectrum of a plutonium sample as obtained with a NaI detector and energy windows selected for the fissile plutonium assay.

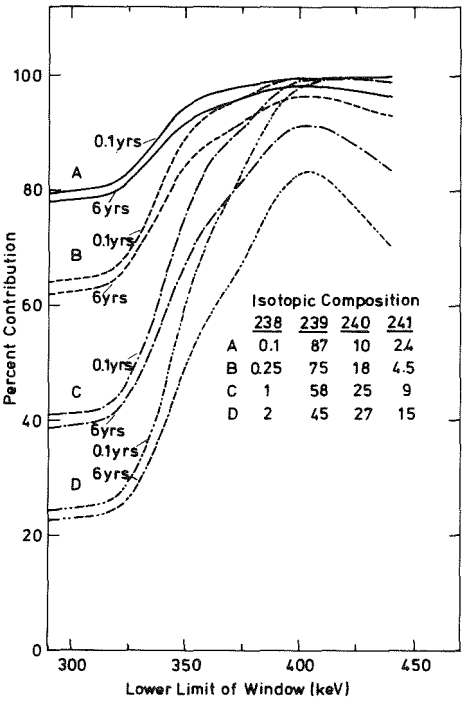

Fig. 2 Percent contribution of ^{239}Pu to the counts in the 400 keV complex. Upper window limit fixed at 470 keV.

isotopic compsotions have been used for this purpose. Some results of these optimization studies are illustrated in fig. 2 where the percent contribution of ^{239}Pu to the counts in the second half of the 400 keV complex as a function of the lower window limit, keeping the upper window limit at 470 keV, as calculated for some typical isotopic compositions is given. For samples having more than 75 % ^{239}Pu the counts in the selected energy interval for *Group 3* can be reasonably assumed to be proportional to the ^{239}Pu content.

Thus in principle one can set up simultaneous equations relating the unknown ^{239}Pu and ^{241}Pu contents to the counts in *Groups 1, 2 and 3*. Before doing this the intral counts C_1, C_2 and C_3 have yet to be corrected for the Compton contribution from higher energy gamma rays in the 650 keV complex which have significant contribution from isotopes other than ^{239}Pu and ^{241}Pu. The correction for this in the three groups has been done by taking a background

window in the 520 keV region *(Group 4)*. The remaining Compton contributions from *Group* 3 to *Groups* 1 and 2 need not be corrected for because they are mainly due to ^{239}Pu and ^{241}Pu and hence can be included in the constants of the equations. Thus, if C_1, C_2 and C_3 are the Compton corrected (for the 650 keV complex) counts per unit time (cps) in the respective groups and if P9 and P1 are the contents of ^{239}Pu and ^{241}Pu in the samples, then

$$\begin{aligned} A \times P9 + B &= C_1 \\ C \times P9 + D \times P1 &= C_2 \\ E \times P9 + F \times P1 &= C_3 \ , \end{aligned}$$

The constants can be solved for from C_1, C_2 and C_3 corresponding to standard samples having known amounts of plutonium and known isotopic composition.

The correction for matrix attenuation effects necessary for dense samples have been performed by transmission measurements with an external plutonium source. The corrected counts so obtained in *Group* 3 is then used to estimate ^{239}Pu and counts in *Group* 2 gives a measure of ^{241}Pu. A transmission measurement for the 208 keV group is not performed because usually the higher absorption coefficient at this energy involves the subtraction of two large quantities leading to low statistical precision. However, the ratio of the counts in *Group* 1 and 2 due to ^{241}Pu, after removing the contribution due to ^{239}Pu, correlates with the measured attenuation at 400 keV in the absence of large localized absorption. Any marked departure from this correlation indicates the presence of localized absorption. The ^{239}Pu content estimated from the counts in *Group* 3 could be in error in such cases.

The NaI technique as described here offers a considerably increased sensitivity as compared to the more elaborate Ge(Li) measurements. The comparison of the ^{239}Pu content measured in a variety of samples using both methods showed good agreement. Thus, the simpler NaI detector can be used with advantage for the assay of fissile plutonium in process wastes.

+On deputation from Bhabha Atomic Research Centre, Bombay (India)

5.1.4 Plutonium Isotopic Analysis by High Resolution Gamma Ray Spectrometry

H. Ottmar and M.R. Iyer[+]

A rather accurate determination of plutonium isotopic ratios can be made by high resolution gamma-ray spectrometry. The isotopic ratio N_i/N_k of two different isotopes i and k deduces from the simple relation

$$\frac{N_i}{N_k} = \frac{P_i}{P_k} \frac{I_k \cdot \lambda_k}{I_i \cdot \lambda_i} \frac{\varepsilon_k}{\varepsilon_i}$$

where P, I, λ and ε are the measured peak area, the absolute branching intensity, the decay constant, and the overall efficiency for gamma rays with energies E_i and E_k from isotopes i and k, respectively. In principle the isotopic ratios can be measured without use of any standards provided the relevant nuclear data, i.e. the half-lives and the branching intensities of the isotopes involved are very accurately known.

In order to test if this prerequisite is sufficiently fulfilled by the body of nuclear data now available for the plutonium isotopes, we have performed gamma-spectrometric isotopic measurements on the plutonium standard samples NBS 946, NBS 947, NBS 948 and BNS 949a. In particular, the measurements have been focused on the isotopic ratio $^{239}Pu/^{241}Pu$ which can easily be measured by gamma spectrometry. For this purpose the following pairs of gamma rays have been used:

Energy (keV)	Emitting isotope	Photon yield (Ref. /1/)
203.52	^{239}Pu	$5.630 \cdot 10^{-6}$
207.97	$^{237}U(^{241}Pu)$	$5.117 \cdot 10^{-6}$
	^{241}Am	$7.600 \cdot 10^{-6}$
419.19	^{241}Am	$2.760 \cdot 10^{-7}$
422.54	^{239}Pu	$1.190 \cdot 10^{-6}$

In all the samples ^{237}U has been in equilibrium with ^{241}Pu, hence its 207.97 keV gamma ray could be used as a direct measure for the ^{241}Pu content. The photon yield given for the 207.97 keV gamma ray includes the alpha branching ratio of $2.46 \cdot 10^{-5}$/2/ for ^{241}Pu decaying to ^{237}U. The 207.97 keV peak from $^{237}U(^{241}Pu)$ has an interfering contribution of a

gamma ray with the same energy emitted by ^{241}Am. To correct for this contribution which amounts to a few percent for older samples, the relative ^{241}Am content must be known. This correction has been made using the pair of gamma rays at 419 keV (^{241}Am) and 422 keV (^{239}Pu).

The efficiency ratio for the two gamma energies 203 and 208 keV was established from the counts under the 148.60 keV peak of ^{241}Pu and from counts under the peaks at 164.59 keV, 207.97 keV and 267.50 keV of ^{237}U along with the gamma branching ratios from ref. /1/. The measured relative efficiencies for each sample were fitted to a parabolic curve and the efficiency ratio for 203-to-208 keV was obtained from this. This procedure was applied to the gamma spectra from samples NBS 946 and NBS 947 and to gamma spectra previously measured from the samples NBS 948 and NBS 949a /3/. The maximum variation in efficiency between energies 203 keV and 208 keV was found to be 2 %.

For the evaluation of the isotopic ratio $^{239}Pu/^{241}Pu$ from the corrected net counts in the 203 and 208 keV peaks, the branching intensities of the two gamma rays and the half-lives of both isotopes must be known. Unfortunately the reported half-lives for ^{241}Pu range from 14 years to 15.16 years. Using these boundary values and the photon yields given above, isotopic ratios $^{241}Pu/^{239}Pu$ as listed in table 1 are deduced from the gamma measurements. The data sets obtained for both half-life values show a bias with respect to the mass-spectrometric data which is most likely due to uncertainties in the nuclear data used.

Table 1 Comparison of $^{241}Pu/^{239}Pu$ weight ratios obtained from gamma spectrometry and mass spectrometry using two different values for the half-life of ^{241}Pu

Standard	Date of gamma measurement	$^{241}Pu/^{239}Pu$ using $T_{1/2}$ = 15.16 y			$^{241}Pu/^{239}Pu$ using $T_{1/2}$ = 14 y		
		Mass spectr.	Gamma	Percent deviation	Mass spectr.	Gamma	Percent deviation
NBS 946	3/76	$3.965 \cdot 10^{-2}$	$4.339 \cdot 10^{-2}$	8.62	$3.900 \cdot 10^{-2}$	$4.007 \cdot 10^{-2}$	2.74
NBS 947	3/76	$4.953 \cdot 10^{-2}$	$5.466 \cdot 10^{-2}$	9.36	$4.871 \cdot 10^{-2}$	$5.048 \cdot 10^{-2}$	3.63
NBS 948	5/74	$4.740 \cdot 10^{-3}$	$5.193 \cdot 10^{-3}$	8.76	$4.707 \cdot 10^{-3}$	$4.796 \cdot 10^{-3}$	1.89
NBS 949a	5/74	$1.609 \cdot 10^{-3}$	$1.751 \cdot 10^{-3}$	8.51	$1.592 \cdot 10^{-3}$	$1.617 \cdot 10^{-3}$	1.57
				Mean 8.81			Mean 2.46

In order to eliminate the present uncertainties in the half-lives as well as alpha and gamma branching intensities, very accurately known isotopic standards should be rather used for calibration purposes in high accuracy isotopic analysis work using gamma ray spectrometry. In this way isotopic ratios are directly related to *ratios* of peak areas which can be much more accurately determined than *absolute* branching intensities. Work following this procedure is in progress.

+ On deputation from Bhabha Atomic Research Centre, Bombay (India)

References

/1/ R. Gunnink, J.F. Tinney; Analysis of Fuel Rods by Gamma Spectroscopy, Report UCRL 51086 (1971)

/2/ R. Gunnink, R.J. Morrow; Gamma-Ray Energies and Absolute Branching Intensities for ^{238,239,240,241}Pu and ^{241}Am, Report UCRL 51087 (1971)

/3/ H. Ottmar; Report KFK 1980 (1974) p. 2-7

5.1.5 Gadolinium Concentration Measurements in Poisoned BWR Fuel Pellets by X-ray Fluorescence Analysis

P. Matussek, I. Michel-Piper, H. Ottmar, and S. Heger

Small amounts of gadolinium are added to part of the fuel for boiling water reactors. Typical concentration levels of gadolinium embedded into the UO_2 matrix of the fuel pellets range from 1 % to 4 %. In a fuel fabrication plant the correct gadolinium content of finished pellets has to be checked for quality control reasons, preferably before loading the pellets into the fuel pins. A potential method to perform these control measurements continuously is X-ray fluorescence analysis. We have investigated the capability of the method for this particular purpose. In view of its potential application in a production environment the present work was aimed at evaluating a measurement system as simple and reliable as possible. Therefore NaI spectrometry was tried rather than high resolution spectrometry with solid state detectors.

A convenient and efficient radiation source for exciting the 43 keV K_α X-rays of gadolinium is ^{241}Am. For our test measurements we have chosen a line source and the "side source" geometry as the most practicable source-

specimen-detector arrangement (fig. 1). The detector used was a 2" x 1" NaI detector. A zircaloy tube having a window of 6 mm width served as sample holder for the pellets.

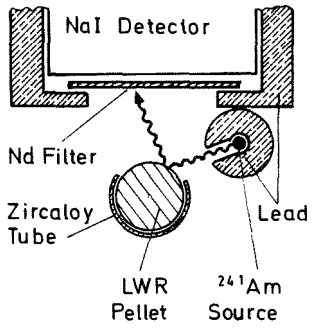

Fig. 1 Geometrical arrangement for the X-ray fluorescence analysis of gadolinium in BWR fuel pellets.

In the lower resolution NaI spectrometry the coherent and Compton scattered radiation from the ^{241}Am source partially interferes with the induced X-rays from gadolinium. This interfering radiation can considerably be suppressed by placing a filter of neodymium between sample and detector (fig. 2). The K-absorption edge of neodymium (43.57 keV) lies just above the energy of the gadolinium K_α radiations (K_{α_1} = 43.00 keV, K_{α_2} = 42.31 keV), hence a thin filter of neodymium (0.25 mm) effectively attenuates gamma radiations with energies above the K_α peak of gadolinium.

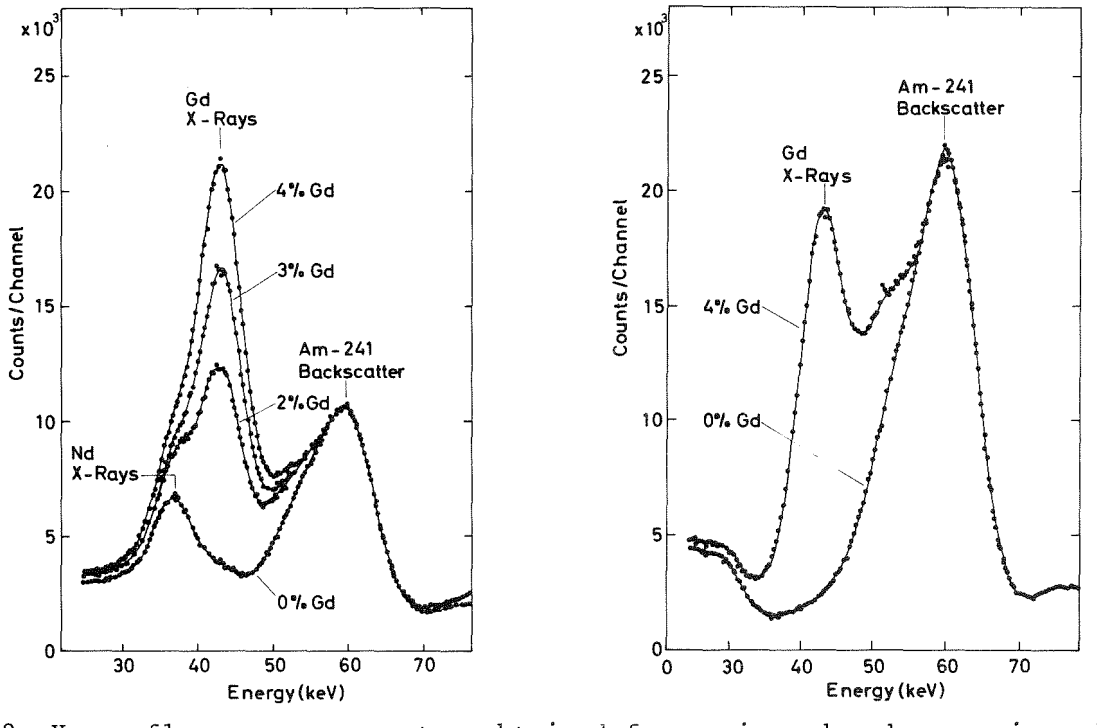

Fig. 2 X-ray fluorescence spectra obtained from poisoned and unpoisoned BWR fuel pellets. Spectra on the left taken with a 0.25 mm thick filter of neodymium placed between sample and NaI detector, spectra on the right taken without filter.

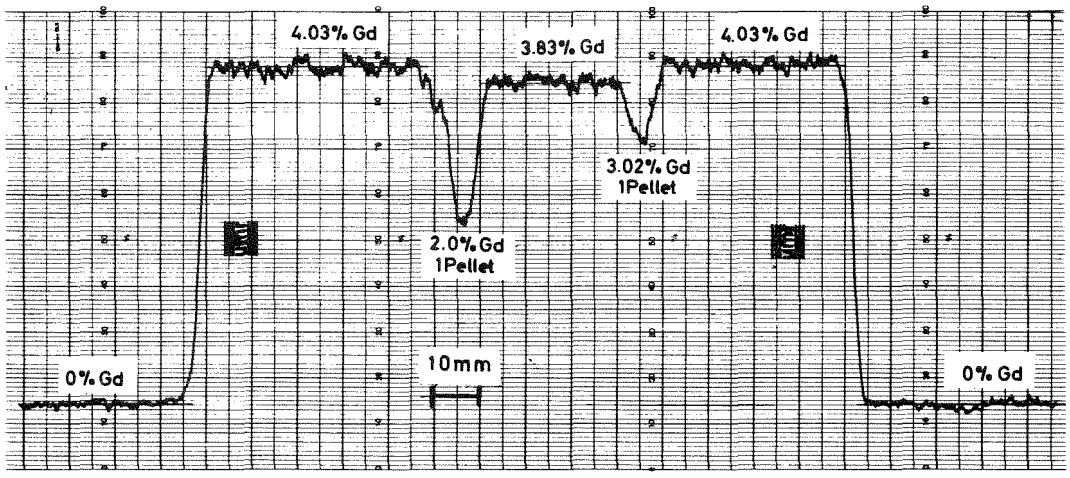

Fig. 3 Stripchart record showing the effect of single "rogue" pellets. Test conducted using a 4 mCi ^{241}Am source with scan speed of 10 mm/min.

Typical net peak count rates in the K_α peak of gadolinium obtained with a 4 mCi ^{241}Am source are in the order of 100 counts/sec and % Gd. A stripchart record of a test run conducted at this source strength is shown in fig. 3. Here a column of fuel pellets with a gadolinium enrichment at the 4 % level has been moved in front of the irradiation source and the gamma detector at a scan speed of 10 mm/min (which corresponds to a scan speed of 1 pellet/min). The intentionally inserted single "rogue" pellets having gadolinium enrichments of 2 % and 3 % are easily detected.

Assuming that the usually occuring discrete gadolinium concentration levels of 1,2,3 and 4 % should be safely discriminated against each other (95 % confidence level) at a scan speed of 1 pellet/sec then an ^{241}Am source strength of only 5 mCi is needed. The gadolinium concentrations ranging from 1 % to 4 % can be determined with an accuracy of 10 % at the same scan speed when source strengths in the order of 100 mCi are used. The total count rate in the NaI detector would then increase to approximately 25000 counts/sec which can be easily managed with standard electronics. Thus, the X-ray fluorescence method based on NaI spectrometry represents a fast, simple and low cost technique for performing gadolinium enrichment control measurements on fuel pellets.

5.1.6 A Portal Monitor for the Detection of Fissile Materials

P. Matussek and I. Michel-Piper

The safeguarding of fissile materials against unauthorized diversion by persons who have access to nuclear facilities is of increasing importance for national as well as international safeguarding authorities. Thus, a portal monitor was developed and tested at the personnel portal of the Karlsruhe SNEAK facility. The monitor was constructed as a lock for persons entering and leaving the fissile material access area. It consists of a detection cell (like a phone box) with two doors arranged opposite to each other. Only one of the doors can be open at a time. The gamma radiation associated with the radiative decay of all fissile material serves as an indicator for the presence of special nuclear material (SNM) carried away. Two large NaI detectors in the lock are used to detect the gamma radiation.

A personnelportal monitor should provide a high sensitivity for small amounts of SNM even under varying background radiation conditions. On the other hand it should not impede the traffic flow through the portal by an undesirable high number of false alarms. Therefore, instead of a fixed alarm threshold a sliding alarm level technique is used: The background radiation count rate and its associated standard deviation are continuously measured as long as the lock is unoccupied. The actual values are updated in preselectable time intervals. An audible and visible alarm is generated when the lock is occupied and the gamma counting rate exceeds the alarm threshold, which is calculated from the previously measured background signals plus n times the standard deviation of the background counts (n selectable from 2 to 5). In the case of an alarm both doors of the cell are automatically locked so that the person carrying nuclear material cannot leave the controlled area. The doors can then only be opened by authorized persons (e.g. security forces, safeguards inspectors). On the other hand, when the lock is occupied and the count rate then measured does not exceed the alarm threshold, the outer door opens and the lock can be left. The electronics and the alarm decision logic are described more in detail in ref. /1/.

The sensitivity of the gamma monitor is influenced by many variables such as size and shielding of the lock, the level and spectral distribution of the background radiation, the type, position and spectral response of the detector, the gamma energy window setting for optimum signal to background ratio etc. Also self-absorption effects and the possible use of shielding materials have to be taken into account when specifying the sensitivity performance for various fissile materials.

The prototype gamma lock installed at the SNEAK facility has inner dimensions of approximately 90 x 130 x 220 cm. The lock is equipped with two 6" x 2" alpha stabilized NaI detectors. The detectors are located at two opposite walls of the cell at different distances from the floor to achieve a fairly homogeneous spatial distribution of the detector response over the whole body of a person staying in the center of the lock. Obviously there are regions of lower sensitivity in the corners of the cell. This problem can be solved by using more and / or larger detectors or by choosing a more appropriate shape for the measuring cell than the rectangular one.

The detection window includes gamma rays from 50 to 500 keV. This window setting seems to be a good compromise for the detection of shielded and unshielded U and Pu with adequate sensitivity. In tab. 1 the minimum amounts of U and Pu are given which can be detected at a 90 % confidence level. The

Table 1 Minimum detectable quantities of fissile material at 90 % confidence level with a false alarm rate <0.1 %. Materials shielded with 3 mm brass.

	Recommended values USAEC Reg. Guide 5.7	SNEAK-lock (material carried on body)	SNEAK-lock (material in the corner)
>90 % ^{235}U	3 g	0.3 g	1.5 g
90 % ^{239}Pu	0.5 g	0.005 g[1)]	0.045 g

[1)] extrapolated value

samples were moderately pressed U_3O_8 and PuO_2 powders of cylindrical shape and shielded with 3 mm brass. The alarm threshold was set to a false alarm rate of less than 0.1 %, i.e. three standard deviations above the mean background counting rate. The minimum detectable quantities are given a) for material carried on the body of a person (average of the four positions top of the head, shirt pocket, pant pocket and inside the shoes) and b) for the worst case position in the corner of the lock. The counting time was 4 sec and the mean background count rate was about 800 counts/sec. For comparison the recommended quantities of the USAEC Regulatory Guide No. 5.7 for doorway monitors are given in the first column of tab. 1.

References

/1/ P. Matussek; Report KFK 1980 (1974) p. 2-37

5.2 ELEMENTAL ANALYSIS

5.2.1 Activation Analysis of Manganese Nodules with 14 MeV Neutrons*

H. Eberle

For the deep-sea exploration of manganese nodules, the Gesellschaft für Kernforschung mbH, Karlsruhe, has developed a sledge, which enables "in-situ"-analysis of these nodules. The technique is based on neutron induced capture γ-spectroscopy with a ^{252}Cf neutron source. The induced γ-rays will be detected by a Ge-detector. The problems of handling and of radiation from the ^{252}Cf source can be reduced by using a neutron generator which can be switched off and a NaI(Tl)-detector system. Experiments were done to find out the expected accuracy of the analysis of manganese nodules by activation analysis using 14 MeV neutrons as an alternative method, which allows the application of a NaI(Tl)-detector. The principle feasibility of this technique is demonstrated, and the problems of the "in-situ"-analysis are discussed.

* Report KFK 2291 (1976)

5.2.2 Investigation of Bulk Density Determination and Filling Level Indication in the MANKA Manganese Nodule Analysis System

H. Eberle

The GfK Karlsruhe has developed a manganese nodule analysis system MANKA, which is based on thermal neutron capture gamma spectroscopy /1/. For an exact analysis of the metal content of the ore nodules the thermal neutron flux distribution and the bulk density in the sample container must be well known in addition to the (n,γ)-spectra /2/. The bulk density is determined from transmission measurements of a 30 mCi ^{228}Th-γ-line source using a NaI(Tl)-scintillation counter. The accuracies indicated in the previous laboratory experiments, which were extrapolated from measurements with a 30 mCi ^{24}Na-source, had to be confirmed experimentally, using a ^{228}Th-source. The transmission measurements were made with freshwater, sea water, ore nodules, and pebble stones. The schematic geometry of the experiment is shown in fig. 1 . The

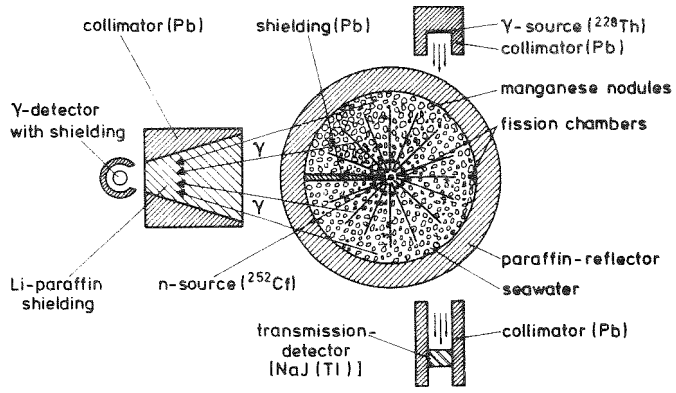

Fig. 1

Schematic layout of the experiment.

measurements of pebble stones served to determine their volume fraction in the sample container because this value is necessary for bulk density calculation. Recording and evaluation of measured data are described in detail in ref. /2/.

The investigations have demonstrated that the total error given in ref. /2/ for bulk density and ore nodule mass determination will not exceed $\pm$ 8 % during 15 min analysing time in the "in-situ"-experiment. It has been taken into account that the analytical system will be employed at the end of 1976 when both a neutron source of higher activity (giving a higher gamma background in the transmission spectrum) and a lower activity ^{228}Th-source will be used.

Because of the lower activity of the ^{228}Th-source the filling level indication in the sample container cannot be realized as planned during the "in-situ"-operation /3/. The counting rate statistics in the transmission spectrum within the ^{228}Th 2614 keV gamma energy range is no longer sufficient for short measurement intervals (about 1-2 s) and simple summation of channel contents to make a distinction between pure sea water and a sea water-nodule mixture. Therefore, the energy range of the 2223 keV gamma line of the hydrogen neutron capture gamma radiation will be used in the transmission spectrum. The advantage of this modification is that the difference of counting rates between sea water and sea water-nodule mixture (>20 %) only depends on the neutron source strength provided that the conditions of measurement are constant. Table 1 shows the relationship existing between the time of measurement t_m and the probability P of erroneous interpretation of the filling level characterized by the standard deviation σ of counting rate differences Δ N for

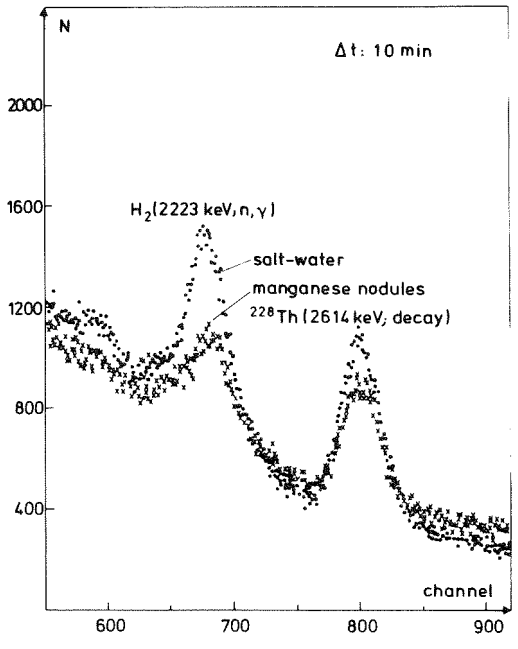

Fig. 2

Part of a transmission spectrum measured with a NaI(Tl) detector (2.6" x 2.6").

sea water and for a sea water-nodule mixture. So, it is possible within a short period of time to decide whether the filling level has been attained in the sample container.

Table 1

P(%)	ΔN	t_m (sec)
31.7	1 σ	0.3
4.5	2 σ	1.0
0.3	3 σ	2.0

References

/1/ J. Lange, U. Tamm, H. Würz; Meerestechnik-Marine-Technologie 6 (1975)50

/2/ H. Würz, H. Eberle; Report KFK 2160 (1975)

/3/ U. Fanger, R. Pepelnik, H. Würz, H. Eberle, Report KFK 1849 (1974) 160

5.2.3 Trace Element Analysis by Proton Induced X-Ray Fluorescence

H. Sobiesiak and F. Käppeler

Trace analysis by proton induced X-rays has been applied to various samples, to ion implanted or evaporated layers as well as to aerosol samples and biological samples.

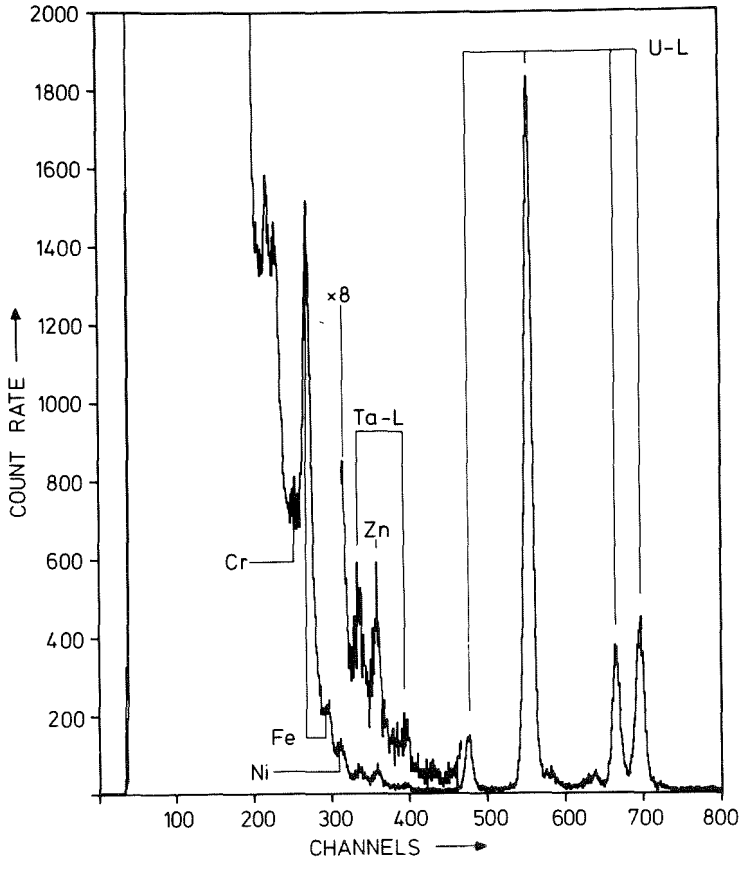

Fig. 1 X-ray spectrum from proton bombardment of an uranium layer evaporated onto a carbon foil. Beside the U-L-lines also traces of Ta, Zn and stainless steel (Fe, Cr, Ni) can be seen.

In fission physics very often extremely thin fissile layers evaporated onto carbon foils are used. Only in thin samples and thin backings the energy loss and straggling of fragments is sufficiently small to allow for corrections without too large uncertainties. In this context it was of interest to investigate whether the evaporated layers of uranium show prominent contaminations, for example from the tantalum boat. Fig. 1 shows a X-ray spectrum of such a sample consisting of 150 $\mu g/cm^2$ uranium on a 30 $\mu g/cm^2$ carbon backing. The dominating peaks correspond to the uranium L-lines, but also small amounts of Ta and Zn were observed. The Cr-, Fe- and Ni-lines indicate the presence of stainless steel.

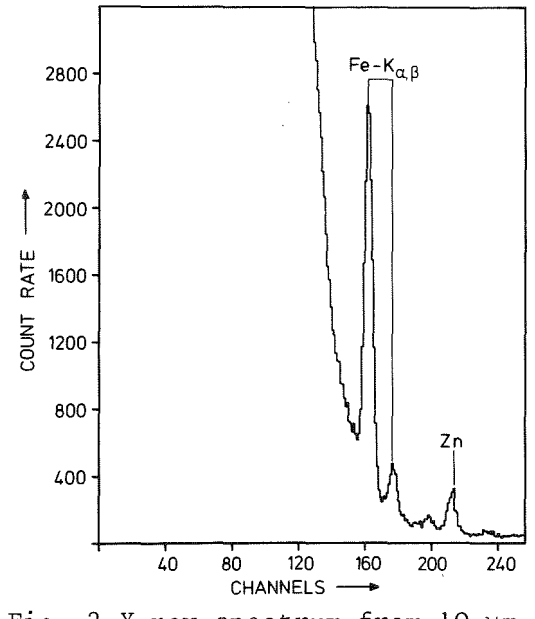

Fig. 2 X-ray spectrum from 10 µm thick cut of a rat brain. The Fe-K-lines from hemoglobin can be used as a measure for the blood supply of the brain.

At the Pathological Institute of the University of Heidelberg the blood supply in brain is investigated as a function of various parameters. It was tried whether it might be possible to measure changes in the blood supply by means of ion induced X-rays. A first attempt was made with a 10 µm thick microtome cut of a rat brain prepared onto a thin, aluminized mylar foil. The measured X-ray spectrum is shown in fig. 2. On the tail of the bremsstrahlung background the Fe-K_α-line from the hemoglobin is well isolated. The count rate is high enough to compare the blood supply in various brain regions with an accuracy of about 2 %.

5.2.4 Suppression of Radioactive Background in Ion Induced X-Ray Analysis*

H. Sobiesiak, D. Heck,and F. Käppeler

The paper describes a method to reduce the decrease in sensitivity of ion induced X-ray analysis by the presence of a radioactive background. Measurements were made using a pulsed proton beam of 5 nA average current with a pulse width of 10 nsec and a repetition rate of 250 kHz. With typically 30 nsec time resolution of the Si(Li)-detector a background suppression of about 40 : 1 was achieved. An improvement of this value is possible by using a smaller repetition rate and a narrower time window.

*Prod. 2nd Int. Conf. on Ion Beam Surface Layer Analysis, Karlsruhe, Sept. 15-19, 1975, ed. by O. Meyer, G. Linker, F. Käppeler, Vol. II (Plenum Press, New York, 1976) p. 803

5.3 MEDICAL APPLICATIONS

5.3.1 Radioactive Purity of ^{125}Xe Samples for Medical Applications

W. Comper[+], S. Göring, and A. Hanser

Previously we reported /1/ studies of the question whether the isotope ^{125}Xe is a better radiopharmaceutical for lung function and blood flow investigations than the normally used ^{133}Xe. This question would be best answered finally by some in vivo investigations.

Radioactive xenon for in vivo investigations should have a high degree of radioactive purity for the following reason: the biological half-lives of inert gases are in the order of one minute. Radioactive contaminations of the xenon samples, however, may be held up in the body of the patient for a long time and can give rise to a high radiation dose. We produce the ^{125}Xe samples by irradiating potassium iodide with deuterons of 47 MeV. The potassium iodide is enclosed in a cover made from copper, zinc and tin solder. After irradiation the ^{125}Xe is heated off from the target and condensed in an ampoule cooled by liquid nitrogen. Such a sample of about 50 mCi has been examined for radioactive impurities by means of a Compton-suppression γ-spectrometer and a high resolution Si(Li) X-ray detector. In addition to the well known γ-peaks resulting from ^{125}Xe, ^{127}Xe, and ^{125}I, the measured spectra showed an extremely weak ^{41}Ar activity and some weak peaks which originate very likely from the decay of ^{125}Xe, too. The identification assignments are based on the precisely measured γ-energies and the observed half-lives. The few unassigned peaks which all have very small intensity are listed in table 1. Most of them decrease with a half-life which is consistent with that of ^{125}Xe. Perhaps these are also to be assigned to the decay of ^{125}Xe. From an irradiated target dummy we have extracted in the manner mentioned above only unimportant, totally negligible amounts of radioactivity. The only clearly recognized impurity from which a significant radiation dose for the patient may result is ^{125}I, the daughter nuclide of ^{125}Xe. This nuclide has to be removed by suitable filters immediately before application, because it is formed continuously from ^{125}Xe.

Table 1 Unassigned peaks in the photon spectrum of the ^{125}Xe sample ranging from 20 to 2000 keV

Photon energy	Half-life	Rel. intensity with respect to the most intense γ-ray of ^{125}Xe
61.7 ± 0.4 keV	∿17 h	1.1×10^{-4}
216.9 ± 0.6 keV	>22 h	0.4×10^{-4} 200 h after irr.
256.18± 0.25 keV	∿17 h	0.4×10^{-4}
535.5 ± 0.6 keV	∿17 h	0.2×10^{-4}
1325.2 ± 0.4 keV	∿17 h	0.2×10^{-4}
1385.25± 0.20 keV	∿17 h	0.6×10^{-4}

To check whether any unallowable impurities are missed by the measurements, we have compiled all nuclides which can be produced directly or indirectly by the irradiation of the covered target. For all γ-emitters among these nuclides we have deduced the lower limits of detection from the measured spectra. This has also been possible in an indirect way for the majoritiy of the pure ß-emitters. The values indicate sufficient purity of the sample. A possible, but not probable contamination of the ^{125}Xe sample by the pure ß-emitters ^{32}P, ^{33}P, ^{35}S, and ^{121}Sn, however, cannot be excluded in this way. This problem may be removed for the first three of these nuclides if we use sodium iodide rather than potassium iodide for target material because ^{32}P, ^{33}P, and ^{35}S are produced from potassium during irradiation.

+Abteilung Reaktorbetrieb und Technik

References

/1/ W.E. Adam et al. ; Report KFK 2223 (1976) p. 76

5.3.2 Recent Developments in the Production of ^{123}I at the Karlsruhe Isochronous Cyclotron

K.H. Assmus, F. Michel+, H. Münzel+, F. Schulz, R. Schütz, and H. Schweickert

In the past year we were asked by several clinical hospitals in the southern part of Germany to produce useful quantities of ^{123}I for application in

nuclear medicine. This was prompted by the recognition of ^{123}I as the most favourable radioisotope of iodine for in vivo applications /1-3/. Its 159 keV gamma ray,which is 83 % abundant, provides ample penetration, is well suited for use with high-resolution γ-cameras, and is detected with more than 80 % efficiency in thin detector crystals. Furthermore, its 13.3 hr half-life and the absence of beta radiation result in a very low radiation dose to the patient. Thus, the dose from ^{123}I is only a few percent of that caused by a comparable quantity of the ^{131}I now in common use.

Therefore,since December 75 a group of the Institut für Radiochemie and the Cyclotron Laboratory is working on a routine method for ^{123}I production at the Karlsruhe Isochronous Cyclotron. The first aim was to produce 20-40 mCi of ^{123}I once every week. The nuclear reaction chosen is ^{124}Te (p,2n) because the energy of our cyclotron is not high enough for the ^{127}I (d,6n)^{123}Xe reaction, whereas high internal and external currents of protons at 26 MeV are routinely available. The best target found so far is enriched tellurium dioxyd /4/ irradiated after the first electrostatic deflector. Fig. 1 shows the TeO_2-target on a platinum backing inside a so-called water target /5/. The beam passes through a 0.1 mm copper window and a 0.1 mm water film onto the target.

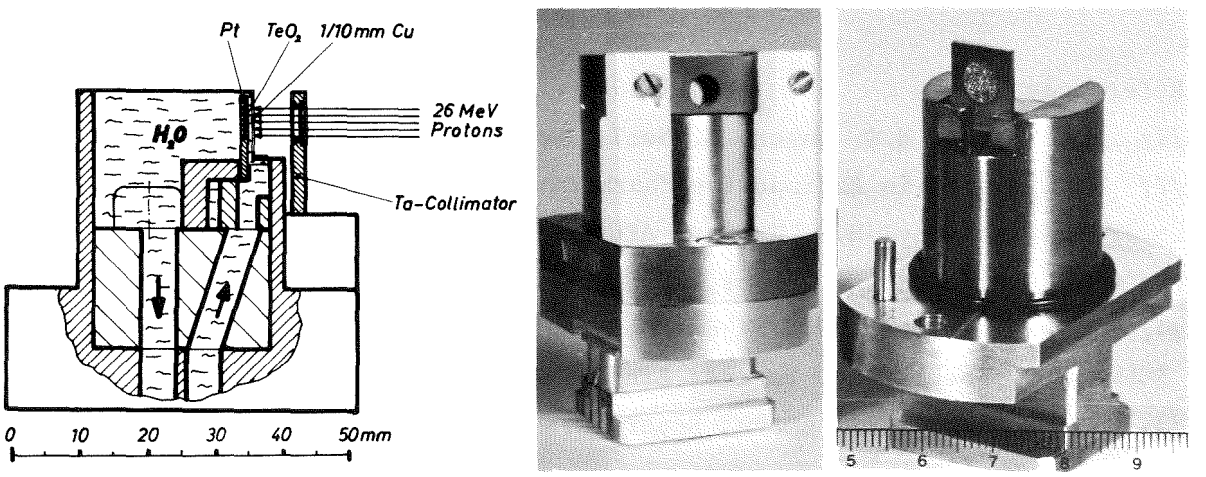

Fig. 1 Principle and photograph of the irradiation set-up for ^{123}I production. The glassy 150 mg/cm^2 TeO_2 (^{124}Te 96 %) is melted into a platinum metal backing. We have tested this kind of target several times at beam currents of 40 µA of protons without any problems.

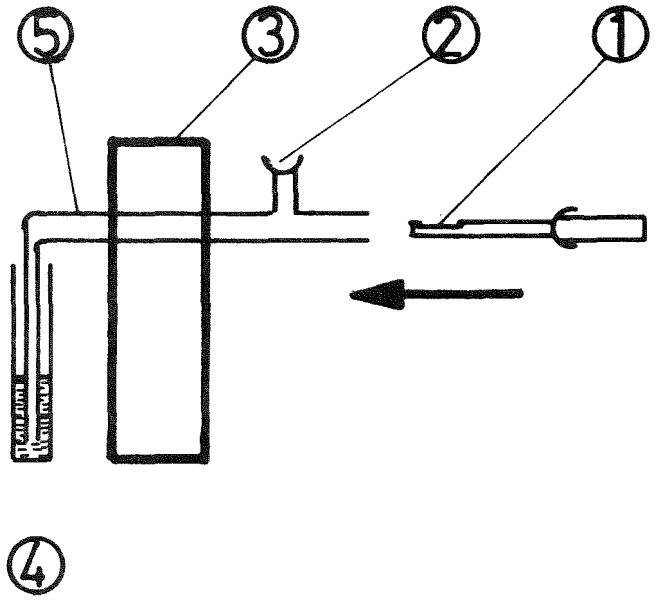

Fig. 2 Apparatus for separation of iodine from the irradiated TeO_2 target:
(1) platinum with TeO ,
(2) O_2 gas flow (20 ml/min),
(3) oven (750°C),
(4) 0.001 M NaOH solution,
(5) quartz tubes.

The extraction of iodine is achieved by dry destillation at 750°C (fig. 2). The yield after extraction is 8 mCi/μAh, and the contamination by ^{124}I is 0.8 %. The production scheme described above will be tested till December 1976 for small quantities (100 mCi once every week) in a pilot study together with the Nuklearmedizinische Klinik rechts der Isar in München and the Deutsche Krebsforschungszentrum Heidelberg.

+Institut für Radiochemie

References

/1/ W.G. Myers, H.O. Anger; J. Nucl. Med. 3 (1962) 183

/2/ W.G. Myers; in Radioactive Pharmaceuticals, eds. G.A. Andrews, R.M. Kniseley, H.N. Wagner; AEC Symposium Ser. 6, Springfield (1966) p. 217

/3/ B.A. Rhodes, H.N. Wagner, M. Gerrard; Isot. Rad. Tech. 4 (1967) 275

/4/ R. van de Bosch, J.J.M. de Goeig, J.A. van der Heide, J.F.W. Terloolen, H.M.J. Theelen, C. Zegers; Eindhoven, private communication (1976)

/5/ F. Schulz, H. Bellemann; Report KFK 685 (1967)

5.3.3 The High Power 14-MeV Neutron Generator Tube KARIN*

K.A. Schmidt and H. Dohrmann

For use in fast neutron radiotherapy and fast neutron activation analysis a compact closed system neutron generator tube based on the (d,t)-fusion reaction has been developed. The source strength of 5×10^{12} n sec^{-1} gives internal irradiation flux densities of 6×10^{10} n cm^{-1} sec^{-1} at a useful probe volume of 25 cm^3. The external neutron beam tissue dose at 90 cm distance from the source outside of a 70 cm long collimator amounts to 20 rd/min. The life expectancy of the tube is several hundred hours.

*Atomkernenergie 27 (1976) 159

5.3.4 Installation of a Neutron Generator Tube for Cancer Therapy

K.A. Schmidt and H. Dohrmann

The clinical model prototype of a fast neutron generator /1,2/ for cancer therapy was installed in 1976 at the German Cancer Research Center in Heidelberg by a licensee (Emile Haefely & Co., Basel, Switzerland). Initial tests with this clinical unit included dosimetry and neutron field mapping. Clinical research on fast neutron cancer therapy will follow shortly.

The neutron tube KARIN is housed in the center of a heavily shielded source head mounted on a rotating gantry (see Fig. 1) which enables to revolve the neutron tube around the patient's couch in a horizontal axis by $\pm$ 120°.

The shield for the source head is designed such as to reduce the RBE-weighted dose of radiation leakage at the outside to less than one percent of the useful radiation directed at the patient through the collimator inserts. The quality of the shielding is verified by measurements of the radiation doses at the outer surface of the source head. Fig. 2 shows the local dependence of the leakage radiation for fast neutron, gamma, and total dose*. The values are

*The dose measurements were performed by K.H. Höver and H. Schuhmacher of the DKFZ to whom we are endebted for communicating their results prior to publication.

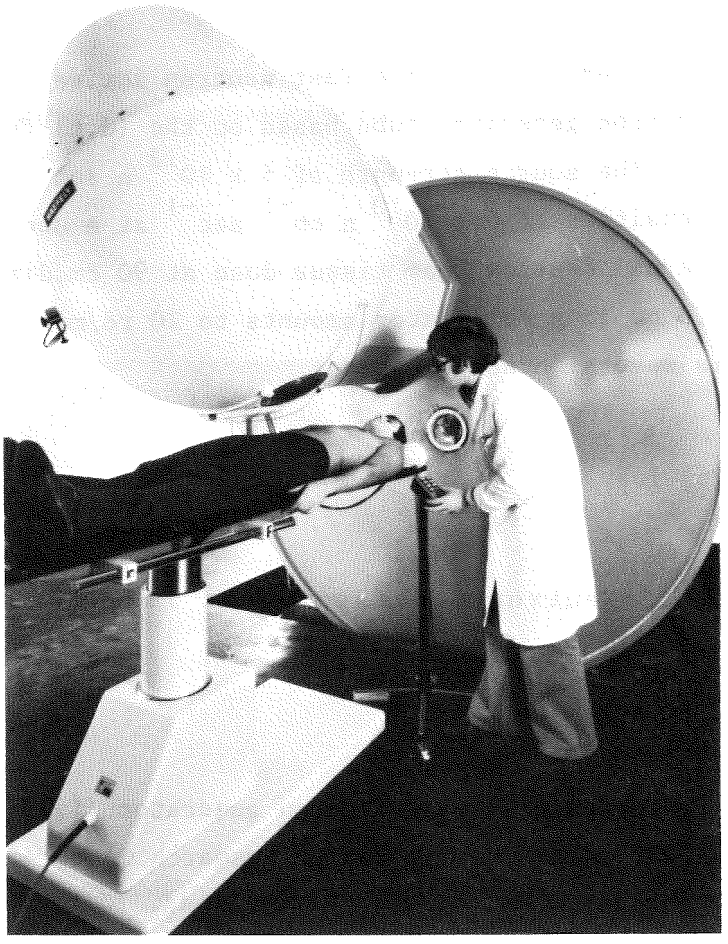

Fig. 1 Source head mounted on a gantry rotating around a patient.

related to a useful neutron dose of 100 rd within the collimated beam at 1 m source-detector distance. The measurements were performed with calibrated thermoluminescence dosimeters, which show sufficient sensitivity and linearity at dose rates of 10^{-2} - 10^{2} rd.

To shield the patient from γ-radiation emitted from activated parts of the tube and the source head, lead shutters are provided with a thickness of 6 cm at the entrance of the collimator insert and of 2 cm at the exit. Interchangeable steel collimators define and permit variation of the size and shape of the treatment field.

A hand-held control (see Fig. 1) positions the treatment couch to accommodate isocentric rotation of the source head and collimator system. Visual centering aids are used for locating the isocenter and for the patient setup. A light source inside the source head projects the effective beam area onto the patient's skin prior to exposure to the neutron beam. The rotating gantry positions the

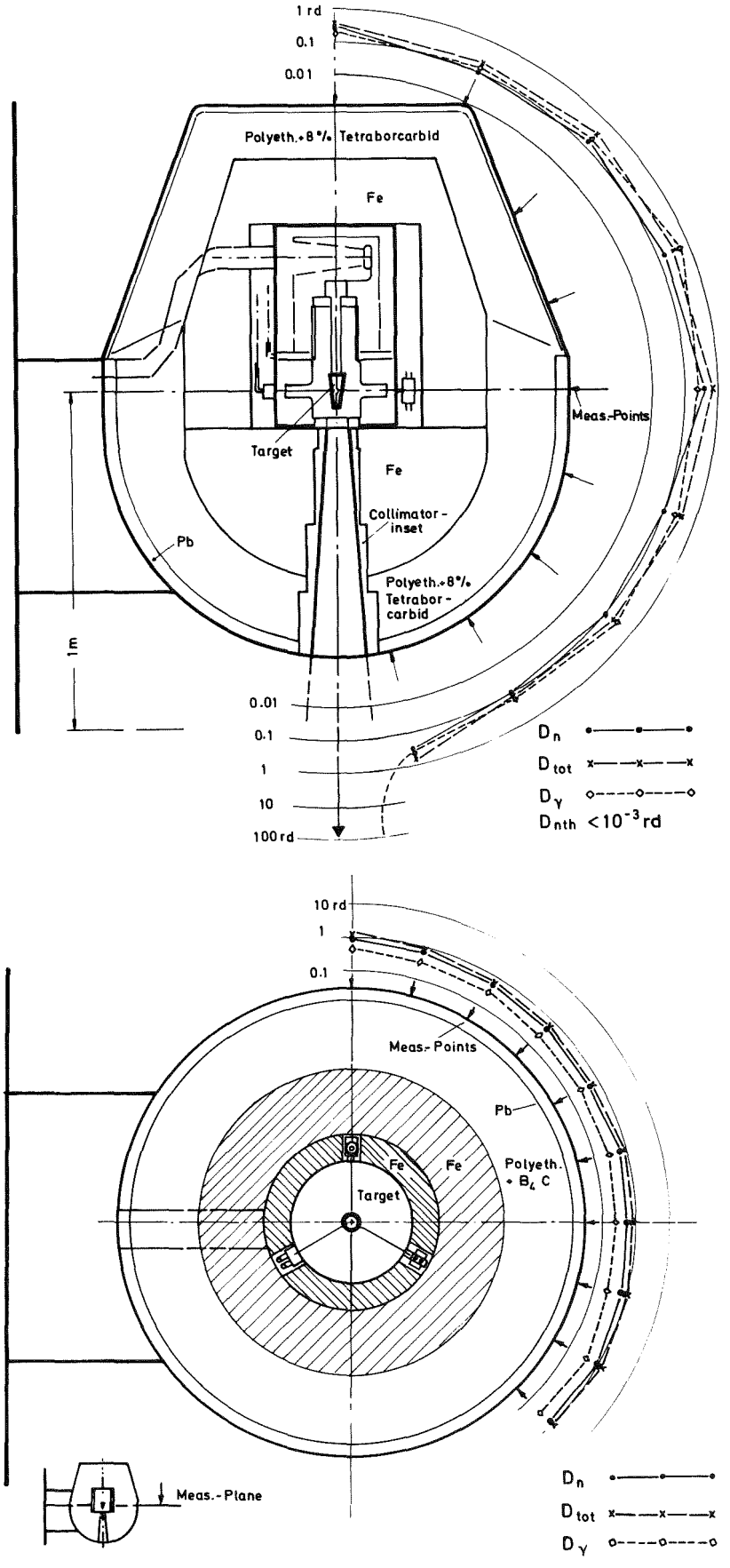

Fig. 2 Leakage radiation outside the neutron generator tube shielding. The values are related to a useful neutron dose of 100 rd within the collimated beam at 1 m source-detector distance.

source head and provides an isocentric motion of the source for multiport treatment or arc therapy, thus allowing location of a specific point on the patient at the isocenter and then rotating the source head around this axis with an accuracy of about 1 mm.

This Haefely-GfK neutron generator offers the same flexibility and mobility of the source head as a betatron. The source head weighs approximately 8.5 tons. The total weight of the neutron generator, including the rotating gantry, is about 25 tons.

A radiation monitoring system controls both the neutron output of the generator and the patient dose. Dose delivery is monitored by a tissue-equivalent ionization chamber positioned in the collimated neutron beam. Redundancy is provided by a fission chamber adjacent to the sealed source but out of range of the collimated beam.

Perfectly stable operation of the KARIN generator tube has been achieved by the automatic gas-pressure control and the fast-acting current-control system of the ring-electrode voltage.The current-control system permits the tube to be switched on and attain full power within a fraction of a second.

References

/1/ K.A. Schmidt, H. Dohrmann; Report KFK 2223 (1975) p. 78

/2/ K.A. Schmidt, H. Dohrmann; Atomkernenergie 27 (1976) 159

6. TECHNICAL DEVELOPMENTS

6.1 CYCLOTRON

6.1.1 Operation Summary of the Karlsruhe Isochronous Cyclotron

F. Schulz and H. Schweickert

During the period of report the machine was in full operation (see table 1). The cyclotron beam was used for irradiations for 7251 hours, which amounts to 88.7 % of the total shift time. Since we needed no shut down time in this period and since the ratio of system failures to the total scheduled shift time decreased to 6.3 %, the available beam time increased by 352 hours as compared to the past year. The recent reduction of the unscheduled shut downs must be partly attributed to the cyclotron computer /1/ which is now in routine use. Again for approximately 10 % of the experimental time the axial injection system was used to study nuclear reactions with polarized deuterons (52 MeV) and high energy $^{6}Li^{3+}$-ions (156 MeV).

Table 1 Operation of the cyclotron from July 75 to June 76

Cyclotron operational	with internal ion sources		with external ion sources		total	
for experiments	6234 h	84.5 %	292 h	36.5 %	6526 h	79.8 %
for beam development and testing new components	359 h	5.0 %	366 h	45.7 %	725 h	8.9 %
time of operation	6593 h	89.5 %	658 h	82.2 %	7251 h	88.7 %
scheduled shut-down for maintenance, repair and installations	366 h	4.9 %	44 h	5.5 %	410 h	5 %
unscheduled shut-down	416 h	5.6 %	98 h	12.3 %	514 h	6.3 %
total shift time	7375 h	100 %	800 h	100 %	8175 h	100 %

According to our failure statistics two special machine components have been improved:

1. New extraction elements have been constructed in our workshop (see fig. 1).

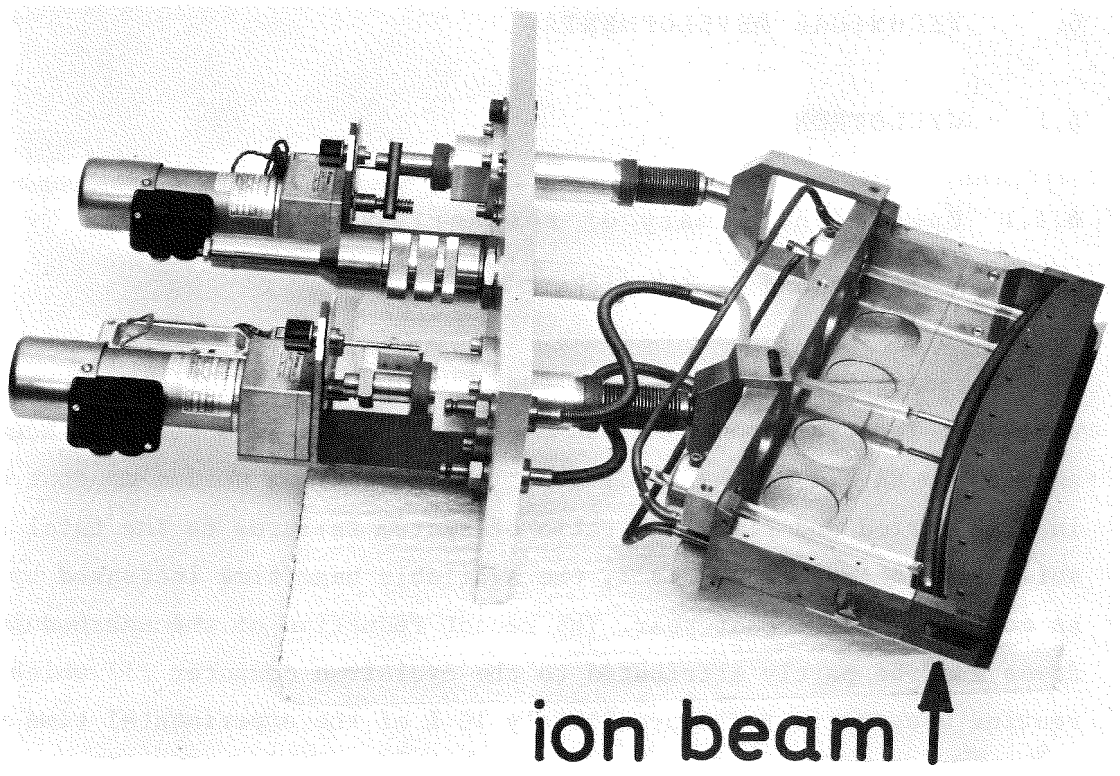

Fig. 1 One of the new extraction elements of the Karlsruhe Isochronous Cyclotron, which can withstand approximately 1 kW of beam power. Except the tantalum anti-septum, all parts which can be seen by the beam are machined out of graphite.

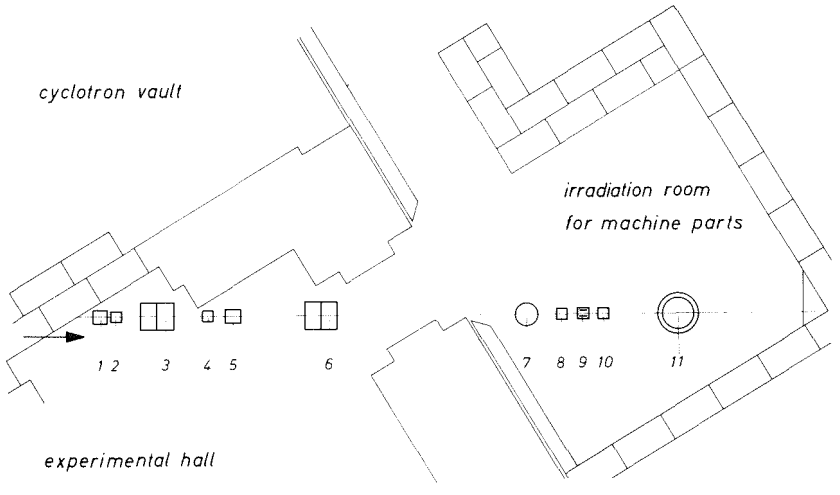

Fig. 2 Layout of the new irradiation room for wear measurements on machine components outside the main experimental hall.(1), (5) x-y-bending elements, (3),(6) quadrupole doublet lenses, (7) diffusion pump, (2),(10) diagnostic boxes, (4), (8) beam scanners, (9) capacitive beam monitor, (11) machine parts.

2. New CAMAC controlled trim coil power supplies have been installed /2/. For a more detailed description of some of the technical improvements we may refer to the following contributions.

For wear measurements on machine components a new beam line outside the main experimental hall (fig. 2) has been completed in May 1976 and tested.

On the user side (see table 2) the tendency observed for several years /3,4/ continued that the number of external (non GfK) experimentalists increases to now 44 %. For the first time more than 50 % of the total available beam time of our cyclotron is used for applied research projects (table 3).

Table 2 User statistic for 1975

GfK - Karlsruhe users

Institut für Angewandte Kernphysik	1977 h	30.3 %
Labor für Isotopentechnik	807 h	12.4 %
Institut für Experimentelle Kernphysik	387 h	5.9 %
Institut für Radiochemie	268 h	4.1 %
Institut für Material- und Festkörperforschung	156 h	2.4 %
Institut für Heiße Chemie	61 h	0.9 %
	3656 h	56.0 %

External users

Universität Saarbrücken	631 h	9.7 %
Freie Universität Berlin	503 h	7.7 %
Max-Planck-Institut für Kernphysik Heidelberg	455 h	7.0 %
Universität Heidelberg	317 h	3.7 %
Technische Universität München	242 h	3.7 %
Universität Mainz	208 h	3.2 %
Universität Erlangen	142 h	2.2 %
Deutsches Krebsforschungszentrum Heidelberg	126 h	1.9 %
Kernforschungsanlage Jülich	123 h	1.9 %
Universität Bonn	53 h	0.8 %
Université Clermont (France)	42 h	0.6 %
Universität Konstanz	21 h	0.3 %
Universität Gießen	4 h	0.1 %
Universität Münster	3 h	0.1 %
	2870 h	44.0 %
Grand total	6526 h	100 %

Table 3 Users statistics for 1975

Solid state physics	1524 h	23.4 %
Nuclear reactions	1234 h	19.0 %
Nuclear spectroscopy	1010 h	15.5 %
Neutron physics	1003 h	15.4 %
Engineering	807 h	12.4 %
Nuclear medicine	383 h	5.7 %
Materials research	328 h	5.0 %
Nuclear chemistry	195 h	3.0 %
Astrophysics	42 h	0.6 %
	6526 h	100 %

References

/1/ Contribution 6.1.3

/2/ Contribution 6.1.4

/3/ G. Schatz, F. Schulz, H. Schweickert; Report KFK-Ext. 18/75-1 (1975)

/4/ F. Schulz, H. Schweickert; Report KFK 2298 (1976)

6.1.2 Computer Controlled Beam Diagnostic at the Karlsruhe Isochronous Cyclotron*

W. Kappel, W. Karbstein, W. Kneis, J. Möllenbeck, D. Hartwig+, G. Schatz, and H. Schweickert

A fast and easy to handle computer controlled beam diagnostic system is built up at the Karlsruhe Isochronous Cyclotron. The computer system is a NOVA 2/10 with 32 k of memory, two disks, two terminals, and a CAMAC branch controller. A 200 m long CAMAC branch connects the 5 crates in the control room, the experimental area, and the cyclotron vault. The beam quality parameters can be measured via interactive programs using a display terminal in the control room. Settings of various parameters of the cyclotron and some external equipment are measured via CAMAC. As a common language for all measuring programs we use BASIC running under the real time disk operating system RDOS. The reasons for the choice of BASIC can be summarized in its interacti-

vity and the way to "write-and-test" programs.

*Proc. of the Seventh International Conference on Cyclotrons and their Applications, Zürich (Switzerland) August 1975 (Birkhäuser, Basel, 1975) p. 538

+Present address: Gesellschaft für Schwerionenforschung mbH, Darmstadt

6.1.3 Further Developments on the Computer Controlled Cyclotron Diagnostics

W. Kappel, W. Karbstein, W. Kneis, J. Möllenbeck, and H. Schweickert

In the last year a first description of our computer controlled beam diagnostic and logging system has been given /1,2/. In the meantime the system has proved to be very helpful for the routine operation of the cyclotron especially for the quick, reproducible and accurate measurement of beam properties and for the detection of imperfect parameter settings. A number of new programs has been added to the CICERO-system (fig. 1). In the following we will give short descriptions of some of these.

Emittance measurement

The emittance measurement described earlier /1,2/ has been extended by a further evaluation section named SIGMAFIT. This program is automatically started after the measurement. A fit for the best ellipse representation of the measuring points is made and displayed on the TV-screen as shown in fig. 2.

Absolute energy measurement

For some applications of the cyclotron, especially for the investigations of wear of machine parts, it is important to know the energy of the external beam precisely. Since in practice the beam energy depends on the operating conditions of the cyclotron it is desirable to have a simple beam energy monitor. The time-of-flight technique in use (figs. 3 and 4) consecutively measures the time of arrival of prompt γ-rays from two graphite targets with respect to a timing signal from the accelerating frequency.

Adjusting the currents of the correction coils

The installation of the new CAMAC controlled power supplies for the correction coils /3/ gives us the possibility to decouple the corrections for

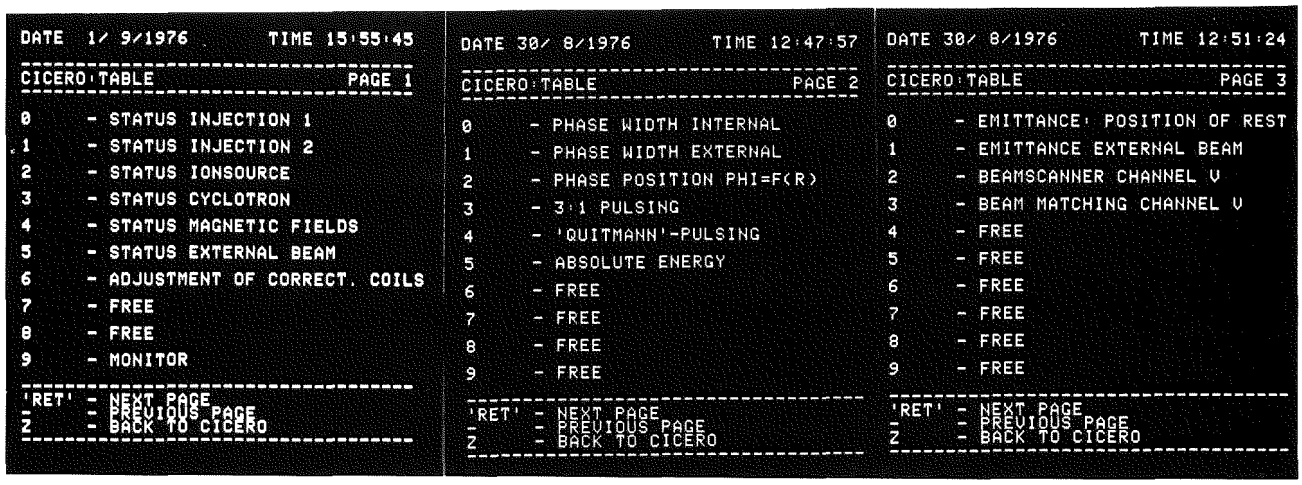

Fig. 1 Lists of measurement programs ready for use as displayed on the television screen in the control room. The cyclotron operator selects the diagnostics program required by input of a number via a keyboard. The computer subsequently excecutes this program and displays the result on the television screen.

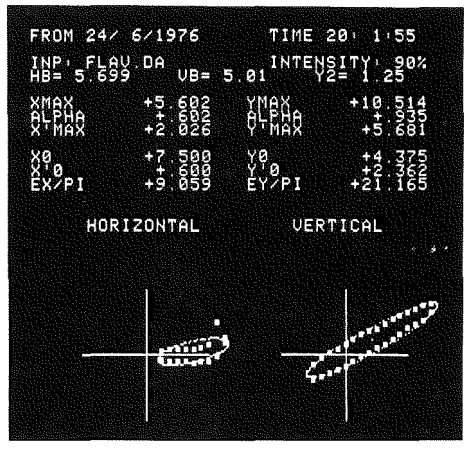

Fig. 2 Results of an emittance measurement performed by the computer at the extracted 52 MeV deuteron beam. Horizontal and vertical emittance ellipses are fitted by the new program SIGMAFIT.

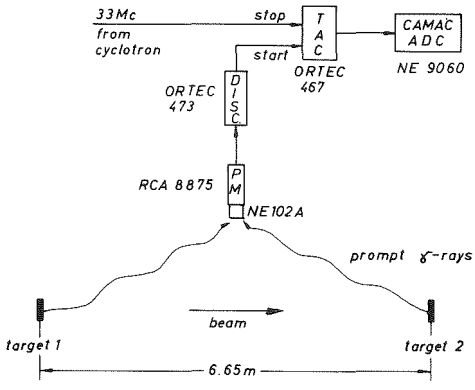

Fig. 3 Schematic diagram of the energy determination for the extracted beam by a time-of-flight technique. The accuracy achieved is ± 50 keV at 52 MeV.

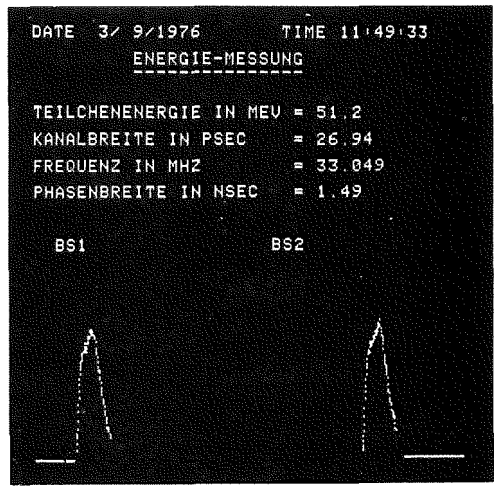

Fig. 4 Typical result of an energy measurement at the external 52 MeV deuteron beam. As in similar programs the computer tracks the operator through the procedure up to this final TV-picture. The time used is 60 sec.

isochronism and the centering of the beam. In fig. 5 the geometrical arrangement of the correction coils is shown.

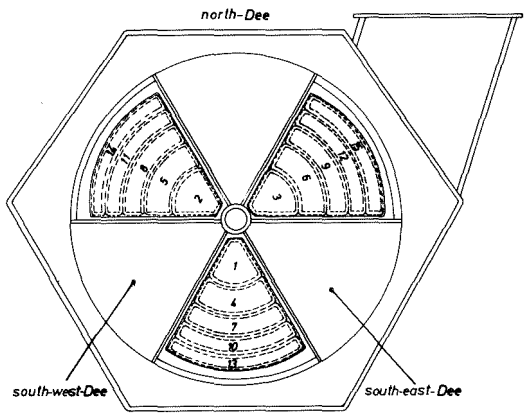

Fig. 5 Geometrical arrangement of the existing correction coils on the pole faces of the hill sectors. It consists of 15 individual pairs of coils each powered by a separate supply.

According to the philosophy represented in fig. 6 it is possible to adjust and monitor the isochronism correction ($\sum I_c$), the amplitude (K) and angle (ϕ) of a first harmonic for the five radii (fig. 7) independently of each other via the control console.

Quality of the 3:1 beam suppression

During operation of the fast neutron time-of-flight spectrometer it is often necessary to test the quality of the 3:1 beam suppression. The hardware for this measurement has been described in detail elsewhere /4/, so it is sufficient to show the final display picture (fig. 8).

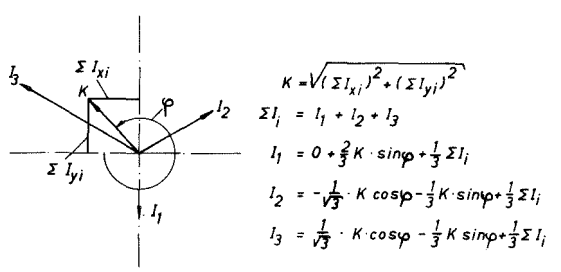

Fig. 6 Definition of the adjustment parameters: $\sum I_c$=sum current; K=amplitude of the first harmonic and ϕ = direction of the first harmonic

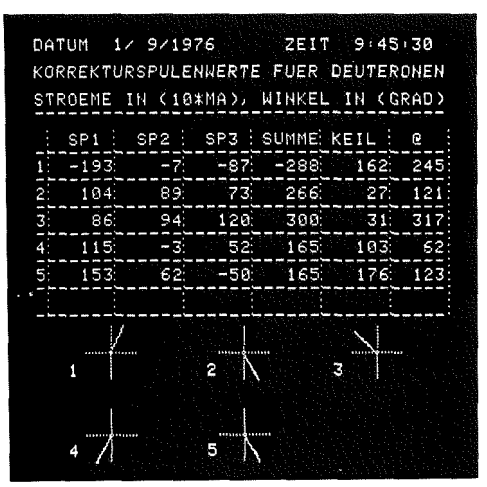

Fig. 7 Typical display picture during the adjustment of the correction currents. The isochronous correction and the first field harmonic (K,ϕ) can independently be varied from the console. Measured actual values are displayed.

Beam scanner

The first two rotating beam scanners /5/ have been tested in connection with the computer (fig. 9).

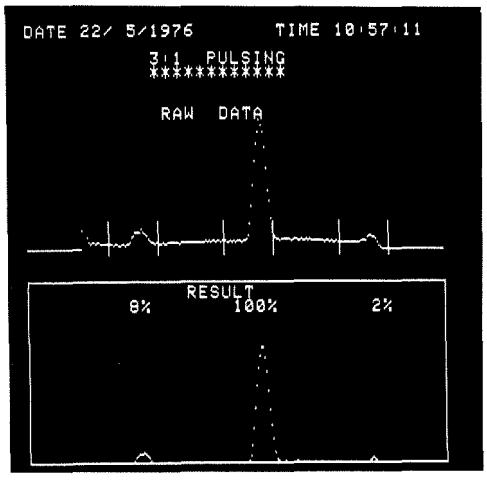

Fig. 8 TV-screen of the computer after the measurement of the 3:1 beam suppression. For demonstration a situation with a poor suppression is chosen.

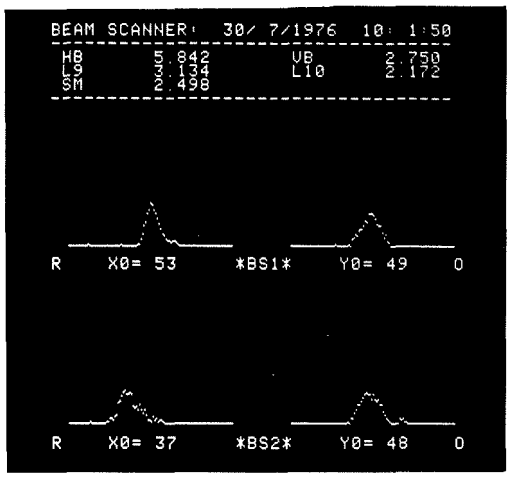

Fig. 9 Display of the beam profile and center taken with the fast quasi-non-intercepting devices. Currents down to 300 nA can be measured; below this limit the used sliding contacts give noise problems.

References

/1/ G. Schatz, F. Schulz, H. Schweickert; Report KFK-Ext. 18/75-1 (1975)

/2/ F. Schulz, H. Schweickert; Report KFK 2298 (1976)

/3/ Contribution 6.1.4

/4/ W. Kappel, J. Möllenbeck, H. Schweickert; Proc. Sixth International Cyclotron Conference, Vancouver, July 1972 (American Inst. of Physics, New York, 1972) p. 358

/5/ G. Bauer, K. Heidenreich, G. Klinger, Ch. Rämer, R. Schütz; Report KFK 2223 (1975) p. 101

6.1.4 New Computer Controlled Power Supplies for the Correction Coils of the Cyclotron

W. Kappel, G. Klinger, and E. Schönstein

The 12 years old power supplies for the correction coils have been replaced by new ones which are controlled and monitored via CAMAC by our Nova 2/10 computer. The principle of this set up is shown in fig. 1. Each coil is supplied by a separate current source with a built in 12 bit BCD digital-

to-analog converter. The digital input of this DAC is defined by a register incorporated in a special CAMAC modul. This register can be loaded and read either by a standard CAMAC dataway operation or in the case of manual operation by an up/down counter. Two clock rates, 2 Hz and 200 Hz, are provided. An additional 3 bit register, which is read by the dataway, serves as a status register for alarm situations at the high current power supplies. The long line transmitter circuits to the power supplies are equipped with optoelectronic coupling boards to give a high noise suppression. the computer control also enables us to check the mechanical and electrical quality of the correction coils by monitoring the applied voltages and circulating currents.

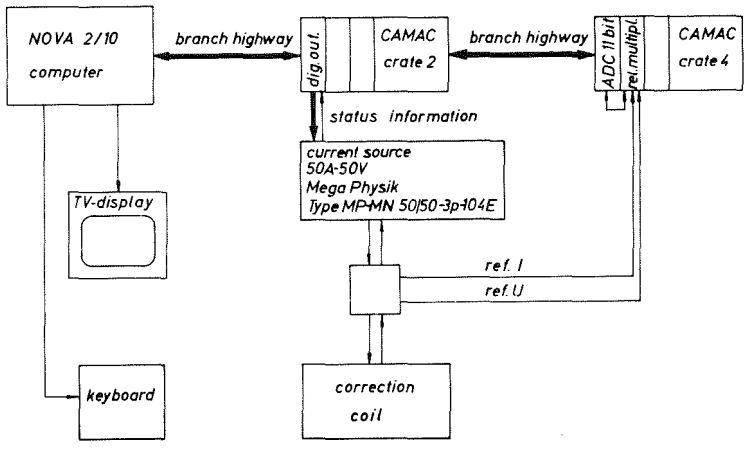

Fig. 1 Simplified block diagram of the circuitry for the new computer controlled power supplies for the correction coils.

6.1.5 Design of the New Correction Coils for the Cyclotron

V. Bechtold, L. Friedrich, Ch. Rämer, F. Schulz, and L. Wiss

In the last year it was decided to build a new set of trim coils for the cyclotron because the coils used until now are partially damaged by radiation. The new coils will give the possibility to accelerate $^{3}He^{2+}$-ions and protons in addition to the e/m = 1/2 particles. The acceleration of protons instead of H_2^+-molecules will result in a higher internal and external beam current for isotope production and in the possibility to inject polarized protons.

Numerical calculations for the trim fields led to a new trim coil configuration consisting of six coils per plate with summing fields /1/. According to these calculations a prototype coil was designed. The coil conductor

is a copper band of 7 x 0.55 mm^2 in cross section which is to be wound tightly around aluminium forms. The power dissipated in the windings of the coils is tranported through a thin insulation layer on the copper band and a thin Kapton foil (0.08 mm) to a copper plate on each side of the coil. These plates are cooled by water flowing through a rectangular cooling channel inserted into the plates. Fig. 1 and 2 show a top view and a cross section of the cooling plate, respectively.

To get the desired field correction, currents up to 50 A per coil are necessary. For these high currents a special vacuum tight feed-through was designed. The feed-through consists of an oxide ceramic flange into which hard silver plated copper bolts and copper pipes are soldered (fig. 3).

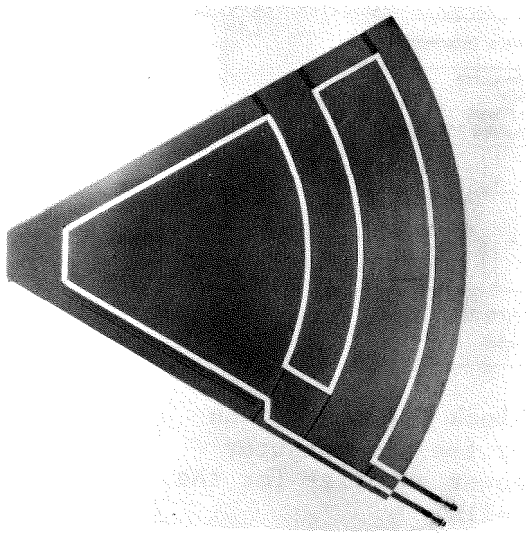

1 Top view of the copper plate with layout of the cooling channel. The plate is 3 mm thick and the inner cross section of the cooling channels is 11.5 x 1.5 mm^2.

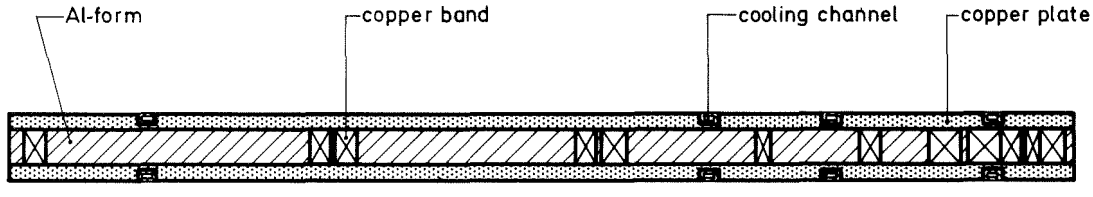

Fig. 2 Cross section of a trim coil with cooling plates on each side.

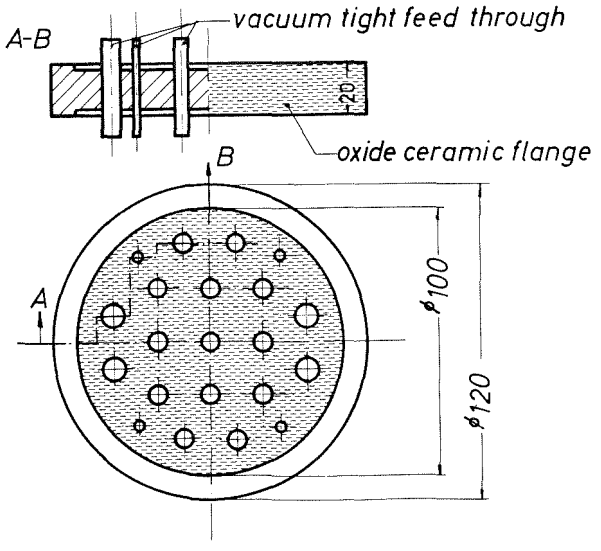

Fig. 3 Oxide ceramic flange with the arrangement of the 13 current and 4 water connections supplying one coil plate. The flange is a special feed-through for high currents.

References

/1/ F. Schulz, H. Schweickert; Report KFK 2298 (1976) p. 75

6.1.6 Capacitive Current Measurements at the Internal Beam of the Cyclotron

G. Haushahn, K. Heidenreich, W. Maier, and E. Röhrl

The aim of the capacitive internal beam probe described below is to measure the extraction efficiency of the Karlsruhe Isochronous Cyclotron without interrupting the beam. Last year we reported about a simple capacitive probe at the external beam line using the second harmonic (66 MHz) of the ion beam pulses to suppress the noise background /1/. A similar technique is now applied to an internal capacitive probe located just in front of the extraction elements in the north east hill sector. A cross section of the very carefully shielded probe is shown in fig. 1. In order to increase the pick-up signal from the ion beam, 30 turns are measured simultaneously with a radial probe extension of 40 mm.

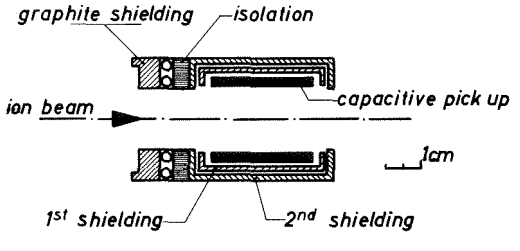

Fig. 1 The triply shielded internal capacitive probe. The probe length in radial direction is 40 mm to increase the signal induced by the beam.

Contrary to the probes at the external beam line the rf-suppression by use of the second harmonic (66 MHh) is not sufficient, since the pick-up voltage is contaminated by a second harmonic originating from the stray field of the dees. This noise voltage from the acceleration system is compensated by an adequate

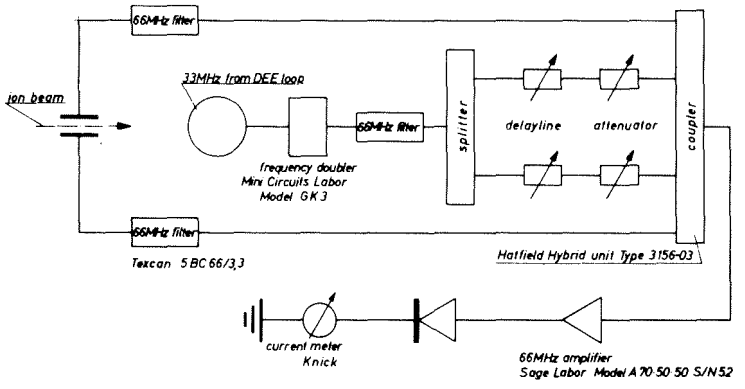

Fig. 2 A block diagram of the non-intercepting internal beam current monitor working on the second harmonic. A compensation technique is used to suppress the pick up of the second harmonic from the rf-system.

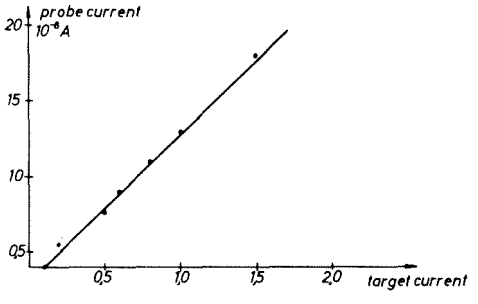

Fig. 3 Calibration curve of the new internal non-intercepting current probe. Currents down to 0.1 μA can be measured very reliably.

circuit shown in fig. 2.

By using this technique a suppression of the second harmonic component of approx. 50 dB has been realized. Thus ion beam currents down to 0.1 μA can be measured very reliably (fig. 3).

References

/1/ G. Haushahn, K. Heidenreich, E. Röhrl; KFK 2223 (1975) p. 97

6.1.7 Status Report of the Axial Injection System at the Karlsruhe Isochronous Cyclotron*

G. Haushahn, J. Möllenbeck, G. Schatz, F. Schulz, and H. Schweickert

A $^{6}Li^{3+}$-ion source and a Lambshift source for polarized deuterons are now in operation at the Karlsruhe Isochronous Cyclotron. Both sources are mounted horizontally outside the cyclotron. A 16 m long injection transport system whose elements are electrostatic quadrupoles and einzel lenses brings the beam up to the cyclotron median plane. The efficiency is drastically improved by using a bunching system with a simulated sawtooth voltage. Maximum

external beam currents are at present 40 nA of polarized deuterons (52 MeV) and 5 nA of $^{6}Li^{3+}$-ions (156 MeV).

*Proc. of the 7th Int. Conf. on Cyclotrons and Their Applications, Zürich (Switzerland), August 1975 (Birkhäuser, Basel, 1975) p. 376

6.1.8 Polarized Deuterons of a Lambshift Ion Source Accelerated by the Karlsruhe Isochronous Cyclotron*

V. Bechtold, L. Friedrich, D. Finken+, G. Strassner++, and P. Ziegler+

At the Karlsruhe Isochronous Cyclotron a Lambshift source has been installed delivering a vector polarized deuteron beam of 0.8 μA within an emittance of 100 mm-mrad at an energy of 10 keV. The distance between the injection system of the cyclotron and the Lambshift source is 16 m. The small emittance of this Lambshift source makes it possible to design a horizontal beam line using only two acceleration and three electrostatic einzel lenses. For beam adjustment small stators of three-phase current motors are used. The whole set-up is completely inserted into a 22 cm diameter tube of iron for shielding the stray field of the cyclotron. A beam of 100 nA polarized deuterons has been accelerated to an energy of 52 MeV and 40 nA have been extracted.

*Proc. 7th Int. Conf. on Cyclotrons and Their Applications, Zürich (Switzerland) August 1975 (Birkhäuser, Basel, 1975) p. 390

+Institut für Experimentelle Kernphysik der Universität Karlsruhe

++Present address: Physik. Institut der Universität Zürich (Switzerland)

6.2 VAN DE GRAAFF ACCELERATOR

6.2.1 Operation of the Van de Graaff Accelerator

A. Ernst[+], D. Roller[+], H. Schreiber[+], and J. Nadasdy[+]

The 3 MV Van de Graaff accelerator was in operation for 5156 hours from July 1975 to June 1976. 4339 hours were made available to and were used by the experimenters. The main fields of research and their share of the beam time were

1.) Surface layer analysis by backscattering, channelling and nuclear reactions	34 %
2.) Neutron cross section measurements for the fast breeder program	33 %
3.) Fundamental research in the field of fast neutron physics	23 %
4.) Materials analysis by proton induced X-rays	10 %

During the above mentioned period there were three major down-times of the accelerator. First the replacement of the accelerator tube became necessary. Then the insulating gas storage system was improved in preparation for the use of SF_6, and a recirculation loop for drying the insulating gas during operation of the accelerator was installed. At the same time, the alignment of the accelerator and of the beam guidance system was checked and corrected. During the last shutdown period, the accelerator terminal had to be modified for the incorporation of four gas bottles and the associated switching and gas flow regulation system in order to meet the demands of the experiments for a greater variety of ions.

On short notice we got the chance to take over a used 2 MV accelerator from another institute of the research centre. This machine was disassembled and has already been mechanically installed at its new site inside the experimental hall of the 3 MV accelerator. Lateron it will be equipped with a penning ion source and will be used mainly for implantation and the production of radiation damage.

[+] Van de Graaff operating group

6.2.2 Present Status of the Computer Based Van de Graaff Control and Supervisory System

A. Ernst[+]

The accelerator control and supervisory program is written in BASIC and is run on a NOVA 2 computer (Data General Corp.) under the RDOS disk operating system. Computer peripherals include a dual floppy disk drive, console typewriter with two tape cassettes, video display, fast pulse ADC, fast level ADC with FET multiplexer, DAC and a CAMAC branch with at the moment 4 crates. Digital inputs and outputs, scalers and slow level ADCs with relay multiplexers are connected via CAMAC. Peripherals not serviced by standard EXTENDED BASIC are controlled by assembler-written subroutines entered via the CALL-statement.

The program has three levels of priority, the highest level comprising the interrupt supervisor and the individual interrupt service routines, also written in BASIC. Interrupts can interrupt the running BASIC-program everytime execution of a program line is completed /1/. Only events requiring rapid response (less than 0.1 s) are enabled to generate interrupts, e.g. sparks in the Van de Graaff generator, where an immediate measurement of the vacuum rise in the accelerator tube yields information on where the spark took place. The intermediate level of priority is taken by clocked tasks, e.g. writing a record of the most important accelerator parameters on cassette tape every 10 minutes. - Lowest priority is given to background programs giving special information on accelerator parameters to the operator such as a program displaying long term stability of the accelerating potential, or the program that determines the pulse width of the proton pulses described earlier /2/.

In addition to this acquisition of accelerator data, many parameters are checked in the background supervisory program for being within preset limits, and in another clocked task the neutron time-of-flight spectrum acquired during the preceding 10 minutes from a monitor detector is automatically analyzed and the maximum neutron energy is calculated and checked.

When a parameter is found to be outside its preset limits, the computer can interrupt data acquisition by the experiment if necessary and can trigger an alarm to call the operator. Further development of the operating system will step by step eliminate the need of calling the operator and will have the

computer itself take the necessary measures to restore correct operating conditions. An example, where this has already been done, is the adjustment of the bunching system:
Especially in the first hours of pulsed and bunched operation of our 3 MV Van de Graaff, the resonance frequency of the buncher high frequency power stage drifts and needs frequent readjustment in order to avoid deterioration of the experimental energy resolution. This is done by the computer in the following way. When the computer finds readjustment necessary, it interrupts data acquisition by the experiment and starts decreasing the motor controlled capacity in the resonant circuit until either resonance has been reached or the high frequency output has dropped by another 20 %. In the latter case the computer starts increasing the capacity, passes the resonance peak, determines the peak high frequency output, and stops at 60 % of the peak level. Then it reverses decreasing the capacity until the peak has been reached. This complicated procedure is necessary to eliminate the effects caused by backlash in the capacity adjustment system and by the force of the air pressure on the vacuum feed-through that moves the capacitor plate slowly until there is no play left. An adjustment of the high frequency phase by the computer is also possible. This automatic adjustment of the buncher has performed excellently over several months of continuous operation.

+Van de Graaff operating group

References

/1/ G. Ehret et al.; Report KFK 2223 (1975) p. 126
/2/ A. Ernst; Report KFK 2223 (1975) p. 110

6.2.3 Ion Optical Calculation of Focusing a 3 MeV Ion Beam to Micron Diameters

D. Heck

Ion induced X-ray or secondary particle emission is frequently used to determine the elemental composition of sample surfaces. For analysis with high spatial resolution the ion beam must be focused to some microns in diameter. Usually this is achieved with a narrow collimator and magnetic quadrupoles /1,2/; the reduced ion optical image of the collimator is projected onto the sample surface by the quadrupole lens system.

To get short measuring times, the beam current should be as high as possible. This requirement is equivalent with a maximum acceptance of the ion optical system. Restricting factors are the image errors. Therefore calculations of different quadrupole systems, including magnetic fringe field effects, have been performed with the program IONBEAM /3/ which uses the transport matrix formalism /4/ extended to 3rd order. It shows, that the dominant aberrations arise from the 4 aperture error coefficients.

The acceptance of quadrupole doublets is generally higher than that of systems with more than 2 quadrupoles, when the image size is kept constant (3μ x 3μ) and the aperture errors are limited ($\leq$ 1 μ). The main features of some systems are listed in table 1. With a doublet of favourable dimensions which will be used at the beam line under construction at the 3 MV Karlsruhe Van de Graaff accelerator, a beam current about 20 % higher than with

Table 1 Lens systems calculated for 3 MeV deuterons. Image size 3μ x 3μ, aperture aberrations $\lesssim$1μ

System	Distance object (cm)	Distance image (cm)	Magnification factors M_x	M_y	max. acceptance parameters $\pm x_o$ (μ)	$\pm y_o$	$\pm\alpha_o$ (mrad)	$\pm\beta_o$	Phase space volume $\mu^2 mrad^2$	δ chromatic (μ)
Harwell quadruplet /1/ $\beta_1=-\beta_4,-\beta_2=\beta_3$; l=18.05 cm, s = 4.2 cm	350	21	0.18	0.18	8.5	8.5	0.62	0.4	18	$\leq\pm$ 0.5
Quadruplet with stigmatic intermediate image (multiple doublet) $\beta_1=-\beta_3,-\beta_2=\beta_4$ l=7.5 cm, s=7cm S=220 cm	200	20	0.021	0.021	71	71	0.12	0.038	23	$\leq\pm$ 0.4
Heidelberg doublet /2/ l = 4 cm s = 3 cm	150	10	0.23	0.043	6.7	35	0.72	0.61	102	$\leq\pm$ 0.22
Doublet l = 10 cm s = 28 cm	250	20	0.52	0.046	2.9	32.4	1.28	0.68	80	$\leq\pm$ 0.73
	250	12	0.46	0.031	3.24	48.2	1.26	0.61	120	$\leq\pm$ 0.73

the Heidelberg doublet system /2/ and more than 4 times higher than with the Harwell quadruplet system /1/ is expected. With a field gradient of 40 T/m it is possible to focuse 3.5 MeV $^4He^+$ ions at a target distance of 12 cm.

References

/1/ J.A. Cookson, A.T.G. Ferguson, F.D. Pilling; J. Radioanalytical Chemistry 12 (1972) 39

/2/ R. Nobiling et al.; Nucl. Instr. Meth. 130 (1975) 325

/3/ Contribution 6.5.7

/4/ K.L. Brown; Report SLAC 75 (1967);
K.L. Brown, S.K. Howry; Report SLAC 91 (1970)

6.2.4 Third Order Transfer Matrix Elements of Octopoles*

D. Heck

The matrix elements of the third order transport matrices for electrostatic and magnetic octopoles are derived. They are needed in ion optical calculations, if octopoles are used as correctors of image aberrations.

* Report KFK 2288 (1976)

6.3 ION SOURCES

6.3.1 Penning Ion Source Improvements

J. Biber, H. Kuhn, and F. Schulz

For the first time an ion source with a grounded reflector was tested inside the Karlsruhe Isochronous Cyclotron. The geometric arrangement of this source is illustrated in fig. 1. Though this arrangement still has to be improved (e.g. exchange of the Al_2O_3 by BN_3 insulators) the accelerated peak beam currents for doubly charged ^3He and ^4He have been increased from 20 µA to 60 µA.

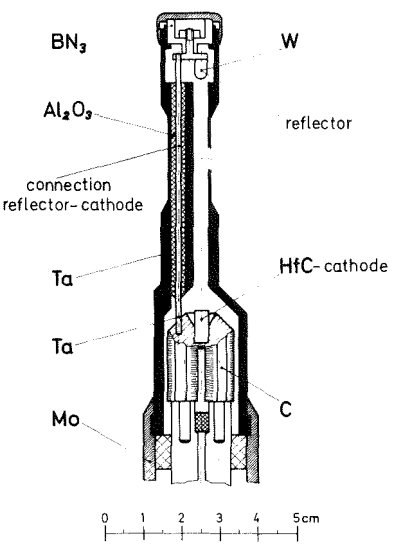

Fig. 1 The structure of the ion source with grounded reflector.

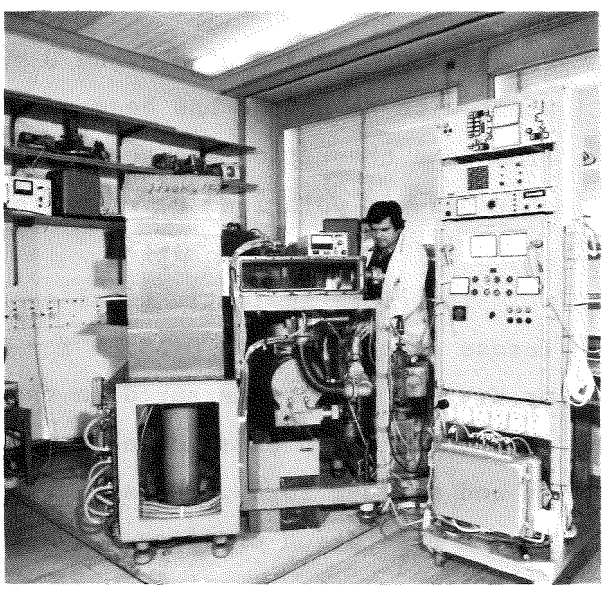

Fig. 2 A recent photograph of the new external Penning ion source. Strong plasma compression will be achieved by a homogeneous magnetic field of 8 kG.

The development on the external $^6Li^{3+}$-sources /1/ was mainly directed towards improving reliability. The position of the plasma was adjusted closer to the extraction slit by appropriate shim rings around the borings in the magnet. In order to reduce impurities inside the source volume, the source is now excited without any buffer gas. The gas inlet is connected to a diffusion pump. Now 500 nA of $^6Li^{3+}$-ions can routinely be produced.

Based on the investigations in the test bench a new external Penning ion source has been built up and will be tested at the end of this year. A

recent photograph of this arrangement is shown in fig. 2.

References

/1/ F. Schulz, H. Schweickert; Report KFK 2298 (1976)

6.3.2 Experimental Investigations of Charge Exchange Processes in Lambshift Sources with Argon and Krypton for Production of D^--Ions*

V. Bechtold, L. Friedrich, and G. Strassner+

The production of D^-- and D^+-ions by collisions of D(1S)- and D(2S)-atoms with Ar and J_2 has been successfully used in polarized ion sources. From some theoretical reasons, it was proposed that Kr might be a more favourable gas for polarized negative ion production.

Therefore inelastic total cross sections for the reaction $D(1S)+X \rightarrow D^{\mp} + X^{\pm}$ (cross section p) and $D(2S) + X \rightarrow D^{\mp} + X^{\pm}$ (cross section γ) - where X = Argon or Krypton - were measured in the energy range of 0.4 - 1.5 keV. It was found that there is no substantial difference between the cross sections p of Ar and Kr and neither for γ. The selectivity S of Kr is somewhat smaller than that of Ar. The absorption cross sections k for metastables in Ar and Kr are almost equal. The neutralisation cross section σ of Ar is much higher than that of Kr. For this reason the use of Ar in Lambshift sources is more suitable for the production of negative ions.

Hence, in judging which charge exchange reaction is more favourable for ion production with Lambshift sources it is necessary to look at the cross sections p and γ as well as at the cross sections k and σ. For optimum polarization a high selectivity and for optimum yield a small difference k-p and a cross section σ much more smaller than k are required.

*Nucl. Instr. Meth. 136 (1976) 361

+Present address: Physik. Institut der Universität Zürich (Switzerland)

6.3.3 LASCO, the Polarized Ion Source at the Cologne HV-FN7 Tandem Accelerator

V. Bechtold, L. Friedrich, and P. Ziegler[+]

The detailed investigation of nuclear reactions with protons and deuterons requires the measurement of analysing powers and polarization transfer coefficients in addition to the measurement of cross sections. The progress in development of polarized ion sources has resulted in beams of more than 100 nA polarized protons and deuterons on target by properly matching source and accelerator. For tandem accelerators the Lambshift source turned out to be most suitable becasue it delivers 0.5 μA negatively charged protons at an emittance of only 1.2 cm rad $eV^{1/2}$. So in Nov. 1973 it was decided to install a Lambshift source of the Karlsruhe design at the tandem accelerator in Cologne.

Whereas the source itself is very similar to C-LASKA which is installed at the Karlsruhe Cyclotron a special preacceleration system and a beam line to match the source to the tandem had to be developed. This is schematically drawn in fig. 1. To reduce variations of the beam envelope the beam is accelerated in three steps to 70 keV. A 10^{o} electrostatic deflection protects the tandem from the neutral background beam.

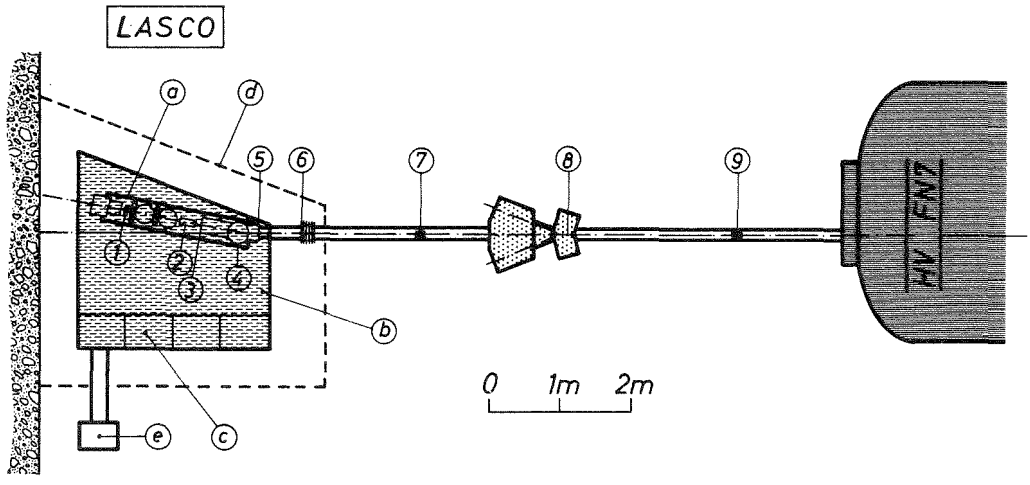

Fig. 1 The Lambshift source LASCO (a) is installed on an insulated platform (b). The electronics (c) is remotely controlled (e). The source is operated on a potential of 70 kV and therefore protected by a fence (d). (1) Cs Cell, (2) Argon cell, (3)(5) accelerating tube lenses, (4) 10^{o} deflection plate, (6) NEC-tube, (7) (9) einzellenses, (8) analysing magnet for other ion sources.

Two einzellenses (10 cm inner diameter and operated with -40 kV) focus the beam through the small diameter drift space in the analysing magnet and match it to the tandem. Since the centre of the acceptance of the tandem is out of the optical axis two steering magnets are provided. The test of the source and the beamline at Karlsruhe were finished achieving a target beam of 500 nA d^--ions with a tensor polarization of P_{yy} = 0.6 measured by the t(d,α)n reaction.

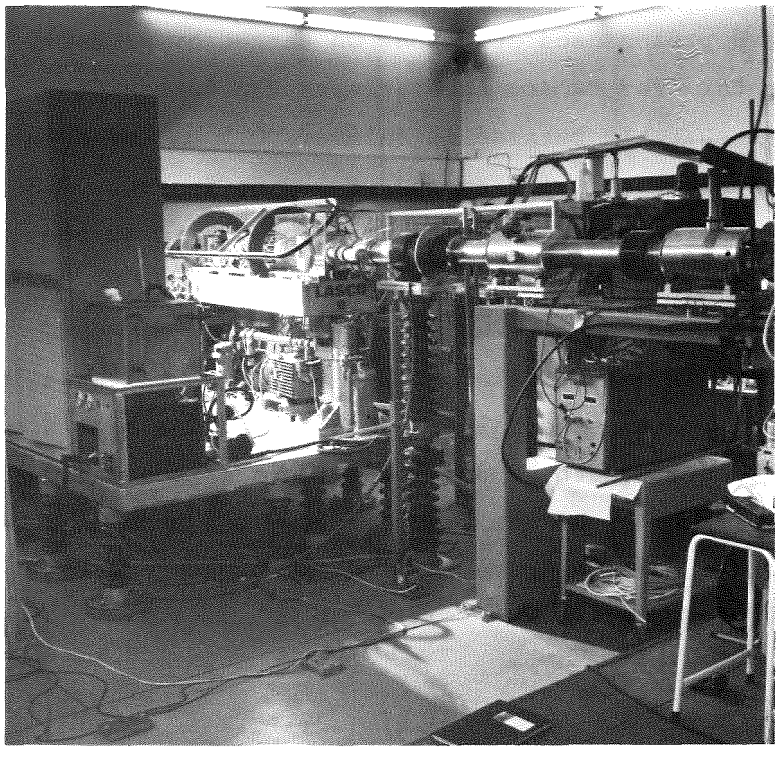

Fig. 2 View of the Lambshift source LASCO installed at the FN tandem accelerator at Cologne.

Immediately after installation in Cologne (Nov. 75, see fig. 2) the source was used for a scattering experiment with polarized protons. The source delivered 400 nA polarized protons and 160 nA could be focused onto the target. The measured maximum polarization was P_{yy} = 0.6. A drift of the measured polarization, never observed at the Karlsruhe polarization experiment, still has to be investigated.

+Institut für Experimentelle Kernphysik der Universität Karlsruhe

6.4 DETECTORS

6.4.1 A Gas Scintillator Arrangement for Measurements of Fission Fragments at High α-Background

B. Leugers and K. Kari

For measurements of neutron induced fission cross sections of highly α-active isotopes the previously used gas scintillation detector was modified. The principle of the design is shown in fig. 1. For the detection of fission fragments an arrangement of several gas scintillation chambers in series is used. The scintillation chambers are made of stainless steel. Each scintillation chamber is separated from its next neighbours by the fission foils. Optical decoupling is provided by the metallized vyns backing of the fission foils. A mixture of 85 % argon and 15 % nitrogen gas is flowing continuously through the counter at slightly above atmospheric pressure serving as the scintillator. Each chamber is viewed by one Valvo DUVP 56 photomultiplier tube. Opposite to each multiplier a fast light emitting diode is mounted (Monsanto MV 1). Fission events are detected by a coincidence of the two adjacent photo multipliers of each fission foil. At high α-background the main problem is

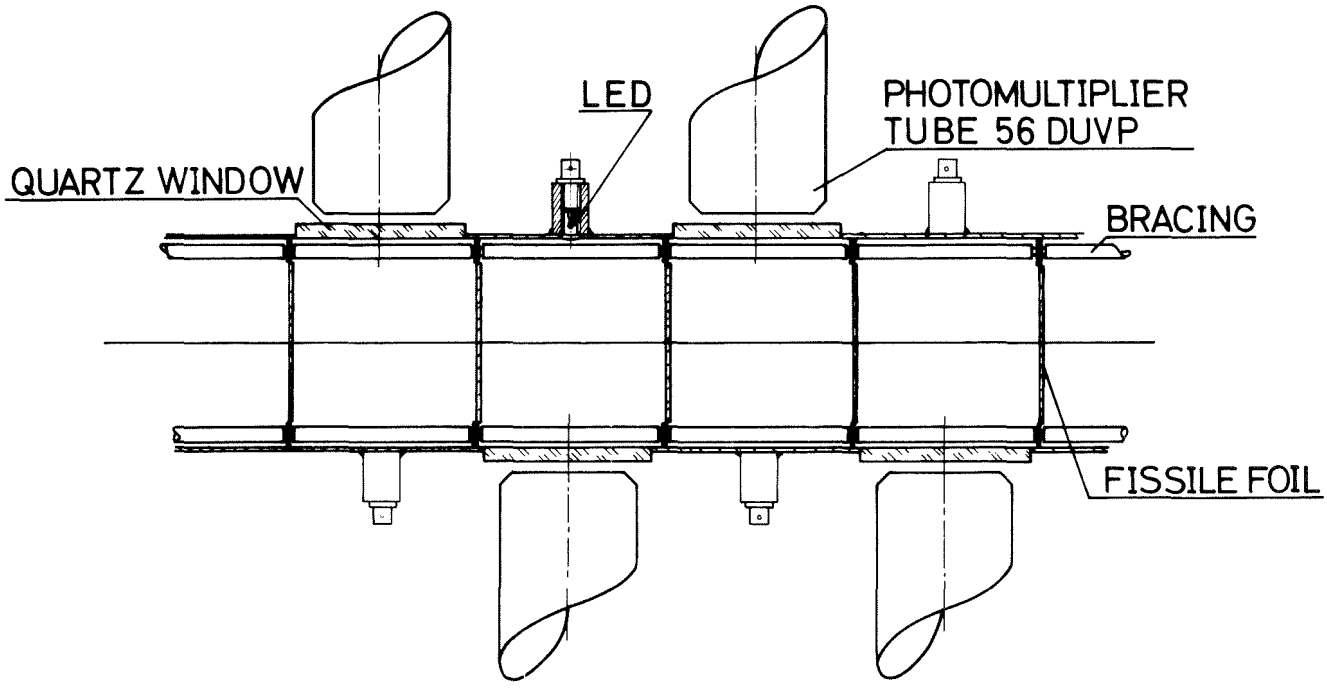

Fig. 1 Fission detector.

the stabilization and control of the gain of the photomultipliers. In this case it is necessary to keep the anode current low and to design the voltage supply for maximum anode current. The resulting voltage of the photomultipliers amounts to about 1600 V. To control the gain of the multipliers, fast light emitting diodes are used, calibrated by the fission fragments of a Cf-252 source. The LEDs are used in combination with a specially developed pulse generator. This generator provides several very fast and constant pulses simultaneously without reflections, which allows an easy control of the timing of the coincidence modules. The LED signals can be separated from the α-background by gating the amplifier and stretcher of the fast photomultiplier signals with a NIM signal provided by the pulse generator. In this way the gain of the photomultipliers was controlled during our measurements.

The new system was used in the measurement of the neutron induced fission cross section of ^{240}Pu. The α-background was about 10^7 sec^{-1}, and at a discriminator threshold of 20 MeV the α-pile-up counting rate still amounted to 4×10^3 sec^{-1}. Using the coincidence technique this rate could be reduced to 1 sec^{-1}, while the rate of fission events was about 10 sec^{-1}. As we used the time-of-flight technique at the Karlsruhe Isochronous Cyclotron in our measurements, the α-pile-up could be easily subtracted as time independent background.

The knowledge of the gain of the multipliers and of the electronic threshold is essential for the detection efficiency of the fission chamber. The efficiency was calculated by a computer program for different neutron energies taking into account the linear momentum given to the nucleus by incident neutrons and the energy loss of the fission fragments in the fission foil itself.

6.4.2 A Spherical Avalanche Detector with Good α-Discrimination

M.A. Kazerouni and F. Käppeler

For fission cross section measurements on highly α-active transuranium isotopes a detector is required with good α-discrimination, very fast timing and long life time. These points can be met only by gas counters. It is obvious that a good α-discrimination can be achieved using the large difference in the specific ionization of α-particles and fission fragments at the begin-

ning of their flight paths. In gas counters this parameter can be adjusted by the counter dimensions and the gas pressure.

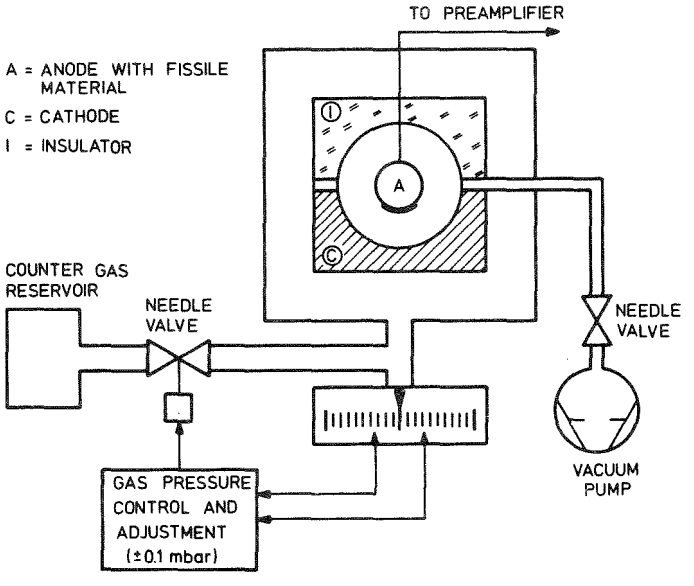

Fig. 1 Experimental set-up of the spherical fission fragment detector with good α-discrimination. Part of the anode is covered by the fissile layer.

The set-up of our prototype counter is sketched schematically in fig. 1. Similar to Dabbs et al. /1/ we have chosen a spherical geometry with the fissile sample on the inner sphere because in this arrangement the differences in all possible ion paths are small. Contrary to Dabbs we are using a low gas pressure in our counter which can be kept constant to $\pm$ 0.1mbar in the interesting range between 1 and 10 mbar. The constancy of the gas pressure is important for long time operation because the pressure strongly determines the detector properties. A constant gas flow is maintained in order to avoid poisoning by desintegration of the counter gas or outgassing from the walls.

The chemical composition and purity of the counter gas seems to be important. Contaminations by oxygen or other electronegative components can cause additional noise pulses. If gases with low vapour pressure are used problems might arise with the insulation of the electrodes. We found hydrocarbons like butane a proper choice.

First measurements were performed with ^{252}Cf sources at a pressure of 5 mbar and a voltage of 1000 V. We got very fast response for fission fragments, the rise times being a few nsec, but for α-particles we observed broad pulses with rise times of about 1 μsec. Most of the α-activity is completely suppressed because the weaker ionization of α-particles is quenched

by the gas. This feature is important because thereby α-pile-up is greatly reduced. The difference in pulse height between α-particles and fission fragments is about a factor of 20.

References

/1/ J.W.T. Dabbs et al.; Proc. of Conf. on Nucl. Cross Sections and Technology, Washington, D.C., March 1975, ed. R.A. Schreck and C.D. Bowman, Vol. I (NBS Spec. Publ. 425, 1975) p. 81

6.4.3 Accurate Calibration of a 50 cm^3 Ge(Li) Detector in the Energy Range from 0.9 to 11 MeV

H. Beer

The efficiency of a 50 cm^3 Ge(Li) detector was determined in the γ-energy range 0.9 to 11 MeV at the Karlsruhe FR2 reactor using the well-known thermal capture γ-ray lines of nitrogen (melamine), chlorine (NaCl), carbon (graphite) and chromium (metal powder). The whole γ-energy interval from 0.9 - 11 MeV was recorded as an 8 K spectrum in a Nuclear Data multichannel analyzer in a typical measuring period of 3-4 h. The normalization of the γ-spectra was performed with calibrated point sources (^{60}Co, ^{22}Na, ^{88}Y; purchased from Amersham Buchler GmbH & Co. KG) located at a distance of 9 cm from the detector. A ^{24}Na source was used to obtain relative line intensities at 1.369 MeV and 2.754 MeV.

Gamma ray transitions above 3.6 MeV were well represented by a double and single escape and a full energy peak. Below this energy only the full energy peak areas were evaluated. Relative full energy peak efficiencies were calculated taking into account the line intensities reported in refs. /1,2/. The data were analysed according to the method of Singh and Evans /3/. Using the function

$$\ln \varepsilon_F = A_o + A_1 E + A_2 E^2 + A_3 E^3, \qquad (1)$$

where ε_F is the full energy peak efficiency and E the γ-ray energy, a least squares fit of efficiency ratios was performed to obtain the constants A_1,

A_2 and A_3. The absolute efficiency values derived from the γ-ray lines of the calibrated sources were applied to determine the constant A_o. Fig. 1 shows the fitted data points of the full energy peak efficiency.

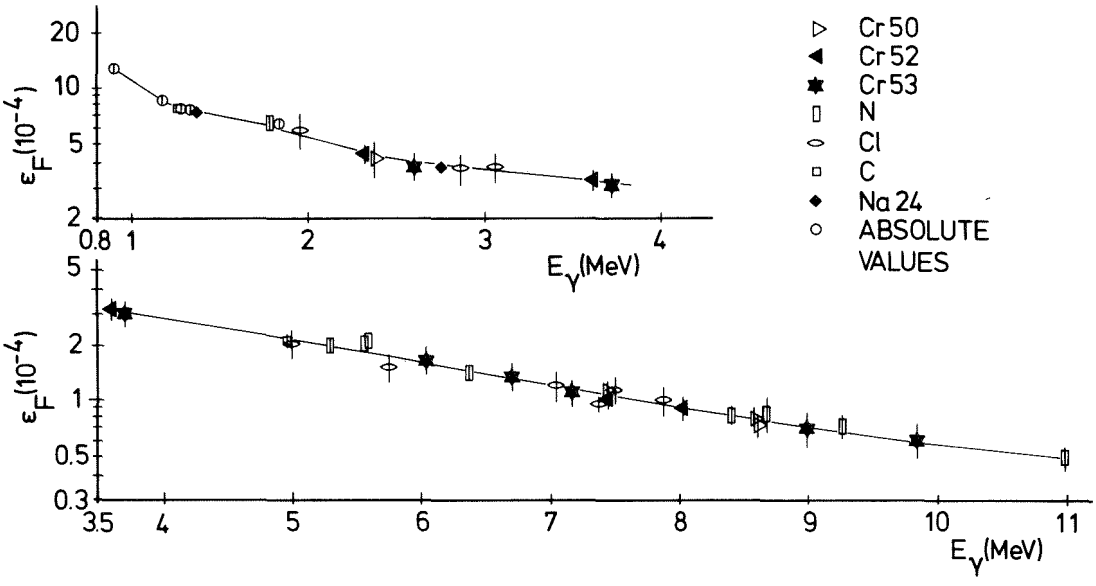

Fig. 1 Full energy peak efficiency of a 50 cm^3 Ge(Li) detector for a point source at 9 cm distance from the detector surface.

The double and single escape peak efficiencies, ε_{DE} and ε_{SE}, were related to ε_F. Least squares fits of the ratios $\varepsilon_{DE}/\varepsilon_F$, $\varepsilon_{SE}/\varepsilon_F$, and $\varepsilon_{DE}/\varepsilon_{SE}$ were carried out. The accuracy achieved in this procedure of efficiency determination was 5 %.

References

/1/ G.E. Thomas, D.E. Blatchley, L.M. Bollinger; Nucl. Instr. Meth. 56 (1967) 325

/2/ G.D. Loper, G.E. Thomas; Nucl. Instr. Meth. 105 (1972) 453

/3/ B.P. Singh, H.C. Evans; Nucl. Instr. Meth. 97 (1971) 475

6.5 COMPUTER DEVELOPMENT

6.5.1 Configuration of the New Cyclotron Experimental Computer

G. Ehret[+], H. Hanak[+], W. Karbstein, and B. Kögel

The old on-line data acquisition system at the cyclotron, a CDC 3100 which is now more than ten years old, does no longer meet today's requirements. Therefore we started to replace this system by a new minicomputer configuration (Data General, Nova 2) step by step. It is planned to replace the old computer completely after a transition time of about one year. Fig. 1 shows the hardware configuration. The standard computer and standard peripherals (left half of fig. 1) are already in use for program development.

This double computer consists of two Nova 2, a conventional periphery and an on-line experimental periphery. The first computer with 32 K of core memory (normally max. for Nova 2), hardware multiply/divide - and floating point processor, conventional input/output devices (console, 2 disks, 2 magnetic tapes, paper tape station, incremental plotter) represents a complete computing center for program development and data evaluation. The second one with the experimental periphery can be regarded as a multichannel analyser. Both computers are connected by their central busses, and so the second computer also serves as an expansion chassis for the additional 64 K core memory (data memory) as well as for other controllers (part of them are made by ourselves) for connecting on-line electronic devices (CAMAC branch, data display, ADC multiparametric system). Instead of a CPU, the second computer has as an essential part a microprogrammed double controller which operates as a memory switch and increment unit /1/. The memory switch controls the data transfer between the 'internal' (main or program) memory and the 'external' (or experiment data) memory or between data memory and the experimental devices connected to the increment unit. The increment unit offers three independent data paths (16 or 32 bits) for list and/or increment mode in DMA to the data memory. An ADC multiparametric system /2/ is connected to these special data paths. Multiparametric system and data display allow the operator to choose the mode of operation and representation of data by hardware switches. The CAMAC branch offers a practically unlimited expansion possibility for all CAMAC devices which are available today. Programming can be done in BASIC or FORTRAN, both running under Data General's Real-

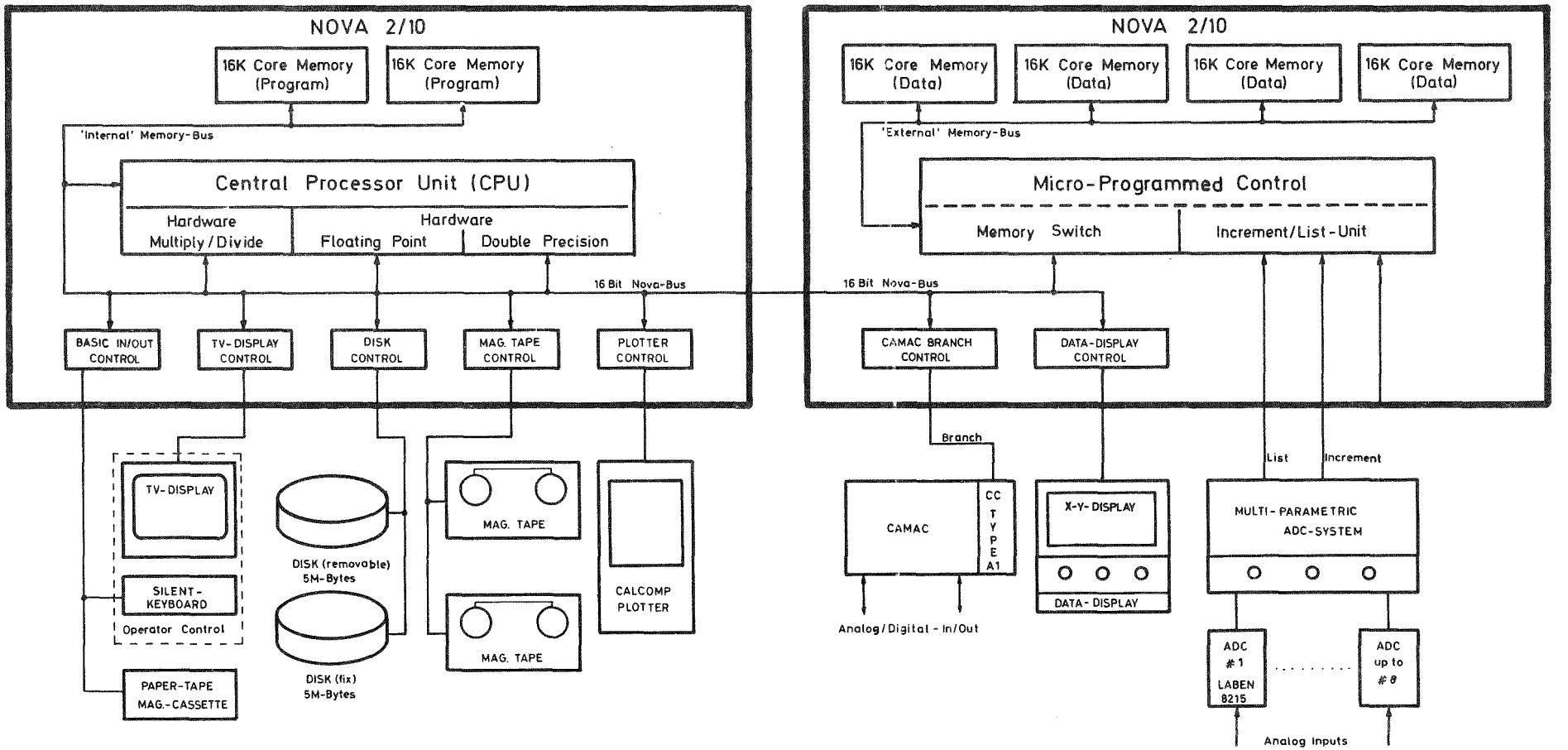

Fig. 1 Hardware configuration of the cyclotron experimental computer.

time Disk Operating System RDOS. Special drivers for the home made and experimental devices are written as assembler subroutines and can be called from the user's BASIC or FORTRAN programs.

+IAK Computer Group

References

/1/ G. Ehret, H. Hanak; Report KFK 2183 (1975) p. 99
/2/ Contribution 6.5.2

6.5.2 An ADC Multiparametric System for Nova Computers

W. Karbstein

Multichannel analysers are less suitable than computers in the field of pulse height analysis if, in addition to data acquisition, complex on-line data evaluation or digital data input (output) are required. This led to the development of special ADC interfaces for various computers. Since modular and computer independent ADC interfaces in CAMAC are not yet available we decided to develop the concept of a hardware multiparametric system which is now being built by Laben.

Fig. 1 shows the whole system schematically. Computer and increment unit are also shown in the picture in order to illustrate the operation of the whole system.

Up to 8 ADCs can be connected to the *ADC-transfer control unit*. Depending on the ADC-mode-switch (one per ADC), the respective ADCs are working in *coincidence mode*, in *single* (or increment) *mode* or are switched off. The modes of operation (coincidence or single) can exist simultaneously and independently from each other. Any ADC of the Laben 8000 Series with or without mixer/router units can be used. In *coincidence* (or list) *mode* data of all ADCs connected in this mode are transferred at end of conversion or after a preselected 'maximum conversion time'. This occupies one data channel of the increment unit in list mode.

In *single* (or increment) *mode* the data of the connected ADCs are switched to a separate output, which can be fed to the second data channel of the increment unit via the window control (for hardware data reduction).

By use of additional *mixer-router/multiplexer*-units (double function) the number of analogue inputs can be increased up to 64. When used as *mixer-router* the first incoming analogue signal on input 1...8 is led to the ADC with the respective binary identification. All remaining inputs are closed, coincidence events are rejected. When used as *multiplexer* only

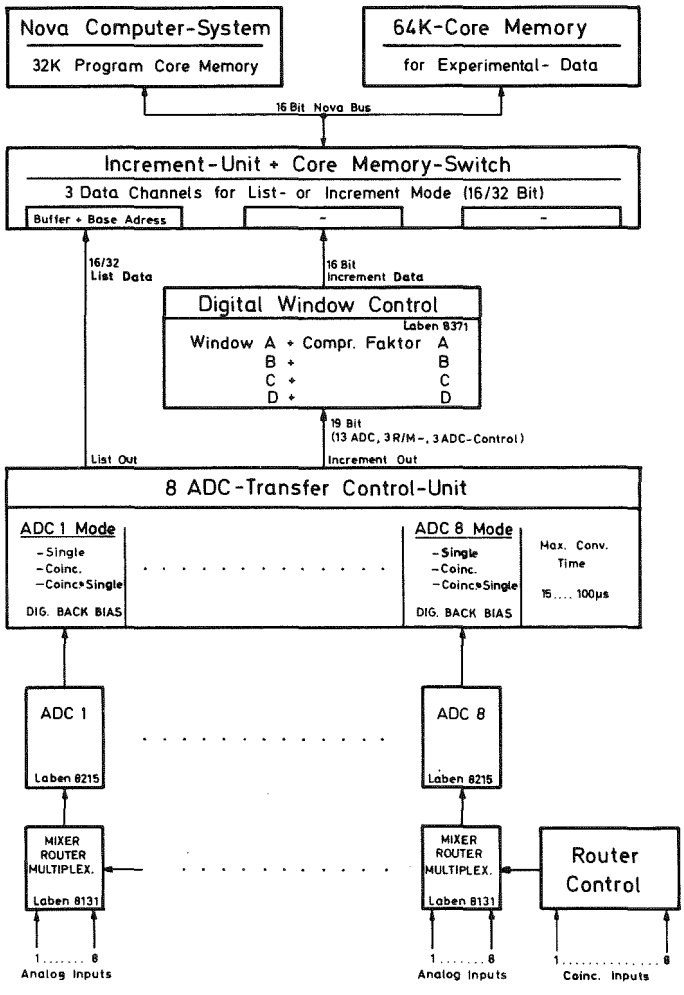

Fig. 1 The ADC multiparametric system as connected to the NOVA computers. The *increment unit* which is a special Nova controller allows the connection of additional 64 K-core memory and also connects three experiment data channels in increment and list mode (16 or 32 bit each).

preselected analogue inputs are opened. This is accomplished by the *mixer-router control* unit which also has 8 inputs. These inputs are normally used for the fast coincidence signals which cause the corresponding multiplexer analogue input to be opened for a preselectable time (1-16 µs).

If each of the 8 ADCs (13 bits) uses an 8 input mixer-router a 512 K-data memory would be required. On the other hand, if not all or non successive inputs are used this would result in empty spaces within the spectra. To avoid this as well as memory address overflow, these spaces are first eliminated by the 'digital backbias' switches (one set for each ADC) and then - if necessary - the spectra are compressed by the *digital window control*. This unit allows the

choice of 4 digital windows. Three of the windows are selectable by octal thumbwheel switches, the fourth window results of the upper limit of window C and the maximum area of 512 K. Within these windows the spectra can independently be compressed by compression factors of 1,2,4...64 and ∞.

The system described here will be equipped with 3 ADCs (Laben 8215, 5 µs fixed conversion time, SK) and 2 mixer/routers (Laben 8131). It gives the operator all the advantages of multichannel analysers (e.g. choosing the modes of operation by hardware switches) as well as the possibilities of a computer system.

6.5.3 A BASIC Data Acquisition and Analysis Program for the Experiment Computer NOVA 2 at the Van de Graaff Accelerator

K. Wisshak and H. Sobiesiak

For data acqusition and data evaluation during experiments with the Van de Graaff accelerator a BASIC program has been developed for a NOVA 2 computer with 32 K memory. The program consists of a main part resident in the memory and subprograms stored as overlays on disk. For data acquisition a 2 K increment area is used, divided into 4 parts with 512 channels each (e.g. time-of-flight and pulse height spectra of two detectors).

The main program comprises all steps which are frequently used or to which fast access is essential. It contains the routines for a software display, it executes commands given as interrupts from a single-bit-control and controls data acquisition. The 16 bits of the single-bit-control are used for simple options like acquire on-off, move marker, expand display, change display, scale etc. In an automatic data acquisition mode the experimental data of different samples, changed after a definite time in a cyclic sequence, are stored on magnetic tape. In addition, for each probe an integral spectrum is stored on disk, containing the data of the increment areas for the individual measurements.

The subprograms can be divided into three groups. The first group consists of programs for data transfer. They render possible transfer between increment area, disk, tape, keyboard and plotter. The second group comprises over-

lays for simple spectrum handling like addition, linear background subtraction, channel compression, integration etc. The last group offers a lot of utilities necessary for data evaluation e.g. determination of peak position, smoothing, linear scale transformation, interpolation, unfolding of a resolution function etc.

The simple and transparent programming in BASIC offers the possibility for other users to adjust the program in an optimum way to their own measurements and to add new subprograms.

6.5.4 An Interactive Beam Transport Optimization Program with Graphic Facilities in BASIC

W. Kneis

Many computer programs for simulation of beam transport systems have been developed over the past decades. Compared with former programs /1,2/ running on batch computers and printing long lists and matrices of beam lines, the programs offered today emphasize the graphic presentation of results and the provision of facilities allowing the user to interact with the program /3,4/. The need for this can be understood by the fact that for all but the simplest problems there is no unique solution for beam optimization. So the user must have the means to impose the right constraints - also during the run - to his optimization to arrive at acceptable solutions. The possibility to interact with the program is also advantageous for finding initial values for iteration.

The beam optics design system, BOD, implemented on a Nova 2 computer consists of three programs:

BODIO - System Input/Output
BODIGA - Graphic Package
BODEONI- Optimization Program

The three programs available under BASIC are connected to each other by a common data base and are controllable via a switchboard with 24 individual switches (fig. 1). The system allows to describe a beam guiding system consisting of drift spaces, quadrupoles (electrical or magnetic), bending elements, edge angles, and coordinate rotation and to display either the resulting phase space ellipses (fig. 2) for the x- and y-subspaces at the

```
BODIO:          9/ 9/1976   17: 4:33
        B O D I O    SWITCHES

 1 - INPUT OF NEW PROBLEM
 2 - DESCRIPTION OF 'BODIGA'
 3 - DESCRIPTION OF 'BODEONI'
 4 - INPUT ELLIPSE FOR START
 7 - INPUT NOMINAL ELLIPSE AT END
 8 - FITTING CONSTRAINTS FOR NOMINAL
     ELLIPSE
10 - INPUT OPTICAL ELEMENTS
11 - INPUT VARIABLE OPTICAL ELEMENTS
12 - CHANGE OPTICAL ELEMENTS
     13 - =0 - DELETE
          =1 - INSERT
16 - PRINT PROBLEM CHARACTERISTIC
19 - START ITERATION -> 'BODEONI'
20 - START RAY TRACING -> 'BODIGA'
21 - BATCH MODE
22 - INPUT FROM DISK
23 - OUTPUT TO DISK
24 - PRINT DISK FILES
```

```
BODIO:          9/ 9/1976   17:52:15
        B O D I G A    SWITCHES

 1 - =0 - DISPLAY ELLIPSE AT END
     =1 - DISPLAY BEAM ENVELOPE
 2 - DO NOT ERASE DISPLAY
 3 - DISPLAY ELLIPSE AT START
 5 - SETTING OF VARIABLE OPTICAL
     ELEMENTS
 6 - PRINT RAY TRACING
 8 - UNIT: [KG] (SLAC)
 9 - UNIT: [KG/CM] FOR Q, [KG] FOR B
19 - CALLED BY PROGRAM
21 - BACK TO 'BODIO' (BATCH MODE)
23 - OUTPUT TO DISK
```

```
BODIO:          9/ 9/1976   18: 7:55
        B O D E O N I    SWITCHES

 2 - DISPLAY ELLIPSE AT END
 3 - DO NOT PRINT ITERATIONS
 4 - PRINT U,T,V
 5 - PRINT XN SUBROUTINE 4000
 6 - PRINT RAY TRACING
 8 - FIT WITH BOUNDARY CONSTRAINTS
 9 - SHORT TERM PRINT OUTPUT
10 - STOP IMMEDIATELY
11 - PRINT ELLIPSE AT END
12 - PRINT VARIABLE OPTICAL ELEMENTS
13 - NO AUTOMATIC STOP IF DIVERGENT
14 - STOP ONLY IF CHIQU<1%
19 - CALLED BY PROGRAM
21 - BACK TO 'BODIO' (BATCH MODE)
23 - OUTPUT TO DISK AUTOMATICALLY
24 - PRINT DISK FILES
```

Fig. 1 Function switches for the control of the BOD-systems.

a) program BODIO

b) program BODIGA

c) program BODEONI

```
BODIGA:          9/ 9/1976   22:47: 2
IN:TK5M4              ** [KG] -  SLAC **

XMAX          4.903   *  1 END:      0.000
ALPHA          .419     19 FKEY:       .250
XTMAX         1.980     20 * CHANGE END *
X0            8.125
XT0            .243

YMAX         11.906
ALPHA          .951
YTMAX         6.314
Y0            1.875
YT0           1.059
```

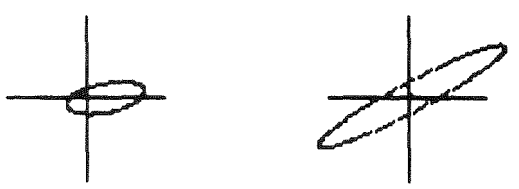

HORIZONTAL VERTICAL

Fig. 2 Specification and display of the horizontal and vertical phase space ellipses.

desired point of the z-axis or to show the beam envelopes in x and y along the beam guiding system (fig. 3). Furthermore it allows to optimize the settings of the optical elements by a least squares iteration method via nominal constraints of the phase space ellipse or boundary constraints. Ray tracing is performed by application of the conventional first order 4 * 4 transfer matrices /1/ to the phase space ellipses. The elements of the phase space ellipse σ are:

$$\sigma = \begin{pmatrix} \sigma_{11} & \sigma_{12} & & 0 \\ \sigma_{12} & \sigma_{22} & & \\ & & \sigma_{33} & \sigma_{34} \\ 0 & & \sigma_{34} & \sigma_{44} \end{pmatrix}$$

with $\sigma_{11} = XMAX^2$ $\quad \sigma_{33} = YMAX^2$

$\sigma_{12} = ALPHA * XMAX * X'MAX$ $\quad \sigma_{34} = ALPHA * YMAX * Y'MAX$

$\sigma_{22} = X'MAX^2$ $\quad \sigma_{44} = Y'MAX^2$

(see fig. 2 and 3).

The desired coordinate system can be chosen by the specification of a beam centroid shift and a reference angle in the bending elements.

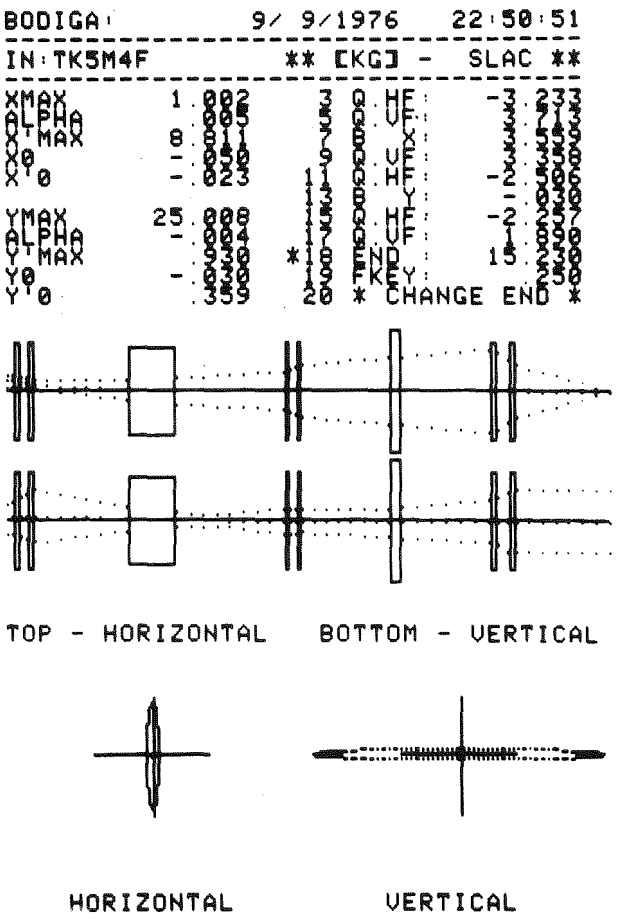

Fig. 3 Graphical and numerical representation of the horizontal and vertical phase space ellipses at END (z=15.23 m) the beam guiding system and the beam envelopes through the system.

References

/1/ K.L. Brown, S.K. Howry; Report SLAC 91 (1970)

/2/ W. Gardner, D. Whiteside; Rutherford High Energy Laboratory, Report NIRL/M/21 (1961)

/3/ B.W. Davis; Nucl. Instr. Meth. 105 (1972) 477

/4/ D.V. Amundson, J.W. Dawson; Particle Accelerators 4 (1972) 19

6.5.5 A Keyboard Input Handler for DGC FORTRAN IV on NOVA 2 Computers

H. Sobiesiak

The "Extended BASIC" language offers a convenient possibility of interactive operation by means of the statement "ON ESC GOSUB", but for many applications this language is too slow, especially if large amounts of data are to be handled. In this case DGC FORTRAN IV (DGC=Data General Corporation) can be used which however has no comparable statement for interactive operation. As FORTRAN is often used in subprograms which are called from the BASIC main program, it was necessary to have an external interrupt possibility for this language, too. As FORTRAN IV interacts with the keyboard input in the same way as with all other files and devices, a special keyboard input handler (KIH) was developed.

Contrary to normal DGC FORTRAN IV where keyboard input is done by the RDOS-system call .RDL, now the keyboard input is performed by task calls (XMT and REC) between the main program and a special keyboard input task. (Thus programs using this input handler have to be multitasking programs). The operation of the KIH can be described in the following way: If the user program demands any ASCII-input (READ- or ACCEPT-statement) first a check is made whether input is required from the keyboard or from any other file and if the input does not come from the keyboard, the normal way (.SYSTEM.RDL) is used. If input from the keyboard is required, the task call REC is issued, and if a character is received it will be echoed on the keyboard printer. At the detection of a NULL, CARRIAGE RETURN or LINE FEED input is terminated. The terminating character will not be echoed leaving it up to the user program to give a CARRIAGE RETURN after the input. When an user program enters the KIH it first issues a REC-call to ensure that the handler is not occupied by another task. On the other hand the KIH itself issues the system call .GCHAR and waits until a character is typed. Each incoming character is compared to a table of ten possible characters which are defined as interrupt characters. If the typed character is identified as one of these ten a

FORTRAN Subroutine linked to this character is called. If the incoming character does not match to any of these ten, 256 is added and the character is then transmitted to the user program by the task call XMT. Of course, also the FORTRAN statement PAUSE was implemented in this handler routine.

The KIH consists of nine subroutines requiring 543_{10} words of memory. Four of these routines are written in ASSEMBLER language and the other five in FORTRAN IV with small (but important) modifications being made after compilation. The program is designed for revision 3.0 of DGC FORTRAN IV.

The KIH was first applied to a plot program for a CALCOMP plotter which is linked to the BASIC program WSTART /1/. The plot program communicates with BASIC by a common file named "FBCOM.CM.". Plotting can be terminated by pressing the ESC-key in which case the pen is positioned back to the beginning of the page, an ERROR flag is written on file FBCOM.CM. and the BASIC program is restored in the memory.

References

/1/ Contribution 6.5.3

6.5.6 Supplementary Subroutines for the Coupled Channels Code ECIS-Karlsruhe

H.J. Gils

The Karlsruhe version of the coupled channels code ECIS /1/ was supplemented by some subroutines for the following purposes in α-particle scattering analyses:

a) Cross sections can be calculated from groundstate (ρ_o) and transition densities (ρ_{tr}) given from theory or from other experiments. Different radial shapes are allowed for proton and neutron densities.

b) For analysing experimental α-particle scattering cross sections in the framework of the folding model /2/ assuming a harmonic vibrator nucleus the radial shape of the transition density can be fitted to the measured data independent from the shape of the transition density.

Both possibilities can be combined. Five different subroutines PØTENT compiled in tab. 1 have been written which have to be substituted instead of the standard version of PØTENT for the folding model of the harmonic vibrational nucleus FØLHVI (cf. ref. /1/ p. 75). A description of the special purposes and of the handling of the subroutines will be given in ref. /3/.

Table 1 Compilation of the supplementary subroutines PØTENT for the coupled channels code ECIS-Karlsruhe. Data of given densities are read and stored in equidistant radial steps by a special subroutine RØDATA. F2: 2-parameter Fermi shape; F2-Di: derivative of F2 independent from ρ_o; F2-Dd: derivative of Fermi shaped groundstate distribution ρ_o.

Name	ρ_o	Shape	ρ_{tr}	Shape	Purpose
PØTOL	given	arbitrary	given	arbitrary	a)
PØTDG	calculated	F2	calculated	F2-Di	b)
PØTO	given	arbitrary	calculated	F2-Di	a),b)
PØTO3P	p:given	arbitrary	p:given	arbitrary	
	n:calculated	F2	n:calculated	F2-Dd	a),b)
PØTO3D	n:given	arbitrary	n:calculated	arbitrary	a),b)
	p:given	arbitrary	p:given	F2-Di	

References

/1/ G.W. Schweimer and J. Raynal; (1973) unpublished

/2/ H. Rebel; Report KFK 2065 (1974)

/3/ H.J. Gils; to be published

6.5.7 Program IONBEAM

D. Heck and E. Kasseckert+

As image aberrations might play an important role on the focusing of ion beams to diameters of some microns /1/, the program IONBEAM has been implemented on the IBM 370/168. This program uses the transport matrix formalism /2/ and operates in a manner similar to the wide spread program TRANSPORT /3/, but moreover it permits calculations up to the third order approximation. The improved Karlsruhe version permits to fit third order

matrix elements, thus geometric image aberration coefficients can be influenced in a desired manner, by tuning suitable correcting elements (e.g. octopoles /4/).

A large variety of elements may be assembled to form a beam line, consisting of

drift spaces,
homogeneous fields with normal , inclined and curved boundaries,
quadrupoles, hexapoles and octopoles, (electrostatic or magnetic),
including fringe field effects,
beam rotations and displacements.

Restrictions exist for a) the number of input parameters ($\leq$ 500)
b) the number of variable parameter ($\leq$ 10)

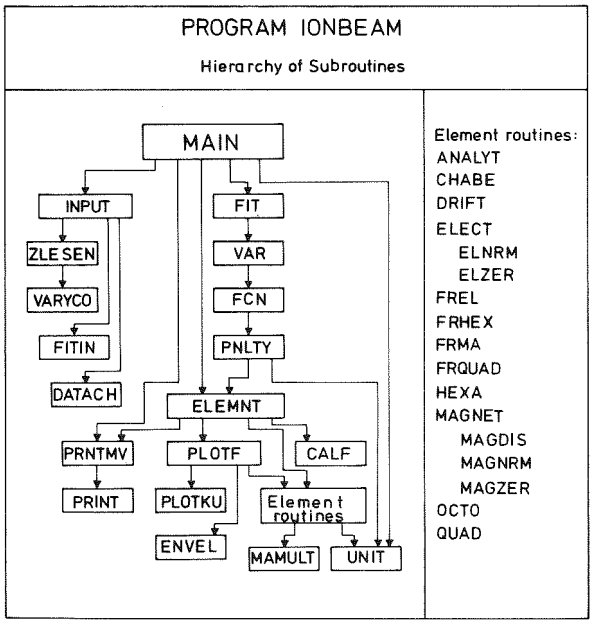

Fig. 1 Flow diagram and list of Subroutines of IONBEAM

The modular composition of the program with subroutines (see fig. 1) easily allows an extension to further elements by adding appropriate subroutines to the list on the right margin of fig. 1. The special matrix multiplication routine MAMULT results in short computation times, typically less than 1 sec for the field gradient fit of a beam line consisting of a

quadrupole doublet. The core memory region request amounts to 156 K bytes.

+ II. Physikalisches Institut, Justus Liebig Universität, Gießen

References

/1/ Contribution 6.2.3

/2/ K.L. Brown; Report SLAC 75 (1967);
K.G. Steffen; High Energy Beam Optics, ed. R.E. Marshak
(John Wiley & Sons, New York, 1965) p. 12

/3/ K.L. Brown, S.K. Howry; Report SLAC 91 (1970)

/4/ D. Heck; Report KFK 2288 (1976)

7. PUBLICATIONS AND CONFERENCE CONTRIBUTIONS

Abdel-Wahab, M.S.; Bialy, J.; Junge, M.; Schmidt, F.K.; Bechtold, V.; Friedrich, L.

Experimentelle Untersuchung der Aufbruchsreaktion dp→ppn am vektorpolarisierten Deuteronenstrahl des Karlsruher Isochronzyklotrons.
Frühjahrstagung DPG und OEPG, Kernphysik, Baden/Österr., 29. März - 2. April 1976.
Verhandlungen der Deutschen Physikalischen Gesellschaft, R.6, Bd 11 (1976) S. 965

Abdel-Wahab, M.S.; Bechtold, V.; Bialy, J.; Friedrich, L.; Junge, M.; Schmidt, F.K.; Strassner, G.

Vektoranalysierstärken der elastischen Deuteron-Proton- und Deuteron-Deuteron-Streuung bei 52 MeV.
Frühjahrstagung DPG und OEPG, Kernphysik, Baden/Österr., 29. März - 2. April 1976.
Verhandlungen der Deutschen Physikalischen Gesellschaft, R.6, Bd. 11 (1976) S. 966

Bechtold, V.; Friedrich, L.; Finken, D.; Strassner, G.; Ziegler, P.

Present State of the Karlsruhe Polarized Ion Source.
4. Internat. Symposium on Polarization Phenomena in Nuclear Reactions, Zürich, August 25-29, 1975

Bechtold, V.; Friedrich, L.; Bialy, J.; Junge, M.; Schmidt, F.K.; Strassner, G.

Elastic and Inelastic Scattering of 52 MeV Vector Polarized Deuterons in ^{12}C.
4. Internat. Symposium on Polarization Phenomena in Nuclear Reactions, Zürich, August 25-29, 1975

Bechtold, V.; Friedrich, L.; Finken, D.; Strassner, G.; Ziegler, P.

Polarized Deuterons of a Lambshift Ion Source Accelerated by the Karlsruhe Isochronous Cyclotron.
7. Internat. Conference on Cyclotrons and their Applications, Zürich, August 19-22, 1975

Bechtold, V.; Friedrich, L.; Strassner, G.; Breuer, H.; Doll, P.; Knoepfle, K.T.; Mairle, G.; Sessler, A.; Wagner, G.J.

Spinbestimmung von 1p-Lochzuständen in ^{15}N mit vektorpolarisierten Deuteronen.
Frühjahrstagung DPG und OEPG, Kernphysik, Baden/Österr., 29. März - 2. April 1976.
Verhandlungen der Deutschen Physikalischen Gesellschaft, R.6, Bd 11 (1976) S. 860

Beer, H.; Ly Di Hong; Käppeler, F.

The Total Cross Section of ^{58}Fe in the Neutron Energy Range 7 - 400 keV.
Neutron Interlab. Seminar CBNM, Geel/Belgien November 12-14, 1975

Beer, H.

Partial radiation widths of $^{58,60}Ni$ and ^{56}Fe resonances.
Neutron Interlab. Seminar CBNM, Geel/Belgien, November 12-14, 1975

Beer, H.; Rohr, G.;

Study of keV-Resonances in the Total Cross Sections of ^{63}Cu and ^{65}Cu.
Z. Physik A 277 (1976) 181

Bräuer, N.; Dimmling, F.; Kornrumpf, T.; Hartrott, M. von; Nishiyama, K.; Riegel, D.; Schweickert, H.

Magnetic Moment of the 8^-, 275 µs State in ^{114}Sb.
Internat. Meeting on Hyperfine Interactions Studied by Nuclear Methods, Louvain, September 10-12, 1975

Buschmann, J.; Faust, H.; Klewe-Nebenius, H.; Kropp, J.; Rebel, H.; Schulz, F.; Wisshak, K.

In Beam Studies of Ir, ^{197}Au (^6Li, xn+yp) Reactions Induced by ^6Li-Ions of up to 156 MeV.
Internat. Symposium on Highly Excited States in Nuclei, Jülich, September 22-26, 1975

Chaffin, E.F.; Dickmann, F.

Der Massentensor in der Dynamik der Kernspaltung.
Frühjahrstagung DPG und OEPG, Kernphysik, Baden/Österr., 29. März - 2. April 1976.
Verhandlungen der Deutschen Physikalischen Gesellschaft, R.6, Bd 11 (1976) S. 970

Chaffin, E.F.; Dickmann, F.

Dynamics of Fission from Saddle to Scission.
APS Spring Meeting, Washington, D.C., April 26-29, 1976, Bull. Am. Phys. Soc. Ser. II, Vol. 21 (1976) No. 4 p. 656

Cierjacks, S.; Schouky, I.

Elastische Neutronenstreuung an ^{16}O und ^{28}Si.
Frühjahrstagung DPG und OEPG, Kernphysik, Baden/Österr., 29. März - 2. April 1976.
Verhandlungen der Deutschen Physikalischen Gesellschaft, R.6, Bd 11 (1976) S. 823-24

Cierjacks, S.; Schmalz, G.; Erbe, D.; Voss, F.

Das verbesserte Neutronen-Flugzeitspektrometer am Karlsruher Isochronzyklotron.
Frühjahrstagung DPG und OEPG, Kernphysik, Baden/Österr., 29. März - 2. April 1976.
Verhandlungen der Deutschen Physikalischen Gesellschaft, R.6, Bd 11(1976) S. 916-17

Cierjacks, S.; Cocu, F.; Haouat, G.; Lachkar, J.; Patin, Y.; Sigaud, J.

Inertial- und Dämpfungseffekte bei der Spaltung von ^{233}U und ^{240}Pu.
Frühjahrstagung DPG und OEPG, Kernphysik, Baden/Österr., 29. März - 2. April 1976.
Verhandlungen der Deutschen Physikalischen Gesellschaft, R.6, Bd 11 (1976) S. 969

Cierjacks, S.

A Neutron Flux Detector for Spectra Measurements between 1 and 30 MeV.
Neutron Interlab. Seminar CBNM, Geel/Belgien November 12-14, 1975

Cierjacks, S.

Partial and Average Level Densities of Nuclear States.
Kolloquiumsvortrag im Kernphysikalischen Institut des Centre d'Etude de Bruyeres le Chatel, Frankreich, 19.3.1976

Cierjacks, S.; Schmalz, G.; Töpke, R.; Spencer, R.H.; Voß, F.

Thick Sample Transmission Measurement and Resonance Analysis of the Total Neutron Cross Section of Iron.
NBS Special Publication 425,
US Department of Commerce, Vol. II, p. 754, Oct. 1975

Cierjacks, S.; Leugers, B.; Kari, K.; Brotz, P.; Erbe, D.; Gröschel, D.; Schmalz, G.; Voß, F.

Measurements of Neutron Induced Fission Cross Section Ratios at the Karlsruhe Isochronous Cyclotron. NEANDC/NEACRP Specialist Meeting on Fast Neutron Fission Cross Sections of ^{233}, ^{235}, ^{238}U and ^{239}Pu, Argonne, Illinois, June 28-30, 1976

Eberle, H.

Aktivierungsanalyse von Manganknollen mit 14 MeV-Neutronen.
KFK-2291 (Mai 1976)

Ehret, G.; Karbstein, W.; Kneis, W.

Basic Subroutines for CAMAC on Nova 2 Computers.
2. Internat. Symposium über CAMAC für Datenverarbeitungsanwendungen, Brüssel, October 14-16, 1975

Eyrich, W.; Berg, M.; Hofmann, A.; Rebel, H.; Scheib, U.; Schneider, S.; Vogler, F.

$^{24}Mg(\alpha,\alpha'\gamma)$ Angular Correlation Measurements at 104 MeV as a Test for the Quadrupole Deformation.
4. Internat. Symposium on Polarization Phenomena in Nuclear Reactions, Zürich, August 25-29, 1975

Eyrich, W.; Gerbig, V.; Hofmann, A.; Scheib, U.; Schneider, S.; Vogler, F.; Rebel, H.

Teilchen-γ-Winkelkorrelationen als Mittel zur Untersuchung von Kernreaktionen.
Frühjahrtagung DPG und OEPG, Kernphysik, Baden/Österr., 29. März - 2. April 1976.
Verhandlungen der Deutschen Physikalischen Gesellschaft, R.6, Bd 11(1976) S. 895

Eyrich, W.; Hofmann, A.; Scheib, U.; Schneider, S.; Vogler, F.; Rebel, H.

Study of Prolate-Oblate Effects by Use of Particle - γ Angular Correlations in the Reaction $^{24}Mg(\alpha,\alpha_1)^{24}Mg$.
EPS Conference on Radial Shape of Nuclei, Cracow, Poland, June 22-25, 1976

Faust, H.; Wisshak, K.; Klewe-Nebenius, H.; Rebel, H.; Gils, H.J.; Hanser, A.

Die L=4 Übergangswahrscheinlichkeit aus der inelastischen α-Streuung an ^{60}Ni und der direkten Beobachtung des $4_1^+ \rightarrow 0^+$ -Übergangs nach dem Zerfall von ^{60}Co.
Frühjahrstagung DPG und OEPG, Kernphysik, Baden/Österr., 29. März - 2. April 1976.
Verhandlungen der Deutschen Physikalischen Gesellschaft, R.6, Bd 11 (1976) S.840-41

Gerve, A.; Schatz, G.

Applications of Cyclotrons in Technical and Analytical Studies.
7. Internat. Conference on Cyclotrons and their Applications, Zürich, August 19-22, 1975

Gils, H.J.

Experimentelle Untersuchungen der Radiusdifferenzen zwischen Protonen- und Neutronendichteverteilung von $^{204,206,208}Pb$ und Studien von Oktupolübergangsdichten durch Streuung von 104 MeV-α-Teilchen.
Dissertation, Univ. Heidelberg 1975
KFK-2225 (November 75)

Gils, H.J.

Isoskalare Übergangswahrscheinlichkeiten aus Streuexperimenten mit α-Teilchen und Untersuchungen der Neutronenkollektivität in ^{208}Pb.
Expertentreffen der Kernphysiker, Schleching, 2.-12. März, 1976

Gils, H.J.; Rebel, H.; Buschmann, J.; Klewe-Nebenius, H.; Nowicki, G.; Nowatzke, W.

Experimentelle Untersuchungen der Unterschiede zwischen den kollektiven Eigenschaften von Protonen und Neutronen in $^{204,206,208}Pb$ durch α-Teilchen-Streuung:
RMS-Radien und Oktupol-Übergangsraten.
Frühjahrstagung DPG und OEPG, Kernphysik, Baden/Österr., 29. März - 2. April 1976.
Verhandlungen der Deutschen Physikalischen Gesellschaft, R.6, Bd 11 (1976) S.857-58

Gils, H.J.; Rebel, H.

Differences between neutron and proton density RMS-radii of $^{204,206,208}Pb$ determined by 104 MeV α-particle scattering.
Phys. Rev. C13 (1976) 2159
EPS Conference on Radial Shape of Nuclei, Cracow, Poland, June 22-25, 1976

Gils, H.J.; Rebel, H.

Ist die Kernoberfläche neutronenreich?
KFK-Nachrichten, 8 (1976) No 1, S.29-32

Hartwig, D.; Kappel, W.; Kneis, W.; Möllenbeck, J.; Schatz, G.; Schweickert, H.

Computer Controlled Beam Diagnostics at the Karlsruhe Isochronous Cyclotron.
7. International Conference on Cyclotrons and their Applications, Zürich, August 19-22, 1975

Haushahn, G.; Möllenbeck, J.; Schatz, G.; Schulz, F.; Schweickert, H.

Status Report of the Axial Injection System at the Karlsruhe Isochronous Cyclotron.
7. International Conference on Cyclotrons and their Applications, Zürich, August 19-22, 1975

Haushahn, G.; Möllenbeck, J.; Schatz, G.; Schulz, F.; Schweickert, H.

Status Report of the Axial Injection System at the Karlsruhe Isochronous Cyclotron.
Frühjahrstagung DPG und OEPG, Kernphysik, Baden/Österr., 29. März - 2. April 1976, Verhandlungen der Deutschen Physikalischen Gesellschaft, R.6, Bd 11 (1976) S. 809

Heck, D.

Third Order Transfer Matrix Elements of Octopoles.
KFK-2288 (April 76)

Käppeler, F.; Ly Di Hong; Rupp, G.

The Total Cross Section of ^{240}Pu and ^{242}Pu between 20 and 560 keV Neutron Energy.
Neutron Interlab. Seminar CBNM, Geel/Belgien, November 12-14, 1975

Käppeler, F.

A Method for Capture Cross Section Measurements of ^{241}Am in the keV Region.
Neutron Interlab. Seminar CBNM, Geel/Belgien, November 12-14, 1975

Käppeler, F.; Naqvi, A.; Ernst, A.; Müller, R.; Gönnenwein, F.

4-Parameter (E,v)-Experiment an korrelierten Spaltfragmenten; (a) Aufbau und Durchführung.
Frühjahrstagung DPG und OEPG, Kernphysik, Baden/Österr., 29. März - 2. April 1976.
Verhandlungen der Deutschen Physikalischen Gesellschaft, R.6, Bd 11 (1976) S. 972

Käppeler, F.; Dickmann, F.

The Energy Gap at the Saddle Point Deformation of ^{236}U.
NEANDC/NEACRP Specialist Meeting on Fast Neutron Fission Cross Sections of ^{233}, ^{235}, ^{238}U and ^{239}Pu,
Argonne, Illinois, June 28-30, 1976

Käppeler, F.; Bandl, R.-E.

The Average Number of Prompt Neutrons, $\bar{\nu}$, from Neutron Induced Fission of ^{235}U between 0.2 and 1.4 MeV.
Annals of Nuclear Energy, 3 (1976) S. 31-39

Kappel, W.; Karbstein, W.; Kneis, W.; Möllenbeck, J.; Schweickert, H.; Volk, B.

Computer Aided Operation of the Karlsruhe Isochronous Cyclotron Using CAMAC.
2. Internat. Symposium über CAMAC für Datenverarbeitungsanwendungen, Brüssel, Oktober 14-15, 1975

Kappel, W.; Karbstein, W.; Kneis, W.; Möllenbeck, J.; Schweickert, H.; Volk, B.

CICERO, ein interaktives Programmsystem für den rechnerunterstützten Zyklotronbetrieb unter Verwendung von CAMAC.
Frühjahrstagung der Studiengruppe für Nukleare Elektronik, Arbeitsgemeinschaft der Grossforschungseinrichtungen, Stuttgart, 22.-24. März, 1976

Kneis, W.; Karbstein, W.

CAMAC with Fortran on a CDC 3100, an Approach Based on IML.
CAMAC Bulletin, No 13 (1975) S. 18-20

Kropp, J.; Buschmann, J.; Wisshak, K.; Faust, H.; Klewe-Nebenius, H.; Rebel, H.

Anregungsfunktionen von (^{6}Li, xn+p)-Reaktionen bei Energien bis E(Li)=156 MeV.
Frühjahrstagung DPG und OEPG, Kernphysik, Baden/Österr., 29. März - 2. April 1976.
Verhandlungen der Deutschen Physikalischen Gesellschaft, R. 6, Bd 11 (1976) S. 891

Krien, K.; Soares, J.C.; Vianden, R.; Bibiloni, A.G.; Hanser, A.

Temperature Dependence of the Quadrupole Interaction of ^{100}Rh in a Cd Lattice.
Hyperfine Interactions, 1 (1975) p. 295-300

Leugers, B.; Kari, K.

Eine Gasszintillator-Anordnung zur Messung von Spaltfragmenten bei hohem α-Untergrund.
Frühjahrstagung DPG und OEPG, Kernphysik, Baden/Österr., 29. März - 2. April 1976.
Verhandlungen der Deutschen Physikalischen Gesellschaft, R. 6, Bd 11 (1976) S. 843

Leugers, B.; Cierjacks, S.; Brotz, P.; Erbe, D.; Gröschel, D.; Schmalz, G.; Voß, F.

The ^{235}U and ^{238}U Neutron Induced Fission Cross Section Relative to the H(n,p) Cross Section.
NEANDC/NEACRP Specialist Meeting on Fast Neutron Fission Cross Sections of $^{233,235,238}U$ and ^{239}Pu, Argonne, Illinois, June 28-30, 1976

Linker, G.; Käppeler, G.; Meyer, O.

Internationale Tagung "Anwendung von Ionenstrahlen zur Materialanalyse".
KFK-Nachrichten, 7 (1975) No 4, S. 23

Matussek, P.; Ottmar, H.

On the Use of Gamma-Ray Spectrometry for In-line Measurements of U-235 Enrichment in a Nuclear Fuel Fabricating Plant.
Internat. Symposium on Safeguarding of Nuclear Materials, Vienna, October 20-24, 1975

Michel, F.; Münzel, H.; Schulz, F.; Schweickert, H.

Statusbericht über die ^{123}J-Produktion am Karlsruher Isochron-Zyklotron.
Jod-123-Panel, Jülich, 13. Februar, 1976

Müller, R.; Gönnenwein, F.; Käppeler, F.; Naqvi, A.; Ernst, A.

4-Parameter (E,v)-Messung an korrelierten Spaltfragmenten;
(b) Auswertung und erste Ergebnisse.
Frühjahrstagung DPG und OEPG, Kernphysik, Baden/Österr., 29. März - 2. April 1976.
Verhandlungen der Deutschen Physikalischen Gesellschaft, R.6, Bd 11 (1976) S. 973

Ottmar, H.; Matussek, P.; Piper, I.

On-line Bestimmung der ^{235}U-Anreicherung an oxidischem Uran in der Prozesslinie einer LWR-Brennelement-Fabrikationsanlage.
Nuclex 75, Basel, 7.-11. Oktober 1975.
Kolloquium C1, Paper; 11 S.

Ottmar, H.; Matussek, P.

In-process control of U-235 enrichment in a LWR fuel fabrication plant.
Internat. Seminar on Nuclear Fuel Quality Assurance, Oslo, May 24-28, 1976

Pinston, J.A.; Roussille, R.; Börner, H.; Koch, H.R.; Heck, D.

Level Structure of ^{149}Nd.
(I). The ^{148}Nd (n,γ) Reaction.
Nuclear Physics A264 (1976) S.1

Rebel, H.

Nuclear Size and Shape Information from Alpha Particle Scattering at 100 MeV.
Symposium on Nuclear Structure: Coexistenz of Single Particle and Collective Types of Excitations, Balatonfuered/Hung., September 1-7, 1975 .

Rebel, H.; Gils, H.J.; Knüpfer, W.

Experimental Studies of Neutron Collectivities by α-particle Scattering and Some Implications for Giant Resonance Excitations.
14. Internat. Winter-Meeting on Nuclear Physics, Bormio/Italy , January 19-24, 1976

Rebel, H.

How to extract Isoscalar Transition Rates from Alpha Particle Scattering Experiments.
Z. Physik A277 (1976) 35

Rebel, H.

Realistische Coulomb-Potentiale bei Coupled-Channel-Rechnungen für die Streuung von α-Teilchen und ^{16}O-Ionen an deformierten Kernen.
KFK-2247 (Januar 76)

Rebel, H.; Geramb, H.V. von

Realistische Coulombeffekte bei Schwellenwertstreuung.
Frühjahrstagung DPG und OEPG, Kernphysik, Baden/Österr., 29. März - 2. April 1976.
Verhandlungen der Deutschen Physikalischen Gesellschaft, R.6, Bd 11 (1976) S. 819

Rebel, H.

Nuclear Matter Distribution from Scattering of Strongly Interacting Nuclei.
EPS Conference on Radial Shape of Nuclei Cracow, Poland, June 22-25, 1976

Roussille, R.; Pinston, J.A.; Börner, H.; Koch, H.R.; Heck, D.

Level Structure of ^{147}Nd. I. ^{146}Nd (n,γ) Reaction.
Nuclear Physics, A246 (1975) S. 380-94

Schmidt, K.A.; Dohrmann, H.

KARIN- ein Neutronengenerator für die Krebstherapie mit schnellen Neutronen.
KFK-Nachrichten, 8 (1976) No 1, S. 20-22

Schmidt, K.A.; Dohrmann, H.

Neutronentherapieanlagen im Deutschen Krebsforschungszentrum Heidelberg
Teil II: Die Hochleistungs-Neutronengeneratorröhre KARIN für 14 MeV-Neutronen
Atomkernenergie 27 (1976) S. 159

Schouky, I.; Cierjacks, S.; Brotz, P.; Gröschel, D.; Leugers, B.

Absolute Flux Determination in Fast Neutron Spectra,
NBS Special Publication 425.
US Department of Commerce, Vol. I, p. 277, Oct. 1975

Schweickert, H.

Status Report on the Karlsruhe Isochronous Cyclotron.
13. European Cyclotron Progress Meeting, Milano, May 6-8, 1976

Schwinn, U.; Mairle, G.; Wagner, G.J.; Rämer, Ch.

Proton Pick-up from Nuclei in the Middle of the 1p Shell.
Zeitschrift für Physik, A275 (1975) S. 241-47

Soares, J.C.; Krien, K.; Freitag, K.; Tischler, R.; Rao, G.N.; Müller, H.G.; Hanser, A.; Feurer, B.

Temperature Dependence of the Electric Quadrupole Interaction of ^{100}Rh, ^{111}Cd and ^{181}Ta in Be Metal.
Internat. Meeting on Hyperfine Interactions Studied by Nuclear Methods, Louvain, September 10-12, 1975

Sobiesiak, H.; Heck, D.; Käppeler, F.

X-Ray Analysis of Radioactive Samples Using a Pulsed Proton Beam.
Internat. Conference on Ion Beam Surface Layer Analysis,
Karlsruhe, September 15-19, 1975

Spencer, R.R.; Beer, H.

Measurement of Radiative Capture in Cobalt-59
Nucl. Sci. & Eng. 60 (1976) p. 390

Voss, F.

Neutron Energy Calibration at the Karlsruhe Time-of-Flight Facility.
Neutron Interlab. Seminar CBNM, Geel/Belgien, November 12-14, 1975

Voss, F.; Schmalz, G.

Präzisionsmessungen der Energien von Neutronenresonanzen im MeV-Bereich.
Frühjahrstagung der DPG und OEPG, Kernphysik, Baden/Österr., 29. März - 2. April 1976.
Verhandlungen der Deutschen Physikalischen Gesellschaft, R.6, Bd 11 (1976) S. 917

Voß, F.; Cierjacks, S.; Erbe, D.; Schmalz, G.

Measurements of the γ-Ray Production Cross Sections from Inelastic Neutron Scattering in Some Chromium and Nickel Isotopes Between 0.5 and 10 MeV.
NBS Special Publication 425, US Department of Commerce, Vol. II, p. 916, Oct. 1975

Wisshak, K.; Hanser, A.; Klewe-Nebenius, H.; Buschmann, J.; Rebel, H.; Faust, H.; Toki, H.; Fäßler, A.

Das Niveauschema von ^{143}Eu.
Frühjahrstagung DPG und OEPG, Kernphysik, Baden/Österr., 29. März - 2. April 1976.
Verhandlungen der Deutschen Physikalischen Gesellschaft, R.6, Bd 11 (1976) S. 912

Wisshak, K.; Hanser, A.; Klewe-Nebenius, H.; Buschmann, J.; Rebel, H.; Faust, H.; Toki, H.; Fäßler, A.

Experimental Studies of the Level Scheme of ^{143}Eu and a Generalized Decoupling Model Description.
Z. Physik A277 (1976) S. 129

8. PERSONNEL

Head of the Teilinstitut Kernphysik: Prof. Dr. G. Schatz

Scientific and technical staff:

Bechtold, V., Dr.	Friedrich, F., Dr.	Nowicki, G., Dr.
Beer, H., Dr.	Gils, H.J., Dr.	Ottmar, H., Dr.
Buschmann, J., Dr.	Göring, S., Dipl.-Phys.	Rebel,H.G.,Dr.,Priv.-Doz.
Chaffin, E.F., Dr.	Hanser, A., Dr.	Rupp, G.
Cierjacks, S., Dr.	Heck, D., Dr.	Schmalz,G.,Dipl.-Ing.
Dickmann, F., Dr.	Käppeler, F., Dr.	Schmidt,K.A.,Dipl.-Phys.
Dohrmann, H., Ing.	Leugers, B., Dipl.-Phys.	Voß, F., Dr.
Erbe, D.	Matussek, P., Dipl.-Phys.	Wisshak, K., Dr.
Eberle, H., Ing.	Michel-Piper,I.,Mrs.,Ing.	Zagromski, S., Ing.
Feurer, B.	Nowatzke, W., Miss	

Guests and research students:

Hensley, F.,Dipl.-Phys.	Kazerouni,M.A.,Dipl.-Phys.	Schouky, I., Dipl.-Phys.
Iyer, M.R., Dr.	Ly Di Hong, Miss	Sobiesiak, H.,Dipl.-Phys.
Kari, K.,Dipl.-Ing.	Naqvi, S.A.A.,Dipl.-Phys.	

Secretarial staff: Mrs. H.M. Friederich, Mrs. E. Maaß

Head of the Cyclotron Laboratory: Dr. H. Schweickert

Scientific and technical staff of the Cyclotron Laboratory:

Ässmus, K.H.	Günther, O.	Kneis, W., Dipl.-Phys.
Bauer, G.	Haushahn, G., Dipl.-Phys.	Kögel, B.
Biber, J.	Heidenreich, K.	Kuhn, H.
Blum, B., Miss	Hirth, W.	Mangold, D.
Depta, A.	Kappel, W.-R., Ing.	Möllenbeck, J., Ing.
Ehret, H.-P.	Karbstein, W.,Dipl.-Ing.	Radtke, G., Ing.
Erdel, E.	Kauther, P.	Rämer, Ch., Miss, Ing.
Franz, J.	Kessel, M.	Röhrl, E.

Schimpf, P.	Seitz, J.	Walsch, V., Mrs.
Schulz, F., Ing.	Seufert, H.	Wiss, L.
Seidel, H.	Volk, B.	

Workshops of the Cyclotron Laboratory:

Ernst, R.	Langenbein, R.	Schönstein, E.
Fehling, H.	Maier, W.	Schütz, R.
Illinger, P.	Ripp, H.	Steigleder, C.
Klinger, G.	Schlenker, G.	

Secretarial staff: Mrs. E. Kirste